Some Studies Of Percolation Phenomena In Disordered Systems

Thesis submitted for the Degree of

Doctor of Philosophy (Science)

in

Physics (Theoretical)

by

SUMANTA KUNDU

DEPARTMENT OF PHYSICS

UNIVERSITY OF CALCUTTA

2019

Dedicated to My Parents

Acknowledgments

Firstly, I would like to convey my sincerest gratitude to my supervisor Prof. Subhrangshu Sekhar Manna for his constant help, support and guidance. Words can not express how valuable were the discussions that we had during the last few years. His encouragements and advice helped me to grow my knowledge and inspired me to develop my attitude towards pursuing research as a career. I am also grateful to him for involving me in several projects and collaborations. All these benefited me a lot to broaden my experience and scientific knowledge.

I am thankful to Prof. Alex Hansen, NTNU, Norway and Prof. Nuno A. M. Araújo, University of Lisbon, Portugal for hosting my visits and giving me the opportunity to work in their research groups. I am also thankful to Prof. Amitava Datta and Prof. Robert M. Ziff for many helpful discussions and valuable suggestions. I would also like to thank Dr. Punyabrata Pradhan for his support and fruitful suggestions. I acknowledge the financial support provided by S. N. Bose Centre.

I take this opportunity to thank my friends, seniors, and juniors for making my stay at the S. N. Bose Centre a memorable one. In this regard, I would like to mention the names of Subhadip Chakraborti, Poulami Chakraborty, Indranil Chakraborty, Anulekha De, Debasish Das Mahanta, Rakesh Das, Arghya Das, Somnath Dutta, Rahul Bandyopadhyay, Anupam Gorai and Swarnali Hait. I express my deepest regards to Biplab Bhattacherjee and Suman Aich for extending their helping hand at several critical situations. Special thanks to my friend Chandreyee Roy. It was a nice experience working with her and she has always been patient and supportive of me. I would always relish the unforgettable memories of SNB days that I had with all of them.

I am eternally indebted to my parents and my sister for their unconditional love, support and encouragements. Especially, I express my deepest respect to my mother, Shyamali Kundu for being an inspiration to me. Finally, I convey my special thanks to Sucheta Sharma who has helped me to move forward during the years.

Sumanta Kundu

List of Publications

Publications Included in the Thesis

1. "Jamming and percolation properties of random sequential adsorption with relaxation"
   S. Kundu, N. A. M. Araújo, and S. S. Manna
   Phys. Rev. E **98**, 062118 (2018).

2. "Double transition in a model of oscillating percolation"
   S. Kundu, A. Datta, and S. S. Manna
   Phys. Rev. E **96**, 032126 (2017).

3. "Colored percolation"
   S. Kundu, and S. S. Manna
   Phys. Rev. E **95**, 052124 (2017).

4. "Percolation model with an additional source of disorder"
   S. Kundu, and S. S. Manna
   Phys. Rev. E **93**, 062133 (2016).

Other Publications

5. "A simple discrete-element-model of brazilian test"
   S. Kundu, A. Stroisz, and S. Pradhan
   Eur. Phys. J. B **89**, 130 (2016).

6. "Network topology of the desert rose"
   S. M. Hope, **S. Kundu**, C. Roy, S. S. Manna, and A. Hansen,
   Front. Phys. **3**, 72 (2015).

7. "Fiber bundle model with highly disordered breaking thresholds"
   C. Roy, **S. Kundu**, and S. S. Manna
   Phys. Rev. E **91**, 032103 (2015).

8. "Scaling forms for relaxation times of the fiber bundle model"
   C. Roy, **S. Kundu**, and S. S. Manna
   Phys. Rev. E **87**, 062137 (2013).

Abstract

The emergence of large-scale connectivity from the small-scale connectedness is the signature of a percolation transition and therefore, the system always exhibits a global connectivity beyond this transition point. The small-scale connectivity is significantly influenced by the disorder present in the system. In the present thesis, we introduce four different lattice percolation models and study how the percolation properties of a system are affected by different sources of disorder.

First, we study the percolation properties of a system by occupying randomly the sites of a square lattice with probability p by disks with uniformly distributed radii. Using three different rules for the criterion of defining a connected bond between two neighboring occupied sites and tuning the parameters characterizing the radii distribution, we find that the percolation threshold always varies continuously within the site percolation threshold to unity. The approach of the percolation threshold to its two limiting values are characterized by two distinctly different exponents and are found to be independent of any specific rule.

Further, we extend this study by considering sinusoidal time variations of the radii of disks with initial random phase angles, but with same maximal radius, on a fully occupied lattice. By tuning the maximal value of the disks radii, two distinct percolation transitions are observed. Interestingly, we find that the global transmission of information is possible even if the clusters are of finite sizes.

In another model, the sites of a regular lattice are occupied by atoms with probability p and then, every atom is colored by selecting randomly one of the n distinct colors with probability q. The bonds having two different colored atoms at their opposite ends are only declared as connected. Accordingly, a non-trivial dependence of the percolation threshold on the values of n and q has been observed.

Lastly, we introduce a random sequential adsorption model where the dimers are adsorbed sequentially and irreversibly onto the sites of a square lattice after going through a well-defined relaxation dynamics. When a new incoming dimer partially overlaps with a previously adsorbed dimer, the relaxation dynamics is triggered and during relaxation, a sequence of dimer displacements occur. The post-relaxation state is a monolayer formation of the adsorbed dimers. We investigate the role of relaxation mechanism on the percolation and jamming transitions. We find that the relaxation dynamics helps the system to percolate in comparison to the model without relaxation.

Using extensive numerical simulations we conclude that although the percolation threshold is dependent on the specific source of disorder, all four variants of the percolation models belong to the percolation universality class.

Contents

Chapter 1

Introduction

1.1 Phenomenon of Percolation

The phenomenon of percolation can simply be described by using the following example. Let us consider a rectangular piece of porous material, such as porous rock containing a collection of pores which are distributed randomly over space. Now, we place the sample horizontally and ask the question, if some liquid is poured on the top surface, will it appear at the bottom? The answer could be yes, or no, depending on the volume fraction p of these pore spaces, i.e., porosity of the material. When the porosity p exceeds a critical value p_c, an interconnected pathway through the pore spaces spanning from the top to bottom of the sample appears and hence the liquid can reach the bottom surface propagating through the pores. The existence of the critical value of porosity in this description is particularly of great interest as the system exhibits many interesting features only in the vicinity this point.

The phenomenon of percolation was first introduced by Broadbent and Hammersley in 1957 [1] to understand the mechanism of charcoal gas masks used in coal mines. For the mask to work properly, the pore spaces within the carbon granules should be sufficiently interconnected such that clean air can penetrate through them while simultaneously blocking the poisonous gas particles by the process of adsorption. This

type of filtration process is often observed in our daily lives. One of the natural examples is rain water which is not directly drinkable, but when it passes through the spaces between the grains of soil from layer to layer, the filtration process takes place. Thus, the impurities are filtered out and water becomes fresh groundwater.

Though percolation was introduced in 1957, later it was realized that the concept essentially was rooted in the study of *gelation* in polymers by Flory in 1940 [2–4]. The process of gelation involves the formation of macromolecules from small monomers [5]. For instance, if we place gelatine, a fluid consisting of a large number of small monomers (sol), in a refrigerator, it starts polymerizing and eventually forms a sufficiently large solid macromolecule (gel) that extends from one end of the system to the other [5]. Similarly, while boiling an egg, gradual formation of the chemical bonds between its constituent small molecules eventually spans the entire system and thus, transforms the egg from liquid-like to solid-like object [6]. The emergence of such a macroscopically connected object is the primary concern in the theory of percolation.

The field of percolation attracted to the statistical physics community when it had been revealed that the models of percolation (described later) exhibit universal features of the *critical phenomena* [7–10]. The critical phenomena are observed only in close proximity to the phase transition point, called the critical point. Different observables either diverge or vanish as the critical point is approached and their behavior close to this point are described by power-laws of the distance from the critical point in the parameter space. For example, when the temperature T of a ferromagnet is increased towards the Curie temperature T_c, the magnetization m vanishes continuously close to T_c as a power law: $m \sim (T_c - T)^{\beta}$ [7]. The exponents characterizing these power-laws are known as *critical exponents*. Typically, their values are found to be non-integer. For instance, it was estimated experimentally that for the ferromagnet $CrBr_3$ the value of the critical exponent $\beta = 0.368 \pm 0.005$ [11]. In the regime $T < T_c$, different domains of the system exhibit correlations resulting in a non-zero net magnetization. The sizes of these correlated domains fluctuate due to thermal fluctuations and as

a result, the magnetization also fluctuates. When T approaches T_c from below, the fluctuations in magnetization become so large that all length scales become relevant. In this regime, the magnetized domains are found to be statistically *self-similar* on all length scales, i.e., the structure of a part of the domain is statistically similar to itself upon repeated magnification [7, 12]. Such self repeating patterns are often observed in nature, such as coastlines, mountain ranges, river networks, Saturn rings, etc., [13–15]. These particular patterns are known as *fractals* and are characterized by the non-integer *fractal dimension*.

The critical behavior of the system is characterized by the set of critical exponents. Remarkably, the experimental values of the critical exponents for different magnetic materials suggest that they are not material specific. More interestingly, the critical exponents obtained for the liquid-gas system are also seen to match with the exponents of the magnetic systems [7, 10]. Very close to the critical point the system specific microscopic details essentially become unimportant and therefore, a class of widely different systems are found to exhibit the same critical behavior. This remarkable feature is called *universality* and the set of critical exponents defines the *universality class*.

The underlying concept of percolation can be applied to study the critical behavior of widely different systems including many great practical applications [6, 16–19]. One of the most common areas where one finds the applicability of the theory of percolation is the extraction of oil from oil reservoirs. The most important task in the oil industry is to predict how much oil one can extract by placing a well at a random location in the oil field. During the oil recovery process, oil contained inside the pores in a reservoir naturally flows through a series of pores. Therefore, for the prediction purposes, oil industry strongly depends on the estimation of the porosity of the sample collected from the reservoir. If the measurement yields a value of the porosity $p < p_c$ of the sample, then the network of pores connecting the well extends only to a small portion of the reservoir and thus, they end up extracting a limited amount of oil. For

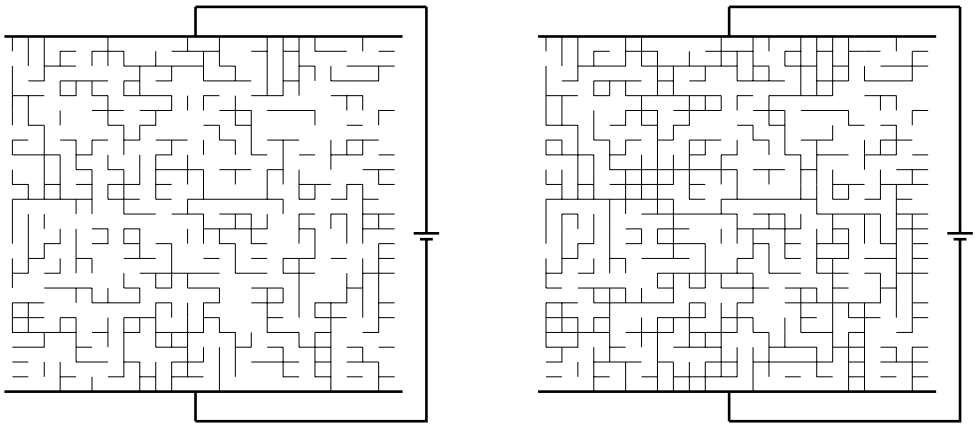

(a) (b)

Figure 1.1: Illustration of the bond percolation model on a 24×24 square lattice for two different values of the bond occupation probability p, namely $p = 0.45$ (a) and $p = 0.55$ (b). A spanning path from the top to bottom of the system exists for $p = 0.55$.

economic purposes, they extract oil only from the reservoirs for which $p > p_c$, resulting in the production of a large amount of oil. Similarly, prediction of the risk of water contamination due to the transport from the nuclear waste deposits essentially requires the knowledge of p_c [20]. Other problems, where the theory of percolation has been proven to be relevant include the propagation of fires in forests [21], spreading of infectious diseases in the form of epidemics [22, 23], propagation of information through wireless sensor networks [24–26], public opinion formation [27, 28], prediction of the agricultural soil quality for optimal yields [20, 29], etc.

The models of percolation provide useful insights about how the large-scale connectivity appears in such diverse types of natural and artificial systems [6, 16–19, 30–32]. In the following, we start by describing two simplest models of percolation on a regular lattice. Consider an electrical network of the mixture of conductors and insulators as illustrated in Fig. 1.1(a). The bonds on the lattice are occupied randomly and independently by the conductors with probability p or they are kept vacant (i.e., they are insulators) with probability $(1 - p)$. The system is placed between two busbars which are connected to an external voltage source. Clearly, for $p = 0$, no conducting bonds are present and the system is an insulator. In the other extreme, at $p = 1$, all

the bonds are conductors and current flows through the system. Therefore, tuning the value of p from zero, at some intermediate critical value of $p = p_c$, known as the *percolation threshold*, the circuit reads a non-zero value of current for the first time. Clearly, at p_c the system undergoes a phase transition from a non-conducting phase to a conducting phase. This particular version of the percolation model is referred as the *bond percolation* in two dimensions [6].

In the context of fluid flow through porous media, the occupied and vacant bonds in the above description correspond to the open pores and solid rock matrix, respectively. For $p > p_c$, if fluid is injected at one side of the system, it will certainly arrive at the other side propagating through the series of open pores. Similarly, in gelation, the fraction of chemical bonds formed between the monomers is represented by the density p of the occupied bonds and hence, the point $p = p_c$ marks the sol-gel transition point. Moreover, the study of Fisher and Essam revealed the one to one correspondence between the model of polymerization and the model of percolation on Bethe lattice [33, 34].

Instead of lattice bonds, the percolation model can also be described by occupying randomly the sites of a regular lattice with probability p, and is recognized as the *site percolation* [6]. In this model, any two adjacent occupied sites are considered as connected. One can imagine this in two dimensions by assigning a metallic disk of radius 1/2 at every occupied site of the lattice with unit lattice constant. A group of such occupied sites interlinked through their neighboring connections forms a *cluster*. Therefore, any two occupied sites, separated at a certain distance, can be reachable by their nearest neighbor connections only if they belong to the same cluster. At any arbitrary intermediate value of p, there exists a number of clusters of different shapes and sizes, the properties of which significantly depend on the value of p [35, 36]. The size s of a cluster is defined as the number of sites in the cluster. The largest one among these clusters monotonically increases in size with increasing the value of p, and an incipient infinite cluster appears in the system when p exceeds a critical value of $p = p_c$. For $p < p_c$, the clusters are all finite sizes and for $p > p_c$, the largest cluster scales

linearly with the volume of the system. Only at $p = p_c$, the largest cluster exhibits self-similar structure.

The term 'infinite' mentioned above is only applicable for the infinitely large system. For a finite-size system, at $p = p_c$, for the first time the size of the largest cluster becomes macroscopically large and it spans between two opposite sides of the lattice. Therefore, in the regime $p > p_c$, there always exists a 'global connectivity' through the spanning path on the largest cluster. This type of cluster is often termed as the 'giant cluster'. Clearly, p_c marks the *percolation transition* point between the 'percolating phase' characterized by the existence of a global connectivity and the 'non-percolating phase' where such a global connectivity is absent.

Unlike the thermodynamic phase transitions observed in the magnetic systems or liquid-gas systems, the percolation transition is completely a geometrical phase transition. However, in a seminal work published in 1969, Kasteleyn and Fortuin demonstrated an interesting mapping between the percolation and the q-state Potts model related to the magnetic system [37]. For $q = 2$, Potts model reduces to the well-known Ising model. Specifically, they showed that the q-state Potts model in the limit $q \to 1$ corresponds to the bond percolation.

Percolation is now regarded as one of the simplest models for studying the order-disorder phase transition. The nature of transition is continuous for both the models described above and they belong to the same universality class. Moreover, the percolation transition is so robust that a large number of variants of the percolation models (some of them are described in Sec. 1.4 and in the subsequent Chapters) exhibit the same critical behavior.

1.2 Percolation Threshold

Precise determination of the percolation threshold p_c is essential in studying the critical behavior of the percolation models, since many non-trivial features are observed only

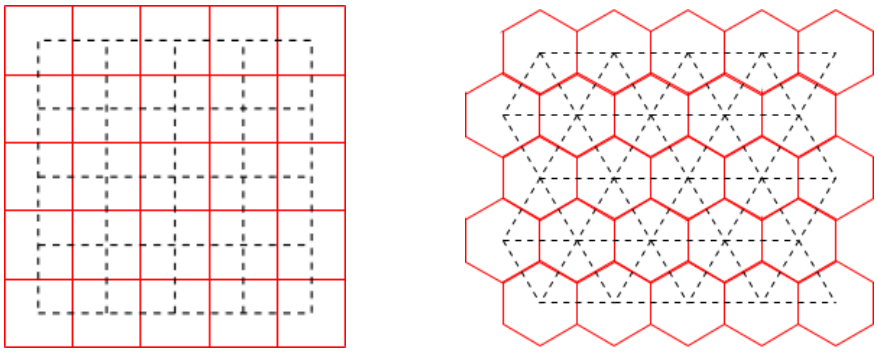

(a) (b)

Figure 1.2: The lattices (red) and their corresponding dual lattices (black). (a) The square lattice is a self-dual lattice. (b) The triangular lattice is the dual of the honeycomb lattice.

in the vicinity of p_c. Unfortunately, there are only a few class of lattice geometries in two dimensions for which the exact thresholds are known [31, 38]. For example, $p_c = 1/2$ for bond percolation on the square lattice. On the triangular lattice, $p_c = 2\sin(\pi/18)$ and $1/2$ for bond and site percolation, respectively. On the honeycomb lattice, $p_c = 1 - 2\sin(\pi/18)$ for bond percolation. The concepts of dual-graph [Figs. 1.2(a) and (b)] and star-triangle transformation are often used in finding these exact values. For example, the bond percolation threshold on a regular square lattice can be obtained using the graph duality as follows. For any bond configuration on the lattice G, there exists a corresponding bond configuration on the dual lattice H such that if a bond is occupied on the lattice, corresponding bond on the dual lattice is kept vacant. Therefore, the sum of the bond densities on the lattices G and H equals unity. This implies that at their corresponding percolation thresholds,

$$p_c^G + p_c^H = 1. \tag{1.1}$$

Since the square lattice is self-dual [Fig. 1.2(a)], it validates the relation $p_c^G = p_c^H$. This eventually leads to $p_c = 1/2$ from Eq. (1.2). However, the site percolation thresholds for the square and honeycomb lattices are still not known exactly. Similarly, exact thresholds for other percolation models in two dimensions such as AB percolation (described

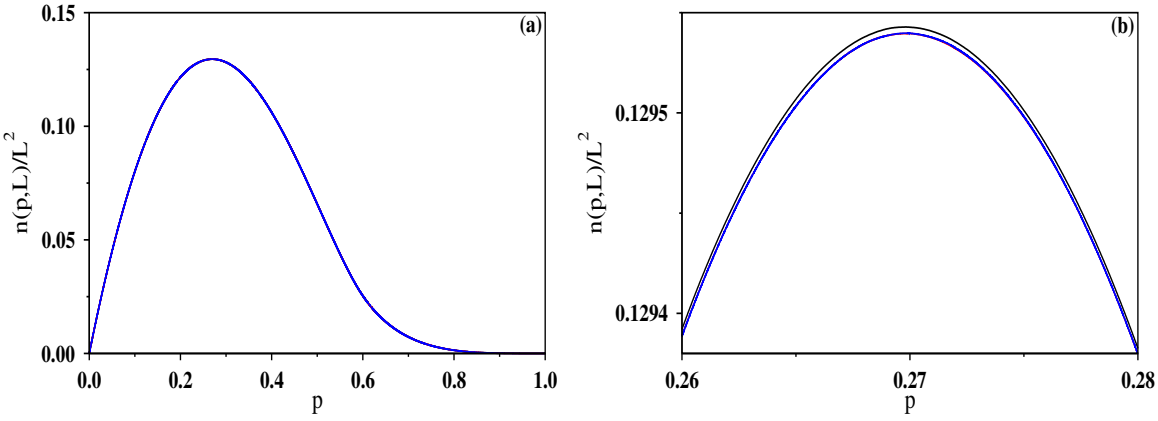

Figure 1.3: (a) Plot of the average number $n(p, L)$ of clusters per site for the site percolation on square lattice of sizes $L = 256$ (black), 512 (red), and 1024 (blue). The maximum of the curves occur at $p \approx 0.2696, 0.2697$, and 0.2698, respectively. The region around the maximum has been zoomed in (b). Apparently, the system size dependence of $n(p, L)$ around this point is negligibly small.

in Sec. 1.4.2), percolation models described in the subsequent Chapters, etc., seem implausible. Furthermore, in higher dimensions exact thresholds are not known for any lattice geometries. In such cases, numerical simulations play a key role in determining the high precision values for p_c. Until now, the best known value of the percolation threshold for the site percolation on square lattice is p_c(sq)=0.59274605079210(2) [39]. Percolation thresholds for many other lattices are listed in Ref. [40]. In the following, we describe a numerical method for evaluating the value of p_c.

1.2.1 Determination of the Percolation Threshold

Let us consider the site percolation model on a square lattice of size $L \times L$ with periodic boundary conditions. One by one, the vacant sites of an initially empty square lattice are occupied randomly and independently. At any arbitrary stage, the fraction of occupied sites is denoted by p. With increase in the value of p from zero, average number of distinct clusters $n(p, L)$ first increases, attains a maximum at $p \approx 0.27$ and after that it decreases when the merging of clusters of different sizes dominate. This variation is exhibited in Fig. 1.3 for the entire range of p. Using Hoshen–Kopelman

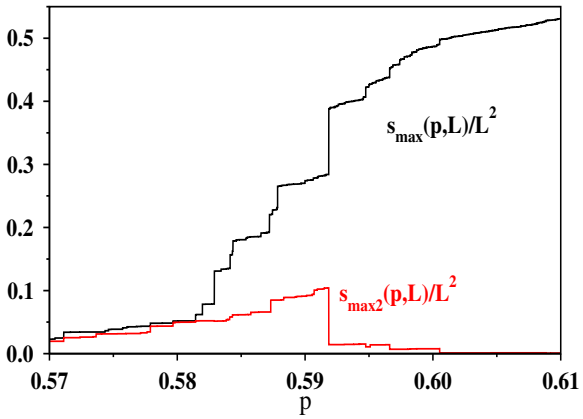

Figure 1.4: Variation of the size of the largest cluster $s_{max}(p, L)$ and the second largest cluster $s_{max2}(p, L)$ scaled by L^2 in a typical run for the site percolation on square lattice of size $L = 512$. The maximal jump in the size of the largest cluster occurs at ≈ 0.5919 for this run.

algorithm [41] or Newman–Ziff algorithm [42], one can efficiently identify different clusters when p is continuously varied. In a typical run, the size of the largest cluster s_{max} increases monotonically with increasing p, but the size of the second largest cluster does not. Near the percolation transition, the second largest cluster may merge with the largest cluster several times and consequently, the largest cluster makes a number of jumps in size (see Fig. 1.4). The maximal jump $\Delta_m s_{max}$ in the size of the largest cluster takes place at a specific value of p, when the maximum of the second largest cluster merges with the largest cluster. This particular value of p is considered as the percolation threshold p_c^α for the configuration α [35, 36, 43]. Averaging over many such independent configurations gives an estimate of the percolation threshold $p_c(L) = \langle p_c^\alpha \rangle$ for the lattice size L. The entire set of calculations is then repeated for different values of L. These $p_c(L)$ value are then extrapolated in the limit $L \to \infty$ using the equation

$$p_c(L) = p_c - AL^{-1/\nu}. \tag{1.2}$$

Tuning the value of ν, the best fit of data by least squares method finally determines the asymptotic value of p_c. We explain the reason of following the Eq. (1.2) for the extrapolation in Sec. 1.3.1.

1.3 Critical Behavior of the Ordinary Percolation

The term 'ordinary' refers to the specific case of percolation where the occupation of sites (bonds) takes place randomly and independently. As mentioned before, the onset of criticality is characterized by the scale-free behavior of several observables. In the following, we enumerate some such quantities related to the percolation. To demonstrate the critical behavior near p_c, we consider the site percolation model on $L \times L$ square lattice.

1.3.1 Correlation Length

Characteristic feature of the continuous phase transition is the divergence of the correlation length. It is a measure of the distance over which the microscopic details of a system are correlated and its value is calculated using a *correlation function* $g(r)$. For the percolation models, the correlation function $g(r)$ is defined as the probability that a pair of occupied sites separated by a distance r belong to the same cluster. This probability is expected to decrease with increasing the distance of separation r. Specifically, it is found that $g(r) \sim \exp(-r/\xi)$, where ξ is the length scale that characterizes the decay of $g(r)$ and is known as the correlation length.

For $p < p_c$, the clusters are all finite sizes resulting in a small finite value for the correlation length ξ, its value increases as p is increased, and when $p \to p_c$, it diverges as

$$\xi(p) \sim |p - p_c|^{-\nu}, \tag{1.3}$$

where ν is the correlation length exponent and its value if 4/3 in two dimensions [6]. Usually, in calculating $g(r)$ the largest cluster is not considered. Consequently, as p_c is approached from both the sides, the correlation length diverges. For a finite-size system ξ can be at most L and that is attained at $p = p_c(L)$ [35]. Thus, from Eq. (1.3) one gets the specific form given in Eq. (1.2): $p_c(L) = p_c - AL^{-1/\nu}$.

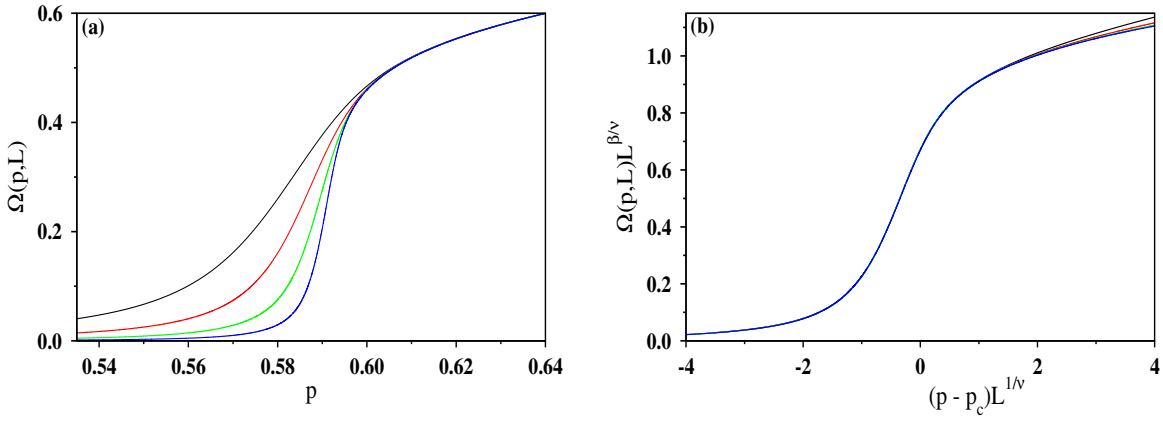

Figure 1.5: (a) The variation of the order parameter $\Omega(p, L)$ has been shown for different values of $L = 128$ (black), 256 (red), 512 (green), and 1024 (blue) for site percolation on square lattice. (b) Scaling plot of the same data using $p_c = p_c(\text{sq})$= 0.59274605079210 [39], $\nu = 4/3$, and $\beta/\nu = 5/48$, exhibiting an excellent data collapse.

1.3.2 Order Parameter

Every phase transition is characterized by an order parameter whose value remains zero in one phase and finite in another phase. For percolation, average size of the largest cluster per site is considered as the order parameter $\Omega(p, L) = \langle s_{max}(p, L)\rangle/L^d$, where d is the Euclidean dimension. When p approaches p_c from the above, the order parameter vanishes continuously in the limit $L \to \infty$ as

$$\Omega(p) \sim (p - p_c)^{\beta}. \tag{1.4}$$

The value of the critical exponent $\beta = 5/36$ in two dimensions [6]. In Fig. 1.5(a), we exhibit the variation of the order parameter with p for different system sizes L. The curves become sharper and sharper when L is increased systematically. To evaluate the critical exponents using finite size systems, usually *finite-size scaling* analyses are performed. This involves suitable scaling of the abscissa and ordinate such that the data for different values of L collapses onto each other and eventually forms a single curve. Figure 1.5(b) shows the scaling plot of the order parameter, implying the following

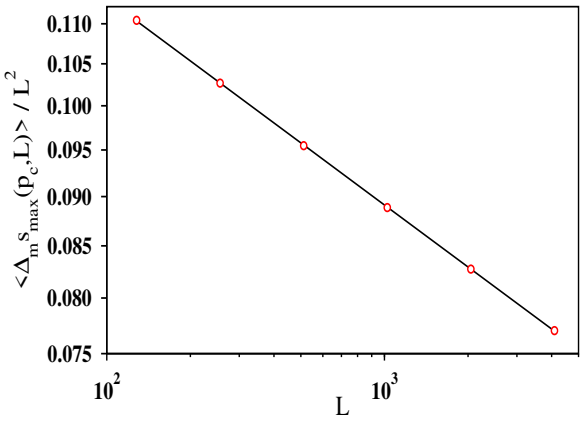

Figure 1.6: For the site percolation on square lattice, the average value of the maximal jump in the size of the largest cluster $\langle \Delta_m s_{max}(p_c, L)\rangle / L^2$ has been plotted against the size L of the lattice on a log-log scale for $L = 128$, 256, 512, 1024, 2048, and 4096. The slope of the fitted straight line is $-0.1039(5)$.

finite-size scaling form

$$\Omega(p, L) = L^{-\beta/\nu} \mathcal{F}[(p - p_c)L^{1/\nu}], \tag{1.5}$$

where $\mathcal{F}$ is called the scaling function. For the regime $p > p_c$, the function $\mathcal{F}[x]$ with $x = (p - p_c)L^{1/\nu}$ obeys a power-law $\mathcal{F}[x] \sim x^{\beta}$, consistent with Eq. (1.4).

Largest Cluster and its Maximal Jump

At $p = p_c$, the scaling form in Eq. (1.5) suggests that $\Omega(p_c, L) \sim L^{-\beta/\nu}$ and therefore, the average size of the largest cluster scales with L as

$$\langle s_{max}(p_c, L)\rangle \sim L^{d-\beta/\nu} = L^{d_f}. \tag{1.6}$$

Therefore, the largest cluster at $p = p_c$ is a fractal with the fractal dimension d_f.

The average value of the maximal jump in the size of the largest cluster $\langle \Delta_m s_{max}(p_c, L)\rangle$ at $p = p_c$ scaled by L^d decreases with L as

$$\langle \Delta_m s_{max}(p_c, L)\rangle / L^d \sim L^{-(d-d_f)}. \tag{1.7}$$

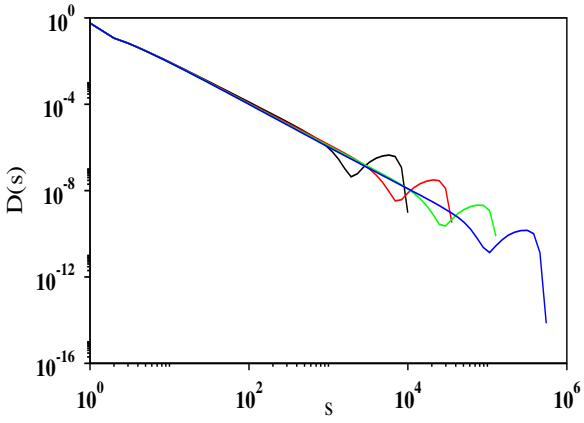

Figure 1.7: The cluster size distribution $D(s)$ at $p = p_c$ has been exhibited on a log-log scale for different values of $L = 128$ (black), 256 (red), 512 (green), and 1024 (blue). The largest cluster has been excluded in the calculation. The slope of the curves in the linear region have been found to be ≈ 2.05.

Figure 1.6 shows the plot of $\langle \Delta_m s_{max}(p_c, L) \rangle / L^2$ as function of L on a double logarithmic scale for the square lattice. An excellent fit of the data by a straight line with a slope $-0.1039(5)$, in close agreement with $d_f - 2$ indicates that the second largest cluster has the same fractal dimension as the largest cluster [43].

1.3.3 Cluster Size Distribution

Near $p = p_c$, the cluster size distribution $D(s)$ obeys the following scaling form

$$D(s) \sim s^{-\tau} \mathcal{D}[(p - p_c)s^{\sigma}], \tag{1.8}$$

where the scaling function $\mathcal{D}[x]$ is a constant at $x = 0$. Therefore, at $p = p_c$, the cluster size distribution follows the power-law:

$$D(s) \sim s^{-\tau}. \tag{1.9}$$

The exact values of τ and σ in two dimensions are 187/91 and 36/91, respectively [6]. In Fig. 1.7, we exhibit the cluster size distribution at $p = p_c$ for four different system sizes on a double logarithmic scale. Since, the largest cluster is fractal at p_c, the cut-off

is seen to grow as L^{d_f}. The second largest cluster also has the same fractal dimension d_f and therefore, even if the largest cluster is excluded while calculating the cluster size distribution, the cut-off still scales as L^{d_f}.

1.3.4 Second Moment

The second moment M_2' of the cluster size distribution is defined as

$$M_2' = \frac{1}{L^d}\Big[\sum_i s_i^2 - \langle s_{max}^2 \rangle\Big], \tag{1.10}$$

where s_i is the size of the cluster i. Clearly, M_2' depends on the value of p and the size of the system L. The function $M_2'(p, L)$ is maximum at a specific value of $p = p_m(L)$ and decreases monotonically on both sides of this point. As L is increased, $p_m(L)$ approaches p_c in the limit $L \to \infty$. At $p = p_c$, the second moment scales with L as

$$M_2'(p_c, L) \sim L^{\gamma/\nu}. \tag{1.11}$$

The exponent γ can be expressed in terms of the exponents ν, d_f and τ as follows. Since the cut-off of the cluster size distribution at $p = p_c$ grows with L as L^{d_f}, the expression of $M_2'(p_c, L)$ can approximately be written using Eq. (1.10) as per the following form:

$$M_2'(p_c, L) \approx \int_1^{L^{d_f}} D(s) s^2 ds \approx L^{d_f(3-\tau)}. \tag{1.12}$$

So from Eqs. (1.11) and (1.12) we get the scaling relation $\gamma/\nu = d_f(3 - \tau)$.

1.3.5 Shortest Path

An arbitrary pair of sites belonging to a cluster are interconnected and thus, they can be reached by traversing a sequence of nearest neighbor distances. A particular sequence constitutes a 'path' and the 'path length' corresponding to that path is defined by the number of distinct nearest neighbor distances on the path. In general, a number of

distinct paths of different path lengths exist between the pair of given sites. The path with the smallest path length ℓ is called the *shortest path*. There may exist more than one shortest paths connecting the two sites and therefore, it is not unique. The concept of shortest path is essential in the context of efficient transportation of matter. For example, the oil industry performs measurements of the shortest path between two wells (one acts as the injector and another one is used for extraction) for the production of oil in an economically viable way. Similarly, in communication systems, for efficient flow of data packets through Internet requires the knowledge of the shortest path.

The average length $\langle \ell(L) \rangle$ of the shortest path between two sites belonging to the spanning cluster, one in the top row and another in the bottom row of the system, is found to scale with the lattice size L at the percolation threshold as

$$\langle \ell(L) \rangle = L^{d_\ell}, \tag{1.13}$$

where d_ℓ is the shortest path fractal dimension. Till now, its exact value even in two dimensions is not known. The best numerically obtained value of d_ℓ in the literature is 1.13077(2) in two dimensions [44].

Further, several different pairs of sites with a certain fixed Euclidean distance of separation can be found on the spanning cluster. Evidently, the shortest path lengths between these pairs of sites are different. It is well-known in the literature that the distribution of the shortest path lengths at the percolation threshold exhibits a power-law with an exponent close to 2.14 [45, 46].

1.3.6 Backbone and Dangling Ends

Consider that there is an Ohmic resistor between every pair of neighboring occupied sites at a given site occupation probability $p > p_c$. So there always exists a spanning cluster of resistors. Now a potential difference is applied between a pair of sites belonging to the spanning cluster, one in the top and another in the bottom row of the lattice.

The set of paths connecting these two sites only carry non-zero current and constitutes the *backbone* of the percolation cluster. Each of the remaining parts of the spanning cluster connects to the backbone through a single site and therefore, no current flows through them. These parts are called the *dangling ends*. Right at p_c, the mass (i.e., total number of sites) of the backbone M_b scales with the lattice size L as

$$M_b(L) \sim L^{d_b}, \tag{1.14}$$

where d_b is the fractal dimension of the backbone and its best known value is $d_b = 1.6434(2)$ [47, 48] for the ordinary percolation in two dimensions.

At p_c the mass of the backbone is negligible compared to the mass of the largest cluster. In other words, the masses of the dangling ends mainly contribute to the mass of the largest cluster. This fact and the self-similarity of the largest cluster immediately implies that the dangling ends are also fractal with the same fractal dimension d_f of the largest cluster. It is well known that the probability distribution of the masses of the dangling ends follows a power-law:

$$D(M) \sim M^{-(1+\lambda)}, \tag{1.15}$$

where M is the mass of a given dangling end and the scaling theory predicts $\lambda = d_b/d_f$. It has also been verified using numerical simulations in Ref. [49].

1.3.7 Percolation Critical Exponents

The critical exponents of percolation are not independent, they are related to one another by scaling and hyperscaling relations. For example,

$$d_f = d - \beta/\nu, \tag{1.16}$$

$$\gamma/\nu = d_f(3 - \tau), \tag{1.17}$$

$$\sigma\nu = 1/d_f, \tag{1.18}$$

$$\tau = 1 + d/d_f, \tag{1.19}$$

$$d\nu = \gamma + 2\beta, \tag{1.20}$$

etc. Many such relations are given in Ref. [50]. In the above relations, the dimensionality d is coupled with the critical exponents and thus, by changing d a different set of critical exponents appear (below the mean-field limit). For a given dimensionality, although the percolation thresholds are different for different lattice geometries, the critical exponents are independent of the lattices and thus, universal. Furthermore, both the site percolation and bond percolation are found to belong in the same universality class. The values of the critical exponents that have been discussed in the above sections are listed in the Table 1.1.

Table 1.1: Critical exponents of the ordinary percolation in two and three dimensions. The exact values are taken from Ref.[6].

d	2	3
ν	4/3	0.87619(12) [51]
β	5/36	0.41809(15) [52]
d_f	91/48	2.52295(15) [52]
γ	43/18	1.805(20) [53]
τ	187/91	2.1890(2) [54]
σ	36/91	0.445(10) [55]
d_l	1.13077(2) [44]	1.3756(6) [44]
d_b	1.6434(2) [47]	1.77(7) [56]

1.4 Variants of Percolation Models

Due to its simplicity in the description and plenty of applicability in a wide variety of fields ranging from physics, biology to engineering, the literature on this topic is vast and expectedly, a large number of variants of percolation models exist in the literature. The generic feature of all these percolation models is the emergence of long-range

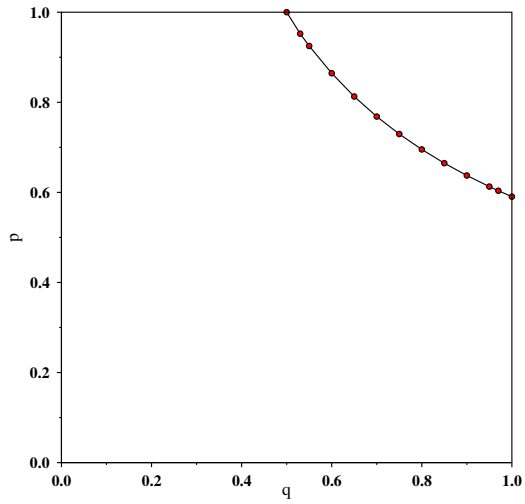

Figure 1.8: Phase diagram of the site-bond percolation on a square lattice, where p and q correspond to the site and bond occupation probabilities, respectively. The data presented here are obtained from our numerical simulation using the lattice size $L = 1024$. The critical curve on the $p-q$ plane separates the percolating region (above) from the non-percolating region (below).

connectivity from the short-range connectedness when the control variable is tuned to the critical point. We briefly describe a few of them in the following.

1.4.1 Site-Bond Percolation

The *site-bond percolation* [57] can be viewed as a combination of both site and bond percolation model. This model was introduced for theoretical understanding of the experimentally observed results of polymer gelation. In a real experiment of polymer gelation, solvent molecules are usually present along with the monomers and depending on the experimental conditions (e.g., temperature) chemical bonds start to form only between the pairs of monomers [5]. Certainly, the gelation is affected by the fraction of volume in system occupied by the solvent molecules. The site-bond percolation is regarded as the simplest model of gelation, which takes into consideration the presence of solvent molecules in the system.

In this model, the sites and bonds of a regular lattice are occupied randomly and independently with two different probabilities of occupation p and q, respectively. The

occupied sites represent the monomers, whereas the vacant sites represent the solvent molecules. Only the occupied bonds having two occupied sites at their opposite ends represent the chemical bonds. Therefore, a sequence of occupied sites connected by the occupied bonds forms a cluster that corresponds to a polymer chain. Depending on the value of p and q, the global connectivity through the alternating occupied sites and bonds is determined by the appearance of such a cluster spanning between two opposite boundaries of the lattice. Clearly, for $p = 1$ and $q = 1$, the model reduces to the ordinary bond percolation and site percolation, respectively. For any general value of $p_c \leqslant p \leqslant 1$, there exists a critical density of bonds q_c, where percolation transition occurs. Therefore, a phase digram can be constructed in the $p - q$ parameter space, where a critical curve divides the entire $p - q$ plane into two regions representing the percolating and non-percolating phases (Fig. 1.8). The critical behavior at all points on the phase boundary has been found to be same as that of the ordinary percolation [58].

1.4.2 AB Percolation

Spins in the antiferromagnetic materials align in a particular (regular) arrangement such that the energy of the system is minimized. Specifically, in the ground state anti-parallel alignment of neighboring spins are energetically favorable and thus, they are assumed to be bonded. Motivated by this antiferromagnetism, Mai and Halley introduced the *AB percolation model* [59] which is illustrated as follows. Initially, all sites of a lattice are occupied with B atoms. Then, the sites are selected randomly one by one and the B atoms at these sites are replaced by the A atoms [36]. At any arbitrary intermediate stage, the fraction of A atoms is denoted by p. According to this model, the bonds which have both A and B atoms at their two opposite ends are declared as connected mimicking the case of antiferromagnetism and form AB clusters. For a given value of p, the density of connected bonds is given by $p_b = 2p(1 - p)$, which has its maximum at $p = 1/2$ and decreases monotonically on both sides of this point. Moreover, p_b is symmetric about this point. This behavior of p_b should

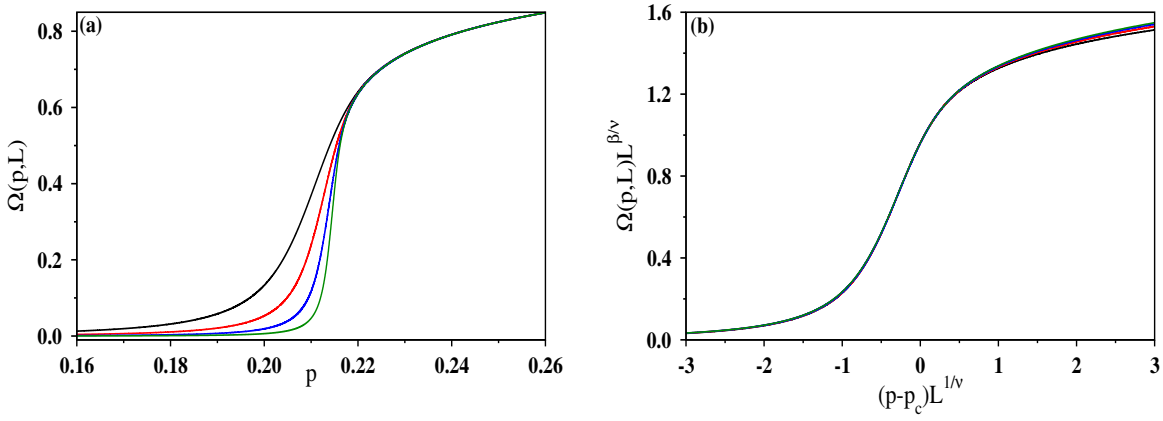

Figure 1.9: For AB percolation, (a) the variation of the order parameter $\Omega(p, L)$ with p has been shown shown for the triangular lattice of sizes L=256 (black), 512 (red), 1024 (blue), and 2048 (green); (b) finite-size scaling plot of the same data. The best data collapse corresponds to $p_c = 0.2155(6), 1/\nu = 0.748(5)$, and $\beta/\nu = 0.103(2)$.

be reflected in the percolation properties of the system also. As p is increased from zero, the average size of the largest cluster increases till $p = 1/2$ and then, its size again decreases monotonically. Because of this, if the largest AB cluster establishes a global connectivity at a specific value of $p = p_c$, the connectivity is lost beyond the point $p = 1 - p_c$. Therefore, for $p_c \leqslant p \leqslant 1 - p_c$, the system is percolating. However, the existence of the global connectivity through the alternating A and B atoms and therefore the existence of p_c, crucially depends on the geometry of the underlying lattice [60, 61]. For example, the spanning AB cluster does not appear on the square lattice [61, 62], but it exists on the triangular lattice [63] and here $p_c \approx 0.215$ [59]. Although, it was first concluded that the universality class of AB percolation in two dimensions is different from the ordinary percolation [59], later it has been argued that it belongs to the same universality class as the ordinary percolation [64–66]. The data obtained from our numerical simulations for the order parameter $\Omega(p, L)$ (defined in Sec. 1.3.2) has been plotted against p in Fig. 1.9(a). The finite-size scaling of the same data has been performed in Fig. 1.9(b) with the scaling exponents consistent (within error bars) with the exponents of the ordinary percolation.

1.4.3 Invasion Percolation

Perhaps, the most simple but appropriate model in the context of flow of two immiscible fluids in porous media is the model of *invasion percolation* proposed by Wilkinson and Willemsen [67]. Imagine a scenario where a porous medium is completely filled with oil and water is injected into the medium at a very slow but constant rate. As a result, the water front advances through the medium by displacing the oil. Clearly, water and oil act as invading and defending fluids, respectively. The water front advances slowly by following the path of least resistance offered by the oil contained in the pores of different sizes on the oil-water interface. During this process a situation may arise when a part of the defending fluid gets trapped in a region surrounded by the invading fluid. Depending on the compressibility of the defending fluid the flow of invading fluid into that region is either prohibited or permitted.

The original model of invasion percolation was studied on a regular lattice geometries representing the porous media, where every site is assigned a number r by drawing its value randomly from a uniform distribution in the range $[0, 1]$. Now, starting from an initial configuration with all sites occupied by the defender, the invader starts growing from a single site (in the simplest case) as follows. At each time step, the number of invader increases by one by displacing the defender from the site having smallest value of r on the interface, while the displaced defender leaves the system [67, 68]. To describe the model more elaborately, let us consider that initially, i.e., at time $t = 0$, a single invader resides at the site (i, j) on a square lattice. At time $t = 1$, the numbers associated with all four nearest neighbors of (i, j) are checked and the site having the smallest number is displaced by the invader. Thus, a cluster of invader of size $s = 2$ is formed. In a similar way, at time $t = 2$, the site with the smallest number is determined from the six perimeter sites of the cluster and then, it is occupied by the invader. This way a single cluster of invader grows with time by following the local properties of the medium, and after a particular instant of time the cluster percolates i.e., it spans across the lattice. At this stage, the density of occupied sites by the invader defines the

percolation threshold p_c.

It is important to note that at an arbitrary intermediate time step when the number $r = r_0$ determines the next site to be invaded, that does not imply that all the sites with $r < r_0$ has already been occupied by the invader. In the subsequent steps, as the interface advances, more and more new sites become available at the interface and consequently, a set of numbers smaller than r_0 may appear.

The properties of the cluster of invader at the percolation point p_c significantly depends on the nature of the displacing fluid as described here. For infinitely compressible defender, one can ignore the trapping mechanism and in this limit the fractal dimension d_f of the cluster at p_c has been found to be same as the ordinary percolation, i.e., $d_f \approx 1.89$. A different value of $d_f \approx 1.82$ has been reported in two dimensions by considering the trapping where the defender prohibits the flow of invader into the trapped region [67]. Furthermore, the value of $d_f \approx 1.82$ was estimated in an experiment where the oil was displaced by the air in a two dimensional network [69].

1.4.4 Continuum Percolation

Instead of lattice geometries, Percolation has also been studied on continuum space. The geological porous media such as fractured rocks, soil, etc., commonly do not possess ordered pores structure as lattice geometries. In general, the pores are found distributed over space randomly and oriented in random directions. Thus, a pore may directly connect many other pores whose number vary from place to place. To study the phenomenon of percolation in such systems the relevant model is the continuum percolation [18, 30]. In a simple minded description of the continuum percolation model, one may consider the following scenario. Lily pads floating at random positions on the water surface of a pond with a certain fixed value for their radii [18, 35]. Here, one finds the minimal density of Lilies required for an ant to cross the pond by walking on the overlapping Lilies. Another real world example where this percolation model is applicable is the Mobile ad hoc network (MANET) [35, 70]. Each mobile device

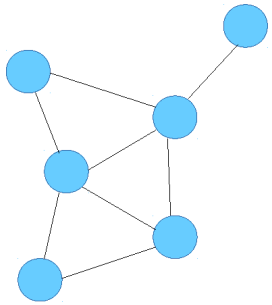

Figure 1.10: Representation of a network with six nodes and eight links.

in a MANET has a fixed range of transmission that is capable of receiving as well as transmitting signals and located at a random position. The main question one tries to address here is how the global connectivity can be established in such a network. Depending on the value of the range there exists a critical density of phones or Lily pads where the long-range correlation first sets in. It is well-known that in continuum percolation the nature of the phase transition is continuous and the model belongs to the universality class of ordinary percolation [30, 71].

1.4.5 Percolation on Networks

Many real-world systems do not have regular structures as the lattice geometries, for examples, the World Wide Web [72, 73], food webs [74], electrical power grids [75], etc., called *networks*. A network consists of a set of *nodes* and *links* connecting the nodes (Fig. 1.10). Sometimes the links are also referred as *edges*. In general, a node may be connected with many other nodes via links whose number may vary from node to node. The number k of links associated with a given node is called its *degree*. Essentially, a network is characterized by its degree distribution $D(k)$, that a randomly selected node has the degree k. A wide variety of real-world networks (mentioned above) exhibit a power-law degree distribution [76]:

$$D(k) \sim k^{-\lambda}, \tag{1.21}$$

where λ is the degree distribution exponent. Such networks are called *scale-free networks*.

Probably, the most simplest model of a growing network is the random graph model introduced by Erdös and Rényi (ER) [77], where starting from a set of isolated nodes N, the links are added sequentially between a pair of randomly selected nodes. At any arbitrary stage, the number of links per nodes in the network is represented by p. As p is increased, the size of the cluster of nodes interconnected through the links increases, and at a critical value of $p = p_c$, a continuous transition occurs signaled by the emergence of a *giant cluster* in the network. It is to be noted that for sufficiently large N the degree distribution of the network is Poissonian [76].

Percolation transition has also been studied on the scale-free networks. Expectedly, a strong dependence of λ [Eq. (1.21)] on the percolation threshold of the network is observed [78–81]. The percolation threshold assumes a finite value for $3 < \lambda < 4$, whereas for $2 < \lambda < 3$ such a percolation transition is absent [79]. More interestingly, different sets of non-trivial critical exponents are found for different regimes of λ [79].

1.4.6 Explosive Percolation

Over several decades after its introduction in 1957, many different variants of percolation model have been introduced. Continuity in the variation of the order parameter curve around the transition point is the basic characteristic of all these models. Therefore, the percolation transition is believed to be one of the most robust continuous transition. However, recently, Achlioptas, D′Souza, and Spencer suggested that a discontinuous transition may be possible in a model of percolation called explosive percolation (EP) [82]. Introducing a competition between a pair of randomly selected vacant edges and occupying the optimal one for the formation of a network leads to a sudden change in the value of the order parameter. The detailed description of the model has been given in the following paragraph.

A slight modification in the formation process of the Erdös-Rényi (ER) network

model describes the original model of EP. One starts with N isolated nodes and then links between pairs of nodes are added sequentially by following an additional predefined rule in the ER model [82]. The formation of a network in this manner is referred as Achlioptas process. Specifically, in each step, instead of selecting one edge as in the ER model, a pair of vacant edges is selected randomly and independently to each other. However, only one of them, which produces a smaller size of cluster, is finally added to the growing network and the other one is discarded. This local modification in the growth procedure of ER significantly changes the percolation properties of the network.

The competition between the edges can be introduced using the product rule [82] as mentioned here. Let s_i, s_j and s_k, s_l are the sizes of the cluster at the ends of the selected two edges between the nodes (i, j) and (k, l), respectively. Now, according to the product rule the link between (i, j) is added to the network if $s_i s_j < s_k s_l$, otherwise (k, l) is added. At any arbitrary stage, the number of existing links per nodes is denoted by p. Clearly, by following this mechanism the clusters of small sizes grow preferentially than the large size clusters. Moreover, this suppresses the growth of the largest cluster and as a consequence, the percolation transition is retarded. For p just below the transition point p_c, moderately large-size clusters are abundant in EP [83], unlike the case of ordinary percolation where the largest cluster is significantly bigger in size than that of the second largest cluster. Coexistence of these similar size clusters raises the question about the existence of a unique largest cluster [84]. Addition of a single link merges such large-size clusters and a giant cluster is formed, leading to an abrupt rise in the order parameter curve at the percolation threshold. This led them to claim that EP model exhibits discontinuous transition [82]. The value of p_c has been found to be 0.888449(2) [85] compared to 1/2 for ER Random graph.

Expectedly, this triggered a burst of activity and attracted a great deal of interest in the physics communities in the field of percolation. Subsequently, a series of research papers appeared attempting to explain the nature of transitions in the models of explosive percolation introducing various rules including its generalization [86–91]. However,

ambiguity in the reported results for the order of transition in EP demanded more careful research. Costa *et al.* first raised the controversy about the order of transition by claiming that a model where small-size clusters grow more preferentially than in the original EP undergoes a continuous transition at the percolation threshold [92]. In this model, node i is selected between a pair of randomly chosen nodes (i, j), if $s_i < s_j$, otherwise j is selected. Similarly, another node is selected from a different pair of nodes (k, l). Finally, a link is placed between these selected nodes. Accordingly, the network grows and the percolation transition occurs at $p_c = 0.923207508(2)$. This implies that the transition in the original EP must be continuous.

Subsequently, evidences from extensive numerical simulations also established that the original EP model although shows a very sharp change in the order parameter for finite size systems and therefore appears like discontinuous transition, it indeed exhibits continuous transition in the asymptotic limit of very large system sizes [83, 85]. Grassberger *et al.* observed a bimodal distribution for the order parameter at the percolation threshold for finite size system. However, the distance between its peaks is observed to decrease as a power-law with system size N leading to a continuous transition in the limit $N \to \infty$ [85]. Later Riordan and Warnke rigorously proved that EP under Achlioptas processes exhibit continuous transition in the asymptotic limit [93, 94]. They argued that depending on the rule for selecting a single link from a finite number of randomly chosen vacant edges and its addition in the network always leads to a continuous transition. However, a discontinuous transition is possible when it is selected from the entire set of vacant edges [90, 93].

Further, EP model has also been studied on scale-free networks [87, 95, 96] and real-world networks [97]. The EP transition under Achlioptas process with the product rule on different lattice geometries is found to have unusual finite-size scaling behavior [85, 98]. However, no concrete claims have been made for its order of transition. Only recently, two models have been proposed on lattice, namely, the 'Gaussian model' [99, 100] and the 'spanning-cluster-avoiding model' [101], and shown that the models undergo

discontinuous percolation transitions.

1.4.7 Directed Percolation

In the case of bond percolation, the spreading of a liquid can take place isotropically in all possible directions through a set of occupied bonds representing channels. A special variant of this model is the situation where a preferred direction is considered for this propagation. Such a scenario resembles the flow of the liquid through a porous medium under gravity. This particular model is known as the directed percolation (DP) and was introduced in 1957 by Broadbent and Hammersley [1].

The model of DP can be described simply on an oriented square lattice where a preferred direction, say the downward direction, is assigned with every occupied lattice bond between a pair of nearest neighbor sites. The bonds act as valves and consequently, a bond restricts the flow along the direction opposite to the direction associated with it [102, 103]. More explicitly, on this lattice geometry a liquid can spread from a site to its only two nearest neighbors situated at the down-left and down-right directions. Evidently, at any arbitrary configuration of occupied bonds, the cluster of sites that can be reachable from a given site by following the directions in DP is a subset of the cluster of sites corresponding to the ordinary percolation.

Accordingly, in DP the clusters grow in size as the density of connected bonds is increased and at a critical value of the bond density long-range correlations first set in. The system undergoes a continuous transition at this point. Due to the imposed direction in the DP model, the long-range correlations that appear at the transition point are not invariant under rotation. As a consequence, two distinctly different correlation length exponents are obtained in two mutually perpendicular directions. Expectedly, the DP model exhibits different universal critical behavior compared to the ordinary percolation [103].

It has been observed that a wide variety of apparently unrelated non-equilibrium systems exhibit the universal critical behavior of DP. Probably, the most common

example of this type of non-equilibrium phase transition is the *active-absorbing* phase transition, in which the system remains in a completely frozen state with no activity at all till a critical value of the control variable is reached [103, 104]. Because of this, the DP is now regarded as the fundamental model for non-equilibrium phase transitions.

1.5 Random Sequential Adsorption

Adsorption is a surface phenomenon which describes the attachment of objects in general onto a surface. The phenomenon of adsorption has applicability in many disciplines of science ranging from physics, biology to engineering including, wide variety of industrial applications. For example, adsorption plays a key role in the process of filtration where activated charcoals are usually used to absorb poisonous gas particles and thus, allowing the purified air to pass through [105]. Adsorption of micron and submicron size colloidal particles on surfaces is another area of great practical importance, as it is the underlying mechanism of the thin films formation for a variety of technological devices, such as photonic crystals, quantum dots, etc., which are generally used for surface coatings and encapsulations [105–113].

Often the adsorption occurs irreversibly and subject to a certain constraint, for instance, adsorption of proteins on the biological membranes [105]. The model of random sequential adsorption (RSA) is known to be the basic model in the field of statistical physics which provides useful theoretical insights about the kinetics of adsorption involved with such irreversible adsorption processes and has been studied quite intensively over the last several decades [114–116]. It was Flory who first introduced a one-dimensional version of RSA to study the interaction among the pendant groups along a linear polymer chain [117]. Subsequently, this model was popularized by Rényi [118] and Feder [119] in the statistical physics community, when it had been realized that the model has ingredients to exhibit the universal features of critical phenomena.

In RSA, the objects are adsorbed sequentially and irreversibly at randomly selected vacant positions on a surface, subject to a constraint that they can not overlap with any previously adsorbed objects. Such interactions among the objects are termed as the excluded volume interaction. In the simplest case, these objects are considered to be inherently immobile, i.e., they can not move out from their position of adsorption [105, 106, 113]. The kinetics of adsorption continues till a jamming state is reached, where no more objects can be adsorbed. Essentially, the structure of the jamming state is very non-trivial and this attracted considerable attention to the scientific community to study many aspects of the model, e.g., the role of the object shape, object size, mechanisms of adsorption, etc. [105, 113, 120–127]. In Chapter 5 of this thesis we introduce a RSA model and describe in greater detail how the properties of the structure depend on the mechanism of relaxation.

1.6 Plan of the Thesis

In the previous sections we have briefly reviewed the literature of percolation, discussed a few variants of percolation models and described percolation as a paradigm of random disordered systems. Furthermore, we have described percolation as a fundamental problem of critical phenomena. In the next four Chapters, we present our study on how the percolation properties of a system are affected by different sources of disorder which influences the small-scale connectivity. In Chapter 2, we study the percolation transitions using a collection of disks with non-uniform radii. We further extend this study by considering an explicit time variation of the disks radii in Chapter 3. In Chapter 4, we generalize the well-known model of AB percolation and examine the percolation properties of the system. In Chapter 5, we investigate the role of relaxation dynamics in a model of random sequential adsorption on the percolation and jamming transitions.

Chapter 2

Percolation Model with an Additional Source of Disorder

2.1 Introduction

In the previous Chapter, we have already described that the percolation transition is signaled by the emergence of long-range correlation and therefore, the system exhibits large-scale connectivity beyond the transition point. In this Chapter [1], we introduce a variant of the percolation model with two different sources of disorder and investigate how these disorders affect the percolation properties of the system. This model may be applicable in the context of wireless sensor networks.

The wireless sensor networks (WSNs) [26, 128] consist of a collection of sensor nodes which are usually deployed in a manner that resembles a regular topology in the form of a grid. The WSNs are commonly used for monitoring various environmental conditions, such as temperature, pressure, humidity, etc. Each sensor node in a WSN may connect to several other nodes and forwards the collected data when the wireless transmission ranges of these sensor nodes overlap. The storage capacities of the sensor nodes are finite and hence it is important to ensure that each sensor can send the

[1]The work reported here is based on the paper "Percolation model with an additional source of disorder", **Sumanta Kundu**, and S. S. Manna, Phys. Rev. E **93**, 062133 (2016).

accumulated data to a base station, otherwise the data packets would be lost. This is often achieved using a multihop radio link connecting the node and the base station through a set of intermediate nodes. In other words, a node can forward the data packets to a base station only when both of them become part of a percolating cluster through the overlapping ranges of transmission of the intermediate nodes.

The transmission range of each sensor node is approximately circular. However, these circular ranges are not uniform in reality. They are affected by temperature variations in the air, obstruction due to the solid objects, and even humidity differences in the environment. Therefore, they are spatially heterogeneous, i.e., they differ from one place to another. So the question is how such spatial heterogeneities in the ranges of transmission affect in establishing the global connectivity in the network. In order to investigate that, we introduce a percolation model using a collection of circular disks with uniformly distributed radii positioned randomly at the sites of a regular lattice. More precisely, by drawing a random value R for the radius of a disk from a uniform distribution $p(R)$, the disk is placed at a randomly selected position centered at the site of a square lattice. Thus the system is spatially heterogeneous mimicking the varying ranges of transmission of the sensor nodes, as these ranges may be compared with the radii of the disks. A bond between a pair of disks is defined to be connected if the radii R_1 and R_2 of the disks at the two ends of the bond satisfy certain predefined rule. Most generally, one divides the whole R_1-R_2 plane into two regions by a closed curve; any point within only one region corresponds to a connected bond. Clearly, there is an additional source of disorder in this model apart from the disorder originated from the random occupation of lattice sites, as in the case of site percolation. Here, based on our publication [35], we have studied the percolation properties of the system by tuning the parameters of the model.

The organization of the Chapter is as follows. We start by describing our model and the method of analysis in Sec. 2.2. We present the percolation properties of the system using three different rules for a bond to be defined as connected, namely, sum

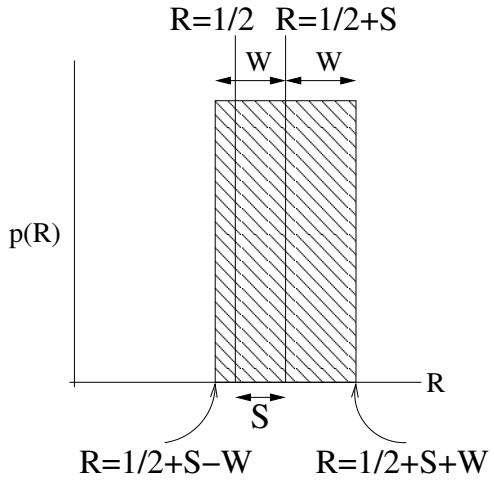

Figure 2.1: A sketch of the two parameters (S, W) uniform rectangular distribution $p(R)$ of the radii R of circular disks. The center of the distribution has been shifted at $R = 1/2 + S$ and it has the width W on both sides of this point.

rule, product rule, and circular rule in Secs. 2.3, 2.4 and Sec. 2.5, respectively. The variation of the bond density with the density of occupied sites has been described in Sec. 2.6. Percolation transition on a fully occupied lattice using uniformly distributed radii of the disks has been described in Sec. 2.7. Finally, we summarize in Sec. 2.8.

2.2 Model and Algorithm

The sites of an initially empty square lattice of size $L \times L$ with periodic boundary conditions are occupied randomly using circular disks of random radii values R. The values of the radii are drawn from a uniform rectangular distribution $p(R)$ of half width W and the center at $R = 1/2 + S$, where S measures the amount of shift of the center of rectangular distribution from $R = 1/2$ (Fig. 2.1). For the simulation, at every step an arbitrary vacant site is randomly selected and then, the center of a disk is placed at this particular site by drawing a random value from the probability distribution $p(R)$ for its radius. Precisely, a random number $r \in \{0, 1\}$ from a uniform distribution is assigned at each lattice site to calculate $R = 1/2 + S + (2r - 1)W$. Clearly, the random occupation of lattice sites is the first source of randomness and the second

source of randomness is introduced through the radii of the disks. In this prescription, a bond is defined to be connected if and only if the radii R_1 and R_2 of disks situated at the two ends of the bond satisfy a certain predefined rule; otherwise it is declared as unconnected. In a general formulation, such a rule is defined on the R_1-R_2 plane by dividing the whole plane into two different regions using an arbitrary closed curve. Any point within one region represents a connected bond, otherwise it is an unconnected one. Clearly, the density of connected bonds changes when the values of S and W are tuned and the global connectivity is determined only through the set of connected bonds. Here, based on our publication [35], we present the global connectivity properties of the system using three different rules for defining a bond to be connected.

To generate a single percolation configuration α with site occupation probability p, we start from an empty square lattice of size L and then drop pL^2 disks with random radii values, one by one, onto the randomly selected vacant sites. All four neighboring bonds of every occupied site are then tested for their possible status: connected or unconnected. Unlike the site percolation, when the four neighboring sites of a given occupied site are all occupied, the number of connected bonds associated with the center site may vary from 0 to 4. A set of occupied sites interlinked by these connected bonds forms a cluster. For any value of p, there exists at least one largest cluster whose size is denoted by $s_{max}(p, L)$ and the order parameter is defined by $\Omega(p, L) = \langle s_{max}(p, L)\rangle/L^2$ as described in Sec. 1.3.2.

The percolation threshold p_c of the system has been determined using the numerical method described in Sec. 1.2.1 in Chapter 1. The value of p, at which the largest cluster merges with the maximal of the second largest cluster and hence executes the maximal jump $\Delta_m s_{max}(p, L)$ in size [35, 36, 43], is recognized as the percolation threshold p_c^α for the particular configuration α. An average over many such independent configurations is considered as the percolation threshold $p_c(L) = \langle p_c^\alpha\rangle$ for the system size L. We repeat the entire calculations for different values of L and estimate the $p_c(L)$ values. Finally, the asymptotic value of p_c in the limit $L \to \infty$ is obtained by extrapolating $p_c(L)$

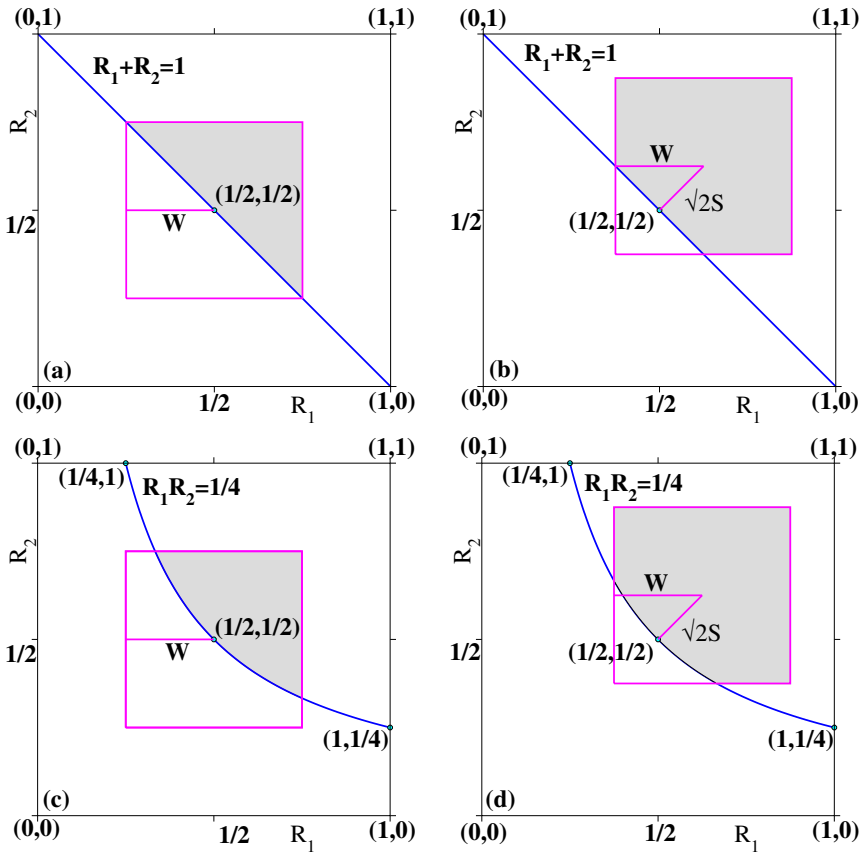

Figure 2.2: On the R_1-R_2 plane, for a specific set of values of $W = 1/4$ and S, the regions corresponding to the connected bonds (grey) and unconnected bonds (white) are indicated. For the sum rule (a) $S = 0$ and (b) $S = 1/8$ and for the product rule (c) $S = 0$ and (d) $S = 1/8$.

against $L^{-1/\nu}$ as given in Eq. (1.2), where the correlation length exponent $\nu = 4/3$ in two dimensions.

2.3 Sum Rule

A bond is declared as connected if and only if,

$$R_1 + R_2 \geqslant 1. \tag{2.1}$$

For a given pair of S and W, the points in the R_1-R_2 plane representing the occupied and vacant bonds, lie within a square box (Fig. 2.2). In Figs. 2.2(a) and (b) we exhibit

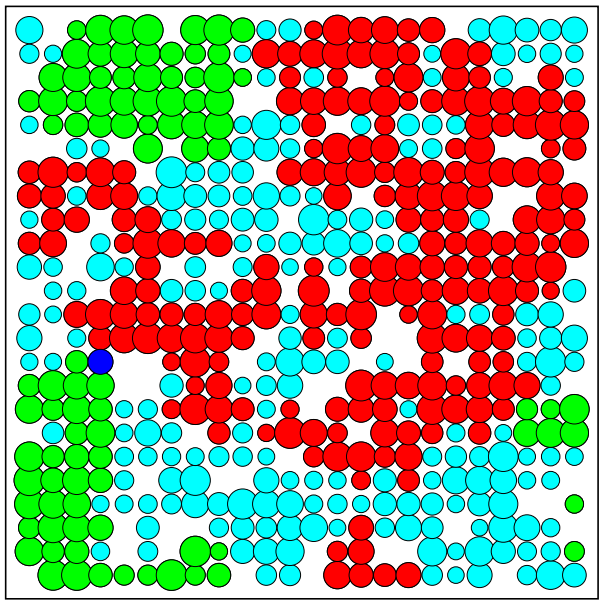

Figure 2.3: A typical percolation configuration of 501 circular disks has been shown on a square lattice of size $L = 24$ (with periodic boundary conditions) using the sum rule for $W = 0.15$, $S = 0$ and $p \approx 0.87$. The largest and the second largest clusters are of sizes 208 (red) and 90 (green), respectively. It exhibits a very specific situation where these two clusters merge due to the occupation of the blue disk and the maximal jump in the size of the largest cluster takes place. Disks at all other occupied sites are painted in cyan.

two specific cases with $S = 0$ and $1/8$, respectively, where W=1/4. We show a typical picture of a percolating configuration for the sum rule in Fig. 2.3.

According to this rule, for $S = 0$ and $W = 0$, the bond between any pair of neighboring occupied sites is connected. Therefore, $p_c(S = 0, W = 0) = p_c(\text{sq})$, where $p_c(\text{sq})$ is the site percolation threshold on square lattice. When $S = 0$ and $W > 0$, in spite of the fact that only half of the disks have radii larger than $1/2$, a global connectivity can still be achieved. The small size disks certainly contribute to the density of occupied sites but may or may not take part in the bond density. Consequently, the growth of the largest cluster is delayed and it takes the higher density of occupied sites to establish the global connectivity. This implies that $p_c(S = 0, W > 0) > p_c(\text{sq})$.

The asymptotic value of the percolation threshold has been estimated using the method described before. Plotting $p_c(L)$ against $L^{-1/\nu}$ with different trial values

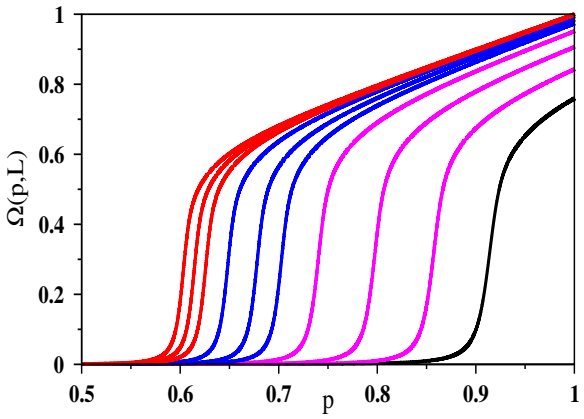

Figure 2.4: For the sum rule, the variation of the order parameter $\Omega(p, L)$ against the site occupation probability p has been plotted for $L = 512$ with red for $S = 0.03$ and $W = 0.04, 0.045, 0.05$; blue for $S = 0.02$ and $W = 0.04, 0.05, 0.06$; magenta for $S = 0.01$ and $W = 0.04, 0.2/3, 0.15$ and black for $S = 0$ and $W = 0.04$; the curves are arranged from left to right.

of ν on a lin-lin scale, the best fit of the data by a straight line is obtained using $\nu = 1/0.7502 \approx 1.333(5)$. Extrapolation of the fitted line in the limit $L \to \infty$ yields $p_c(S = 0, W > 0) \approx 0.9191(2)$. As the region corresponding to the connected bonds equals to the unconnected bonds (Fig. 2.2), the probability of finding a connected bond between two neighboring occupied sites is $1/2$ for all values of $W > 0$ and consequently, $p_c(S = 0, W > 0)$ is independent of W. Further, the average size of the largest cluster scaled by L^2 has been found to decay like $L^{-0.105}$ and this gives an estimate of $d_f = 1.895(5)$ compared to the exact value of $d_f = 91/48$ [6]. We also observed that the configuration averaged value of the maximal jump in the size of the largest cluster $\langle \Delta_m s_{max}(p_c, L) \rangle / L^2$ varies as $L^{-0.104}$. Equating the power to $d_f - 2$ one gets $d_f = 1.896(5)$. This clearly indicates that the largest cluster and the second largest cluster are fractal objects with the same fractal dimension d_f.

For different (S, W) pairs, the variation of the order parameter $\Omega(p, L)$ against the site occupation probability p has been exhibited in Fig. 2.4. Because of the small size disks, the value of $\Omega(p, L)$ converges in the limit of $p \to 1$ to a maximum value which is well below unity and depends on the precise values of the parameters S and W.

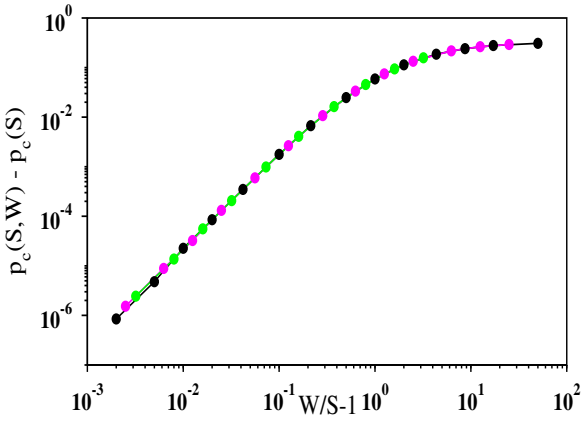

Figure 2.5: For the Sum Rule, the scaling plot of $p_c(S,W) - p_c(S)$ against $W/S - 1$ has been shown for $S = 0.1$ (green), 0.01 (magenta) and 0.001 (black). The values of $p_c(S)$ required to make the curves straight in the limit $W/S \to 1$ are 0.5927675, 0.5927684, and 0.5927662, respectively which are very close to $p_c(\text{sq})$. The slopes of the linear portions are 1.96, 1.93 and 1.94 respectively, giving $\zeta_S = 1.95(5)$.

For $S = 0$, the curve is independent of W. However, for a fixed non-zero value of S, the sharp rise in the order parameter curve shifts towards the higher values of p with increasing W, whereas for a fixed value of W, the curve shifts towards the smaller values of p with increasing the value of S.

For a given non-zero value of W, the region corresponding to the connected bonds [Fig. 2.2(a)] increases as $S > 0$ is increased and thus, the percolation threshold $p_c(S,W)$ decreases. Evidently, $p_c(S,W) = p_c(\text{sq})$ for $S \geqslant W$. For $0 < S < W$, the asymptotic values of $p_c(S,W)$ in the limit of $L \to \infty$ are calculated as before using Eq. (1.2). It appears that $p_c(S,W)$ for different values of S and W depends only on the ratio W/S. To investigate how the values of $p_c(S,W)$ approach the value $p_c(\text{sq})$ in the limit $W/S \to 1$, we performed a scaling analysis. Precisely, we plot the $p_c(S,W) - p_c(S)$ against the scaled variable $W/S - 1$ for three different values of S and for each S many W values and then tune the values of $p_c(S)$ to obtain a good data collapse as shown in Fig. 2.5. The curves for different S fit to a very nice straight line as $W/S - 1 \to 0$ indicating a scaling form

$$p_c(S,W) - p_c(S) \sim (W/S - 1)^{\zeta_S}, \tag{2.2}$$

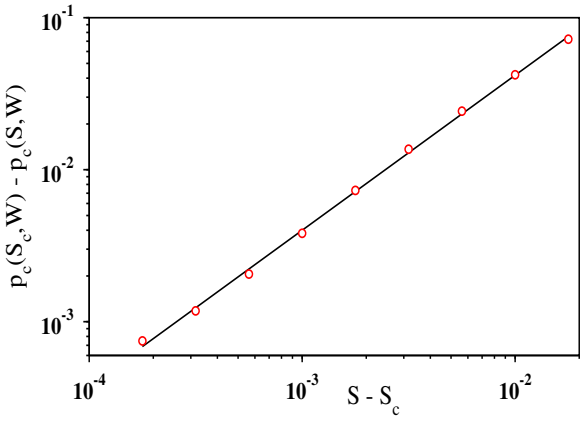

Figure 2.6: For the Sum Rule and for $S < 0$, the difference $p_c(S_c, W) - p_c(S, W)$ has been plotted against $S - S_c$ on a log-log scale for $W = 1/4$ with $p_c(S_c, W) = 1$ at $S_c = -0.0201(5)$. The resulting plot gives a straight line with slope $\eta_S = 1.02(3)$.

where we estimated $\zeta_S = 1.95(5)$. Expectedly, we find that the best tuned values of $p_c(S)$ are consistent with $p_c(\text{sq})$.

On the other hand, when S takes negative values and its absolute value is increased, the area in Fig. 2.2(a) representing the unconnected bonds increases, the connected are decreases and therefore, the percolation threshold increases. Clearly, for a given value of W there exists a specific threshold value of $S = S_c$ when the percolation threshold reaches unity, i.e., $p_c(S_c, W) = 1$. For $S < S_c$, the density of connected bonds is not sufficient to establish the global connectivity. Numerically, we estimated $S_c = -0.0201(5)$ for $W = 1/4$. It has been observed that the percolation threshold approaches unity as

$$p_c(S_c, W) - p_c(S, W) \sim (S - S_c)^{\eta_S}, \tag{2.3}$$

with $\eta_S = 1.02(3)$ (Fig. 2.6). For other W values $S_c(W)$ varies, but $S_c(W)/W$ remains constant.

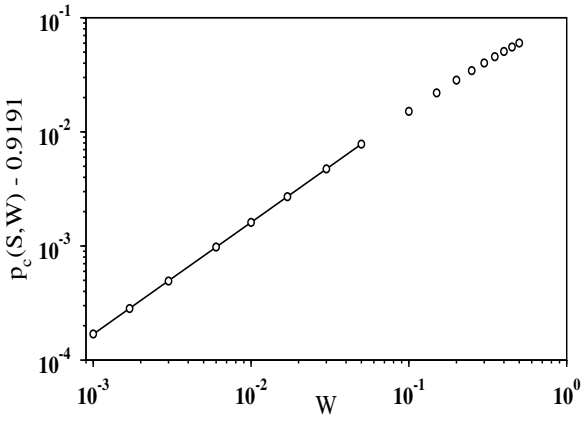

Figure 2.7: For the product rule and $S = 0$, the difference $p_c(S, W) - 0.9191$ of the percolation threshold has been plotted against the width parameter W using a log-log scale. The slope of the fitted straight line has been measured as 0.98(5).

2.4 Product Rule

A bond between a pair of neighboring disks is said to be connected only when the following condition is satisfied:

$$R_1 R_2 \geqslant 1/4. \tag{2.4}$$

The regions representing the connected and unconnected bonds determined by the product rule are shown in Figs. 2.2(c) and (d) for $S = 0$ and $1/8$, respectively, using $W = 1/4$.

It can be seen from the Fig. 2.2(c) that for $S = 0$, the probability of finding a connected bond decreases with increasing the value of W. Consequently, unlike the case of sum rule, the percolation threshold $p_c(S = 0, W > 0)$ increases with W. In the limit $W \to 0$, the percolation threshold $p_c(S = 0, W > 0)$ approaches a value 0.9191(2) (Fig. 2.7). This is because, the line $R_1 + R_2 = 1$ is the equation of the tangent to the curve $R_1 R_2 = 1/4$ at $W = 0$.

For a general value of $S > 0$, the order parameter $\Omega(p, L)$ plots are quite similar to those of the sum rule, but for same (S, W) pairs the $p_c(L)$ values are slightly larger. For $S > 0$, we find that a relation like in Eq. (2.2) is valid here as well. A scaling plot of $p_c(S, W) - p_c(S)$ against $W/S - 1$ gives a very nice data collapse (not shown)

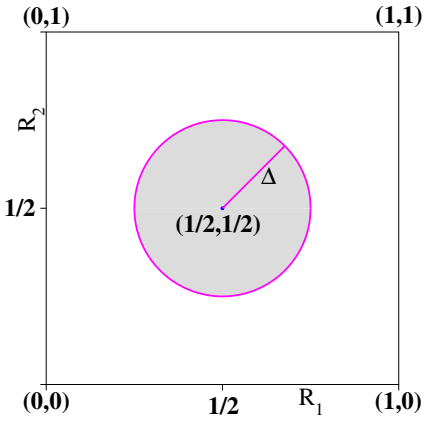

Figure 2.8: A circular region with radius Δ on the R_1-R_2 plane for $S = 0$ and $W = 1/2$. A point (R_1, R_2) representing the radii of the disks at the opposite ends of a bond, corresponds to a connected bond if the point lies inside the circle.

and we find $\zeta_P \approx 1.93(10)$. Further, shifting the value of S to the negative values, the percolation threshold increases and finally reaches unity at a specific value of $S = S_c$, i.e., $p_c(S_c, W) = 1$. We obtained $S_c = -0.0117(5)$ for $W = 1/4$. Similar to Eq. (2.3), the approach to this limit is again characterized by a power-law with exponent $\eta_P \approx 1$.

2.5 Circular Rule

Here a circular region, centered around the point $(1/2, 1/2)$ of radius Δ in the R_1-R_2 plane, is selected (Fig. 2.8). The radii R of the disks are again distributed by $p(R)$ but only $S = 0$ and $W = 1/2$ are used. The region inside the circle represents the connected bonds whereas, the outside region represents the unconnected bonds. Therefore, the condition for a bond to be declared as connected is

$$(R_1 - 1/2)^2 + (R_2 - 1/2)^2 \leqslant \Delta^2. \tag{2.5}$$

Evidently, the percolation threshold $p_c(\Delta, L)$ depends on the value of Δ. It has been observed that if the size of the circular region is too small, the size of the largest cluster becomes minuscule even when the site occupation probability $p = 1$. As the value of Δ

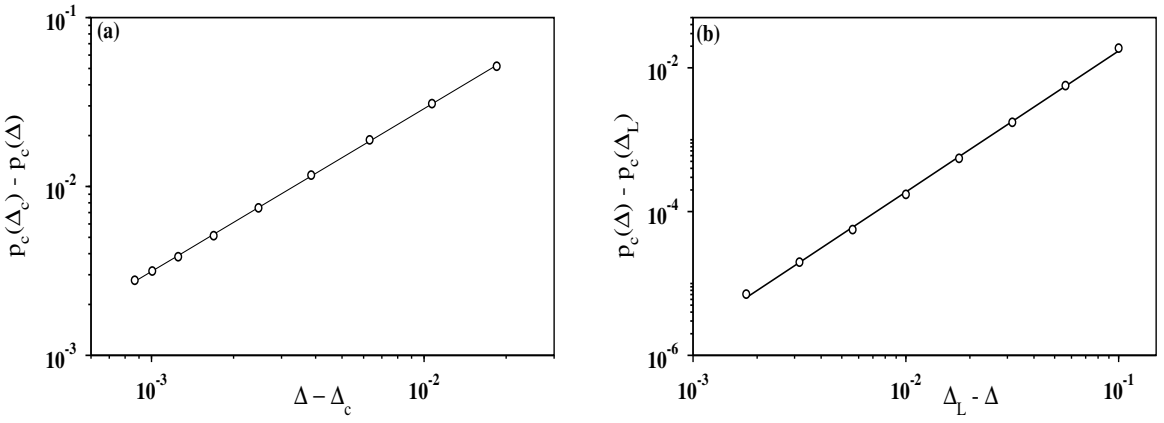

Figure 2.9: For the circular rule, (a) the differences of the percolation thresholds $p_c(\Delta)$ for different values of Δ from $p_c(\Delta_c) = 1$ at $\Delta_c = 0.3488(5)$ has been plotted on a log-log scale. The slope of the straight line is $\eta_C = 0.96(5)$. (b) The differences $p_c(\Delta) - p_c(\Delta_L)$ has been plotted against $\Delta_L - \Delta$ using $\Delta_L = 1/\sqrt{2}$ and $p_c(\Delta_L) = 0.59275371$ for the best fit. Clearly, $p_c(\Delta_L)$ is very close to $p_c(\text{sq})$. The fitted straight line has a slope $\zeta_C = 1.96(5)$.

is increased, more and more bonds appear in the system and eventually they contribute to the global. Consequently, there exists a threshold value of $\Delta = \Delta_c$ such that a percolation transition can occur only when $\Delta > \Delta_c$. Clearly, the percolation threshold at Δ_c is $p_c(\Delta_c) = 1$. As before, we observe that $p_c(\Delta_c) - p_c(\Delta)$ varies as $(\Delta - \Delta_c)^{\eta_C}$. The least-squares fit of the numerical data yields $\Delta_c = 0.3488(5)$ and $\eta_C = 0.96(5)$ [Fig. 2.9(a)]. Further, with increasing the value of Δ monotonically, the region of unconnected bonds continues to shrink and as a consequence, the percolation threshold $p_c(\Delta)$ decreases. Finally, $p_c(\Delta)$ approaches its limiting value $p_c(\text{sq})$ at $\Delta = \Delta_L = 1/\sqrt{2}$ when all points in the R_1-R_2 plane correspond to the connected bonds. We find that in the limit $\Delta \to \Delta_L$, the percolation threshold approaches $p_c(\text{sq})$ in the same way as in the case of sum rule and product rule. Precisely, our numerical data suggests that $p_c(\Delta) - p_c(\text{sq}) \sim (\Delta_L - \Delta)^{\zeta_C}$ with $\zeta_C = 1.95(5)$. Figure 2.9(b) demonstrates this clearly.

2.6 Variation of Site and Bond Densities

In the site percolation, the bond density grows with the site density as $q(p) = p^2$. In comparison, in our case, for any value of $W > 0$ this form is modulated by a function as $q(p) = \mathcal{H}(S, W)p^2$. For the sum rule,

$$\mathcal{H}(S,W) = \begin{cases} 1/2 + S/W - S^2/(2W^2) & \text{for} \quad S \geqslant 0, \\ 1/2 - S/W + S^2/(2W^2) & \text{for} \quad S \leqslant 0. \end{cases} \tag{2.6}$$

For the product rule, there exists a threshold value S_W, such that

$$4W^2\mathcal{H}(S,W) = \begin{cases} (S+W)^2 + (S+W) - \ln(1+2S+2W)/2 & \text{for} \quad S \leqslant S_W, \\ 4W^2 - (S-W)^2 - (S-W) + \ln(1+2S-2W)/2 & \text{for} \quad S \geqslant S_W, \end{cases} \tag{2.7}$$

where $S_W = [(1+4W^2)^{1/2} - 1]/2$. For the circular rule, the expression of $q(p)$ is very straightforward and is given by

$$q(p) = \pi\Delta^2 p^2. \tag{2.8}$$

Our numerically estimated values of $q(p)$ are in close agreement with these expressions.

2.6.1 Comparison with Site-Bond Percolation

Here, we compare our model with the site-bond percolation [57, 58], where lattice sites and bonds both are occupied randomly and independently. In this model, the global connectivity is determined through a sequence of alternating occupied sites and bonds, as described in Sec. 1.4.1. In comparison, in our model when two neighboring sites are occupied, the status of the bond between them either connected or unconnected is immediately determined, subject to the fulfillment of certain condition. Hence our model is somewhat a correlated bond percolation problem, where local correlations are

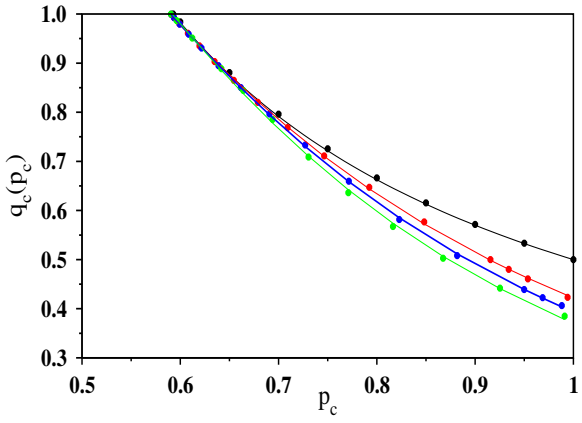

Figure 2.10: Critical values of the site p_c and the bond q_c occupation probabilities are plotted for the site-bond percolation [58] (black), sum rule (red), product rule (blue), and the circular rule (green). The solid lines are the best-fit forms given in Eq. (2.9).

present.

To show the difference between these two models with an enhanced clarity, let us consider a situation when the bond occupation probability is $q = 1/2$. For $S = 0$ and $W > 0$, our model simply gives $q = 1/2$, where the percolation threshold is found to be $p_c \approx 0.9191$. Clearly, this value is completely different from the site-bond percolation on square lattice, where $p_c = 1$ when q is set at $1/2$ [58].

Similar to the site-bond percolation, we construct a phase diagram as shown in Fig. 2.10. A critical curve in this phase diagram divides the entire phase space into two regions, namely, the percolating and the non-percolating regions. Therefore, every point on the phase boundary between the two regions signifies a critical point, represented by $[p_c, q_c(p_c)]$. The data for the site-bond percolation have been collected from [58]. For comparison, similar phase boundaries for our model using the sum, product and the circular rules have also been shown in the same plot. In general, all four phase boundaries are distinctly different, but they meet only at the point $[p_c(\text{sq}),1]$.

For the site-bond percolation, the functional form of the critical curve is $q_c(p_c) = B/(A + p_c)$ [58]. In the phase diagram, the black solid line represents this curve. For

our model, we have observed that a modified functional form

$$q_c(p_c) = B/(A + p_c^{\theta}) \tag{2.9}$$

fits the data very well. The best fit corresponds to $\theta = 2.41, 2.70$, and 2.81 for the sum, product and circular rules, respectively. For this analysis we have used $W = 1/4$ for the sum and product rules.

2.7 Percolation on a Fully Occupied Lattice

A very interesting special case of our model is the situation when all sites of the square lattice are occupied ($p = 1$) by disks of uniformly distributed radii $R \in \{0, R_0\}$. This is the only source of disorder present here. A related model in continuum percolation considers disks of randomly selected radii [129, 130]. In this version of the model, the parameter R_0 acts as a control variable similar to the site occupation probability p. Imposing periodic boundary condition along the horizontal direction and the open boundary condition along vertical direction, the set of connected bonds are determined by the sum rule. Clearly, for any value of $R_0 < 1/2$, the density of connected bonds is strictly zero. When R_0 is continuously increased, more and more bonds get connected. Consequently, the size of the largest cluster of sites interlinked by the connected bonds also increases and for a critical value of $R_0 = R_{0c}$, the largest cluster connects two opposite sides of the lattice through a spanning path across the system. Therefore, the system exhibits global connectivity only for $R_0 > R_{0c}$.

2.7.1 Spanning Probability and Order Parameter

The spanning probability $\Pi(R_0, L)$ is defined as the probability that an arbitrary percolation configuration has a cluster spanning between the top and the bottom boundaries of the lattice. In Fig. 2.11(a), we plot $\Pi(R_0, L)$ against R_0 for three different

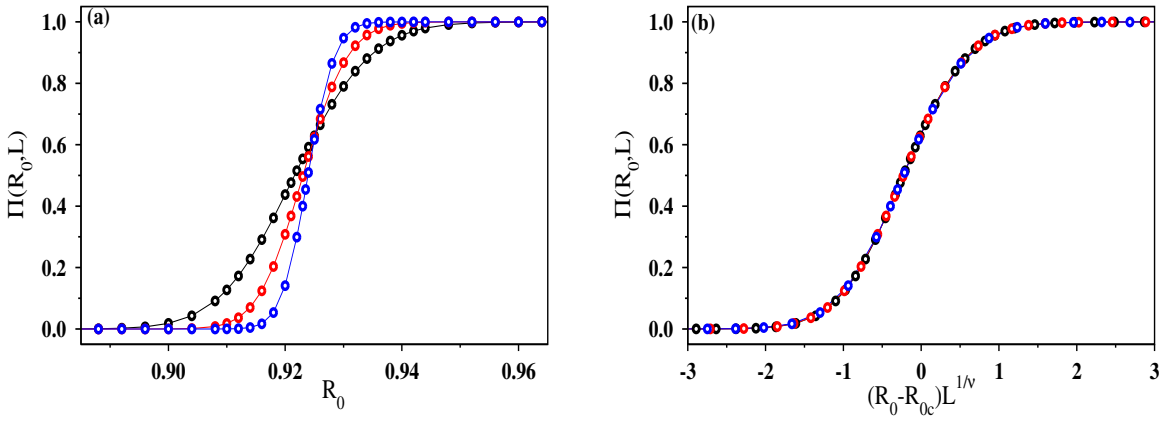

Figure 2.11: (a) Plot of the spanning probability $\Pi(R_0, L)$ against R_0 for the system sizes $L = 256$ (black), 512 (red), and 1024 (blue). (b) Finite-size scaling of the same data in (a) with $R_{0c} = 0.925$, $1/\nu = 0.75$ exhibits an excellent data collapse.

system sizes which meet at approximately same value of $R_0 = R_{0c} \approx 0.925(5)$. To estimate precisely the value of percolation threshold R_{0c}, we first calculate $R_{0c}(L)$ for individual system sizes using $\Pi[R_{0c}(L), L] = 1/2$ and then, the $R_{0c}(L)$ values are extrapolated in the limit $L \to \infty$ using an equation similar to Eq. (1.2) with $\nu = 4/3$. This gives an estimate of $R_{0c} = 0.925(5)$. A finite-size scaling analysis of $\Pi(R_0, L)$ has been done in Fig. 2.11(b). Plotting $\Pi(R_0, L)$ against the scaled variable $(R_0 - R_{0c})L^{1/\nu}$ with $1/\nu = 0.75$, we obtain an excellent data collapse for all three system sizes [Fig. 2.11(b)], indicating a finite-size scaling form

$$\Pi(R_0, L) \sim \mathcal{F}\Big[(R_0 - R_{0c})L^{1/\nu}\Big]. \tag{2.10}$$

In Fig. 2.12(a), we have plotted the order parameter $\Omega(R_0, L) = \langle s_{max}(R_0, L)\rangle$ against R_0. A similar finite-size scaling analysis has been performed for $\Omega(R_0, L)$ and we find that the usual scaling form as in Eq. (1.5)

$$\Omega(R_0, L) \sim L^{-\beta/\nu}\mathcal{G}\Big[(R_0 - R_{0c})L^{1/\nu}\Big] \tag{2.11}$$

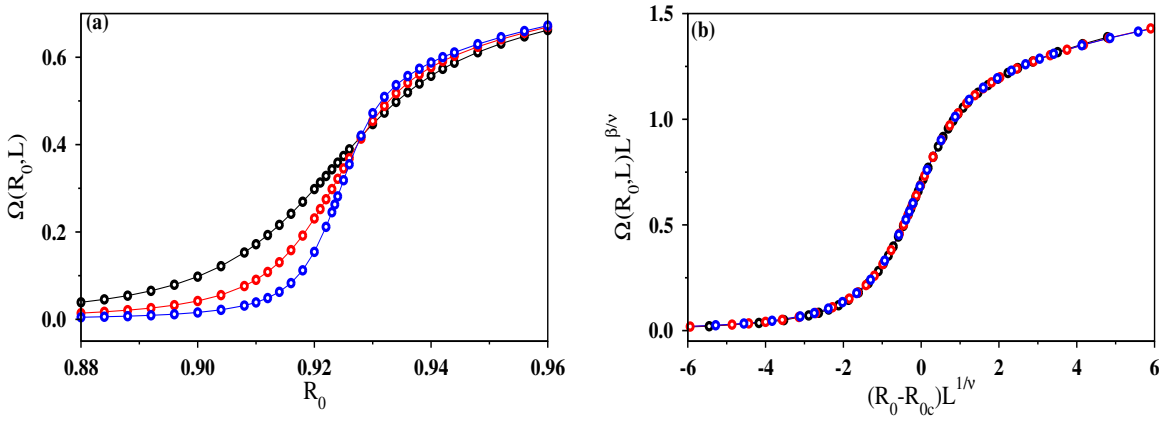

Figure 2.12: (a) Variation of the order parameter $\Omega(R_0, L))$ against R_0 for the system sizes $L = 256$ (black), 512 (red), and 1024 (blue). (b) Finite-size scaling plot of the same data using $R_{0c} = 0.925$, $1/\nu = 0.75$ and $\beta/\nu = 0.11$ exhibits a very nice data collapse.

works very well [Fig. 2.12(b)]. The exponents ν and β bears the same meaning as the ordinary percolation. Our best collapse of the data corresponds to $1/\nu = 0.75$ and $\beta/\nu = 0.110(5)$. Expectedly, these values are consistent with the exact values of the two dimensional percolation exponents $\nu = 4/3$ and $\beta = 5/36$, i.e., $\beta/\nu = 5/48 \approx 0.1042$ [6]. The entire set of calculation has been repeated using the product rule and the results are found to be very similar to those of the sum rule except $R_{0c} = 0.978(5)$.

2.8 Summary

Motivated by how the global connectivity is established in a wireless sensor network with non-uniform ranges of transmission of the sensor nodes, we have introduced and studied a model in the framework of percolation theory. Precisely, we have studied the global connectivity properties of a system using a collection of circular disks with uniformly distributed radii mimicking the non-uniform transmission ranges of the sensor nodes. Sites of a square lattice are occupied randomly by disks with probability p as in the site percolation and after occupying a given site, the center of a disk is assigned to the site by drawing a random value R from a uniform distribution for its radius.

Clearly, there exists two different sources of disorder in the model. According to this model, a bond between a pair of neighboring occupied sites is said to be connected if the disks with radii R_1 and R_2 situated at these sites fulfill certain condition. Such a condition is most generally described by dividing the whole R_1-R_2 plane into two regions by a closed curve of any arbitrary shape: points within one region correspond to the connected bonds, whereas the other region represents the unconnected bonds. The study of three different rules for the criterion of defining a connected bond under this general formulation always indicates that the percolation threshold varies continuously within $p_c(\text{sq}) \leqslant p_c \leqslant 1$. The nature of the percolation transition is continuous, but the approach of the percolation threshold to its two limiting values are characterized by two exponents ζ and η. These exponent values are found to be same (within error bars) for all three specific rules considered here. Moreover, our analysis even on a fully occupied lattice by disks with uniformly distributed radii $R \in \{0, R_0\}$ reveals that a percolation transition can occur by tuning the maximal radius R_0 of the disks. Estimation of different critical exponents lead us to conclude that our model exhibits universal features of the ordinary percolation transition and therefore, both the models belong to the same universality class.

Chapter 3

Double Transition in a Model of Oscillating Percolation

3.1 Introduction

Obtaining the large-scale connectivity is a matter of great importance in different scientific disciplines including physics, biology and several areas of communication systems. Inability to achieve such global connectivity might result in some serious effect on today's world, especially on human life. For instance, fatal consequences can occur due to any sudden interruptions during aviation communication which is extremely important for pilots and crews to be in touch with other flights and air traffic controllers. The disorder in the ranges of transmitters and receivers associated with this kind of electronic communication systems often causes such interruptions. In the previous Chapter, we have discussed how the spatial heterogeneity in these ranges affects the global connectivity properties of the system. Additionally, effect of temporal fluctuations of the transmission ranges on the connectivity in large-scale has been studied in detail in this Chapter [1].

Most commonly, wireless sensor networks (WSNs) [26] are used for such communi-

[1]The work reported here is based on the paper "Double transition in a model of oscillating percolation", **Sumanta Kundu**, A. Datta, and S. S. Manna, Phys. Rev. E **96**, 032126 (2017).

cation purposes. As described in the previous Chapter, every sensor node in a WSN receives, stores and transmits the data packets wirelessly. Hence a sensor node can forward the data packets to another node situated at a far apart distance through overlapping radio transmission ranges of intermediate nodes. Moreover, such multi-hop relaying enables the low power and limited storage capacity sensor nodes to connect with the base station where the collected data packets are finally aggregated. It is well-known that the transmission ranges of the sensor nodes fluctuate temporally due to noise and interference [131–133]. As a result, the communication between a node and the base station through a multi-hop path may be interrupted. Since each sensor node has very little buffer space and packets that cannot be immediately transmitted are usually dropped, it is therefore important to know when such a path exists enabling the node to forward its packets to the base station without any need for buffering the packets in intermediate nodes. In reality, such temporal variations exist in above-ground [132, 133], above-ground to underground [134] and aerial-sensor networks [135]. The speed of variation of these transmission ranges is usually much slower compared to radio transmission speed and hence a multi-hop path persists for a long enough duration for transmitting packets in a WSN.

Here, based on our publication [128], we introduce and study a percolation model which provides useful theoretical insights about how the global connectivity can be achieved in the presence of such time-varying transmission ranges in a WSN. In particular, our goal is to find the ranges in the values of the model parameters within which an uninterrupted global transmission of information can be ensured. In the model, the sites of a regular square lattice are occupied by circular disks of time-varying radii $R(t)$ which pulsate sinusoidally. This scenario mimics the temporal variations of the transmission ranges of the sensor nodes as these ranges may be compared with the radii of the disks. The disks start pulsating with initial random phase angles which makes the system heterogeneous. A lattice bond is defined as connected if and only if the disks at the two ends of the bond overlap. Accordingly, as the system evolves with time

the configuration of connected bonds changes and due to initial random phase angles different bonds remain connected for different durations of time. In general, sometimes the bond configuration connects the two opposite sides of the system through a spanning path and sometimes does not. Thus, the system oscillates between percolating and non-percolating phases with time. The duration of time the system remains in the percolating phase is dependent on the value R_0 of the maximal radii of the disks and thus, R_0 acts as the control variable in the model. In the time-averaged description, the system always exhibits a global connectivity through the set of connected bonds when R_0 exceeds a critical value R_{0c} in the limit of asymptotically large system. A consideration of propagation of information with infinite speed within a cluster lead us to identify two distinct transition points. Clearly, in the regime $R_0 > R_{0c}$ information transmits instantly through the entire system. More interestingly, global propagation of information is even possible for $R_0 < R_{0c}$, where there exists only isolated finite-size clusters and a finite amount of time is required for the information propagation. This time increases as R_0 is decreased and diverges as $R_0 \to R_0^*$. At this point the system undergoes another percolation transition. The critical behavior of the system at both the transition points have been studied here throughly. This study may also be relevant in the context of disease spreading in a population in the form of an epidemic, spreading of computer viruses through the Internet, and even for rumor spreading in the social media, etc.

The organization of this Chapter is as follows. We start by describing the model of oscillating percolation in Sec. 3.2. The variation of the order parameter and the spanning probability are described in Sec. 3.3. In Sec. 3.4, we discuss the dependence of the percolation properties on the frequencies of the pulsating disks. In Sec. 3.5, we have observed the existence of a second percolation transition point defined in terms of two time scales for the speed of information propagation through a series of finite-size clusters of connected bonds. In Sec. 3.6, we discuss the role of a shift parameter on the percolation transitions. A phase diagram is constructed by generalizing the model in

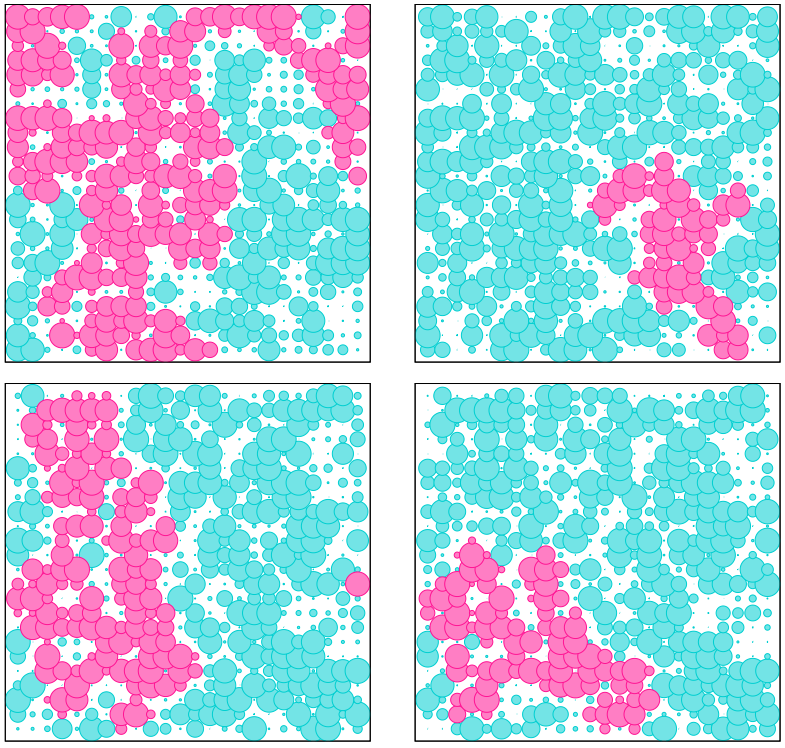

Figure 3.1: Snapshots of the time dependent percolation configuration have been shown on a square lattice of size $L = 24$ with periodic boundary conditions along the horizontal direction. The radii of all the disks having angular frequency $\omega = 1$ pulsate with time as per Eq. (3.1) and are different at a given time t due to the random initial phases $\{\phi\}$. For $R_0 = 0.85$, the snapshots are taken at $t = 150dt, 300dt, 500dt$ and $600dt$ (clockwise from top-left corner), where $dt = \pi/L^2$. The largest cluster painted in magenta sometimes spans the entire lattice and sometimes does not.

Sec. 3.7. Finally, we summarize in Sec. 3.8.

3.2 Model

Every site of a regular square lattice of size $L \times L$ with unit lattice constant is assigned a circular disk of radius $R(t)$ that varies with time t. For simplicity, we consider a periodic variation of the radii of the disks. The radii varies in a sinusoidal manner as

$$R(t) = (R_0/2)[\sin(\omega t + \phi) + 1], \tag{3.1}$$

where R_0 is the maximal radius of a disk; ϕ and ω are the two parameters which denote the phase angle and the angular frequency, respectively. Therefore, R_0 is the only control variable of the model and its value is tuned in the range between $[0, 1]$. Initiall a phase angle is associated with every lattice site by drawing its value randomly from a uniform probability distribution $p(\phi) = 1/2\pi$, $0 \leqslant \phi < 2\pi$ and accordingly, a disk of radius $R(0)$ calculated using Eq. (3.1) at time $t = 0$ is placed with its center at the site. The disorder in phase angles which has been mentioned here is specifically quenched disorder. With this only source of randomness, the radii of the disks start pulsating between $[0, R_0]$ according to Eq. (3.1) and as a consequence, the disks configuration evolves with time in a completely deterministic fashion. A periodic boundary condition has been imposed along the horizontal direction and an open boundary condition along the vertical direction.

Overlapping of the nearest neighbor disks is considered as the criteria for determining the set of connected bonds at any particular instant of time t. Since the lattice constant is unity, for a connected bond between a pair of neighboring disks of radii $R_1(t)$ and $R_2(t)$ the condition

$$R_1(t) + R_2(t) \geqslant 1, \tag{3.2}$$

must be satisfied. This is referred as the 'sum rule'. The bonds which do not satisfy Eq. (3.2) are unconnected bonds. Due to the periodic nature of the time evolution of the disks the connection status (i.e., connected / unconnected) of every bond over a period $T = 2\pi/\omega$ would be repeated *ad infinitum*. Evidently, the bond configurations at two successive time steps are correlated. Typically, a bond remains connected state for a certain interval of time and then in the unconnected state. At a given instant of time, there exist several clusters of sites interlinked through the connected bonds. These clusters are of various different shapes and sizes. Depending on the value of R_0, during the time evolution the largest one among these clusters sometimes spans between two opposite boundaries of the lattice and therefore establishes global connectivity,

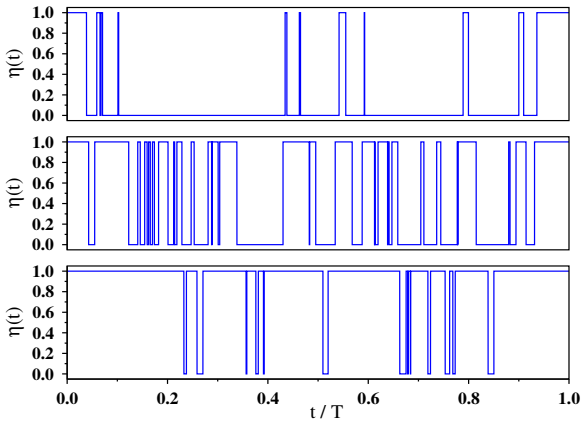

Figure 3.2: For $\omega = 1$ and $L = 128$, the phase representing variable $\eta(t)$ has been plotted with t during a period T for $R_0 = 0.88$, 0.90 and 0.92 (from top to bottom). The value of $\eta(t) = 1$ and 0 correspond to the percolating and non-percolating phases, respectively.

and sometimes does not. In Fig. 3.1, we demonstrate this using the snapshots of the percolation configurations taken at four different instants of time for a fixed value of R_0. Therefore, within one period of time T, the system in general switches between the percolating and non-percolating phases. We define a flag $\eta(t)$ =1 and 0 for the percolating and non-percolating phases, respectively, and its variation is exhibited in Fig. 3.2. On increasing the value of R_0, more and more bonds would be connected for more longer duration of time and consequently, the average residence time in percolating phase increases with R_0. To estimate how much the disk configuration becomes different from its initial configuration in time t we define a hamming distance $\Delta(t) = \max\{|R_i(t) - R_i(0)|\}$ calculated over all sites i. For a given time t, the quantity $|R_i(t) - R_i(0)|$ differs from site to site due to initial random phase angles and has a functional form $R_0 \cos(\omega t/2 + \phi) \sin(\omega t/2)$. Maximizing this quantity with respect to ϕ finally yields $\Delta(t) = R_0 \sin(\pi t/T)$.

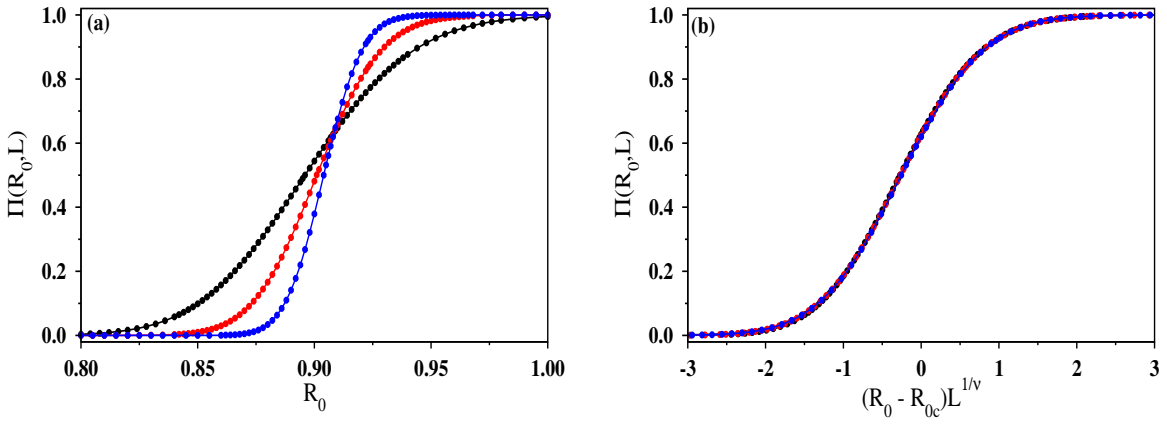

Figure 3.3: For $\omega = 1$, and the system sizes $L = 64$ (black), 128 (red), and 256 (blue) (arranged from left to right). (a) The spanning probability $\Pi(R_0, L)$ has been plotted against R_0. (b) Finite-size scaling plot of the same data with $R_{0c} = 0.908(5)$ and $1/\nu = 0.75$ exhibits a very nice data collapse.

3.3 Order Parameter and Spanning Probability

The order parameter $\Omega(R_0, L)$ is defined as the average size of the largest cluster scaled by L^2. In this problem, it is doubly averaged with respect to time between 0 and T and over many initial configurations $\mathcal{C}$ characterized by different sets of random phase angles $\{\phi_i\}$. Therefore,

$$\Omega(R_0, L) = \langle\langle s_{max}(R_0, L)\rangle_T\rangle_{\mathcal{C}}/L^2. \tag{3.3}$$

We also calculate the probability of finding the system in the percolating state where there exists at least one cluster spanning between the top to the bottom of the lattice. This particular quantity is termed as the spanning probability $\Pi(R_0, L)$.

In numerical simulations, time is incremented in equal steps of $dt = T/(2L^2)$. Imposing periodic boundary conditions along the horizontal direction, the global connectivity is determined along the vertical direction. Therefore, the geometry of the system under study is essentially a cylinder. Both the quantities $\Omega(R_0, L)$ and $\Pi(R_0, L)$ are estimated for a large number of values of $1/2 < R_0 \leqslant 1$ with a minimum increment of $\Delta R_0 = 0.001$.

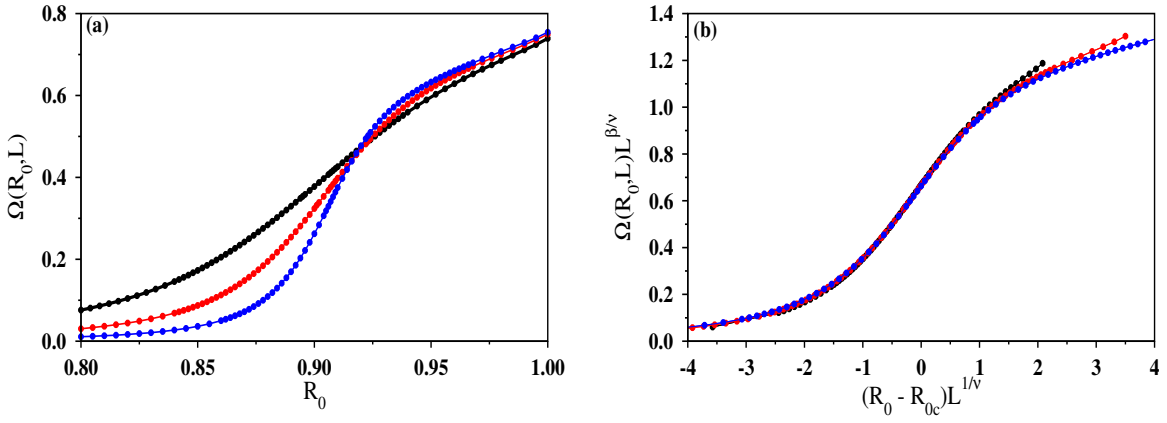

Figure 3.4: For $\omega = 1$, (a) variation of the order parameter $\Omega(R_0, L)$ as defined in Eq. (3.3) with R_0 has been shown for the system sizes $L = 64$ (black), 128 (red), and 256 (blue) (arranged from left to right); (b) finite-size scaling of the same data using $R_{0c} = 0.908(5)$, $1/\nu = 0.75$ and $\beta/\nu = 0.114(5)$ exhibits an excellent data collapse.

In Fig. 3.3(a), $\Pi(R_0, L)$ has been plotted against R_0 for three different system sizes using $\omega = 1$ for all disks. These curves intersect approximately at the point $[R_{0c}, \Pi(R_{0c})]$. By visual inspection we estimate $R_{0c} \approx 0.90$ and the spanning probability $\Pi(R_{0c}) \approx 0.63$ which is quite consistent with the value 0.636454001 [136] obtained using Cardy's formula [137]. For a more precise estimation of R_{0c} we define $R_{0c}(L)$ for individual system sizes by $\Pi[R_{0c}(L), L] = 1/2$. The $R_{0c}(L)$ values are estimated by linear interpolation of the data in Fig. 3.3(a) and then these values are extrapolated to $L \to \infty$ to obtain R_{0c}. Tuning the value of R_{0c} the difference $R_{0c} - R_{0c}(L)$ has been plotted against $L^{-1/\nu}$ and the best least-squares fitted straight line passes the origin closely for $R_{0c} = 0.908(5)$. Here we used $\nu = 4/3$, the correlation length exponent of the ordinary percolation. Further, a finite-size scaling analysis has been performed in Fig. 3.3(b), where we plot $\Pi(R_0, L)$ against $(R_0 - R_{0c})L^{1/\nu}$. An excellent data collapse for all three system sizes in Fig. 3.3(b) indicates the finite-size scaling form

$$\Pi(R_0, L) \sim \mathcal{G}\Big[(R_0 - R_{0c})L^{1/\nu}\Big]. \tag{3.4}$$

We repeat the whole set of analyses for the order parameter $\Omega(R_0, L)$. In Fig. 3.4(a),

we exhibit the variation of $\Omega(R_0, L)$ against R_0 for the same three system sizes and the corresponding finite-size scaling plot has been shown in Fig. 3.4(b). The collapse of data onto a single curve indicates the following scaling form

$$\Omega(R_0, L)L^{\beta/\nu} \sim \mathcal{F}\Big[(R_0 - R_{0c})L^{1/\nu}\Big]. \tag{3.5}$$

Our best data collapse corresponds to $\beta/\nu = 0.114(5)$ which is consistent (within error bar) with the exact value of $\beta/\nu = 5/48 \approx 0.1042$ with $\beta = 5/36$ [6] for the ordinary percolation.

3.4 Percolation with Distributed Frequencies

Now we consider the situation where each disk is randomly assigned a frequency ω_1 with probability f and frequency ω_2 with probability $1 - f$ with previously prescribed random phase angles. The time period $T_{(\omega_1,\omega_2)}$ has been calculated numerically for a large number of pairs of angular frequencies, where the frequencies are the rational numbers. Since for two rational numbers a/b and c/d, HCF$(a/b, c/d)$ = HCF(a, c) / LCM(b, d), HCF and LCM being the highest common factor and lowest common multiplier, respectively, we find the following functional form

$$T_{(\omega_1,\omega_2)} = 2\pi/\text{HCF}(\omega_1, \omega_2). \tag{3.6}$$

This is found to be independent of $0 < f < 1$. A generalized form of the above expression for T can further be given for the mixture of N distinct frequencies $\omega_1, \omega_2, ..., \omega_N$ as

$$T_{(\omega_1,\omega_2,...,\omega_N)} = 2\pi/\text{HCF}(\omega_1, \omega_2, ..., \omega_N). \tag{3.7}$$

Using the mixtures up to five distinct frequencies we numerically verified the above formula. For example, the time period has been estimated using the plot of $\Delta(t)$

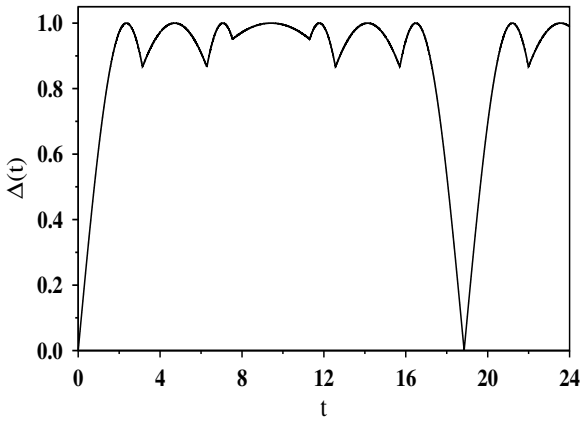

Figure 3.5: Plot of $\Delta(t)$ against t for $L = 64$, $R_0 = 1$ and for one initial configuration. The system is composed of three different types of disks characterized by their own frequencies: $\omega_1 = 1/3, \omega_2 = 2/3$ and $\omega_3 = 4/3$. Here, we find that the minimum value of $\Delta(t) = 2.96 \times 10^{-4}$ is at $t = 18.85$. The numerical estimate of $T = 18.85$ matches considerably well with the value of $T = 6\pi$ calculated using Eq. (3.7).

against t in Fig. 3.5 for three distinct frequencies. The value of $\Delta(t)$ close to zero for the first time for t sufficiently larger than zero indicates the re-occurrence of the initial configuration. We found that the transition point R_{0c} is not dependent on the frequencies ω_1 and ω_2 of the disks.

This model is further extended by assigning a distinct frequency to each disk drawing them from a uniform distribution $p(\omega)$ between [0,1]. In this case, T is very large and therefore we run the simulations up to a finite time $t = 10\pi$, in steps of $dt = 2\pi/(2L^2)$. Surprisingly, the transition point $R_{0c} = 0.908(5)$, the crossing probability ≈ 0.63 and the set of critical exponents remain unaltered within our numerical accuracy i.e., they do not depend on the actual number of distinct frequencies.

here we give an explanation for this frequency independence. Let $p(R)$ be the probability distribution of the radii of the disks. We argue that $p(R)$ is independent of time using Eq. (3.1). Introducing a variable $Q = \omega t$, the joint distribution function $p(Q, R)$ can be expressed in terms of the distribution functions of the two mutually independent variables Q and ϕ as, $p(Q, R) = p(\omega t)p(\phi)|J(Q, R)|$, where $J(Q, R)$ is the Jacobian of the transformation. This follows directly from the conservation of

probability. Finally, the marginal distribution of R is calculated from $p(Q, R)$ and has the form

$$p(R) = 1 \Big/ \left(\pi\sqrt{RR_0 - R^2}\right), \tag{3.8}$$

independent of the distribution of $p(\omega)$. Here we note that for a system having a uniform distribution of disk radii between $[0, R_0]$, the transition occurs at $R_{0c} = 0.925(5)$ [35]. The form of $p(R)$ in Eq. (3.8) has also been verified numerically and the matching is very good (not shown here). Using this equation one can calculate the probability for that a bond is connected. Neglecting local correlations and equating the bond formation probability to 1/2, the random bond percolation threshold on a square lattice, one obtains an approximate estimate of $R_{0c} = 1$.

3.5 The Second Percolation Transition

In this section we exhibit that a second percolation transition exists in terms of the passage time for information propagation. For this description we consider that information propagates with infinite speed within a cluster of connected bonds i.e., spreads instantly to all sites of the cluster irrespective of the site of its introduction. This implies that for $R_0 > R_{0c}$ there exists a spanning cluster across the system through which information can be transmitted at the same time instant from one side of the system to its opposite side. On the other hand, for $R_0 < R_{0c}$ there are finite isolated clusters of connected bonds which dynamically change their shapes and sizes.

Now we introduce the second mechanism for information propagation. We assume that the sites of an isolated informed cluster of connected bonds retain the information with themselves forever. In a latter time during the time evolution, this informed cluster may merge with another uninformed cluster and information would then propagate instantly to the sites of the new cluster. It is therefore apparent that if one waits long enough, may be several multiples of the time period T, it is likely that information would propagate through the system even when $R_0 < R_{0c}$. More elaborately, all sites

at the top row of the square lattice are given some information at time $t = 0$. This information is instantly transmitted to all sites of all clusters that have at least one site on the top row. All these sites are now informed sites and they keep the information with them. Since time is increased in steps of dt, at the next time step the status of every bond is freshly determined and some new sites (clusters) may get linked to these informed sites through a fresh set of connected bonds. Immediately, the information is transmitted again to all sites of all these clusters. In this way the information spreads to more and more sites of the entire lattice. Sometimes it may happen that the spreading process pauses for few time steps, though the status of different bonds are still changing. We assume that the spreading process terminates permanently when the information reaches the bottom of the lattice. The time required on average for this passage is denoted by $T_I(R_0, L)$. Since the average number of connected bonds in the system decreases when the value of R_0 is decreased, this average information passage time increases. Finally, $T_I(R_0, L)$ diverges when R_0 approaches R_0^* from above. Therefore, we recognize R_0^* as the second critical point of percolation transition.

All the bonds do not take part in the information propagation. Accordingly, we classify the whole set of bonds into two categories as described in the next subsection.

3.5.1 Live and Dead Bonds

Figure 3.6 illustrates that the phase difference $\Delta\phi = |\phi_2 - \phi_1|$ between the two pulsating disks at the ends of a bond plays a crucial role in determining the connectivity status of the bond. For $R_0 = 1/2$, the bond is connected only at a single instant within the time period T if the disks are in the same phase, whereas, for $R_0 = 1$ the bond remains always connected if the disks are in the opposite phase. This implies that for $1/2 < R_0 < 1$, a bond is connected within a period T only when the phase difference of the two end disks lies within a certain range. For a bond to be connected at least once during the whole time evolution, the maximum value of the sum $R_1(t) + R_2(t)$ must be

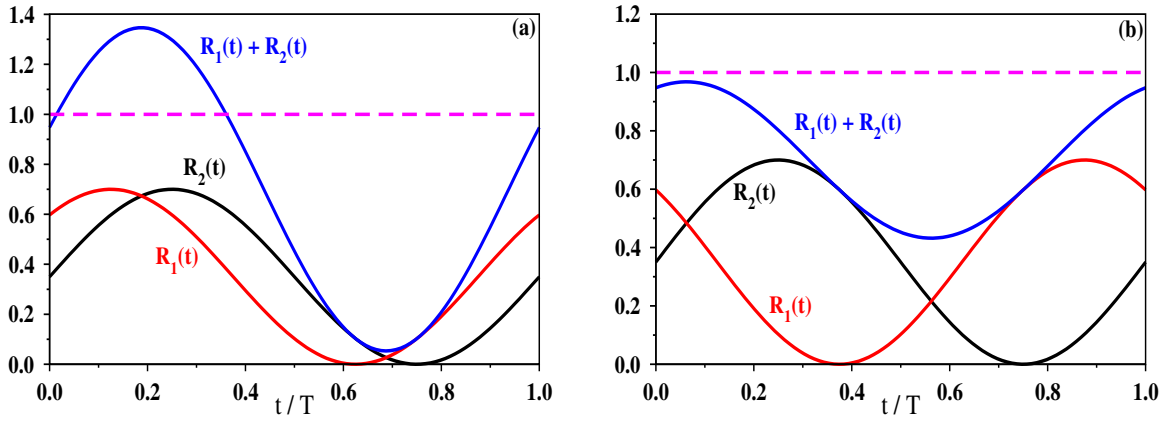

Figure 3.6: Schematic representation of the live and dead bonds. Using $R_0 = 0.7$ and $\omega = 1$, the time variations of the radii of the disks at the ends of a bond have been shown for two different values of the phase difference $\Delta\phi$. For $\Delta\phi = \pi/4$ (a), the bond is a live bond as it remains connected for a certain duration of time, whereas the bond with $\Delta\phi = 3\pi/4$ (b) is a dead bond.

greater than unity which gives

$$R_0[\cos(\Delta\phi/2) + 1] \geqslant 1. \tag{3.9}$$

This immediately implies that for a connected bond

$$\Delta\phi \leqslant \Delta\phi_c = 2\cos^{-1}\Big(1/R_0 - 1\Big). \tag{3.10}$$

This range increases with increasing the value of R_0.

Evidently, some bonds remain unconnected forever for which $\Delta\phi > \Delta\phi_c$. We call these bonds as the "dead" bonds. In contrast, the remaining set of bonds dynamically changes their connectivity status within a period T and are referred as the "live" bonds. Therefore, the sets of connected bonds that appear at different times during the time evolution are the subset of these live bonds. In general, at any instant of time the dead bonds co-exist with the live bonds and the corresponding bond densities are represented by p_d and p_l, respectively. Expectedly, p_d increases when R_0 is decreased from 1 and it approaches unity as $R_0 \to 1/2$. As the distribution of the phase angles $p(\phi)$ is uniform,

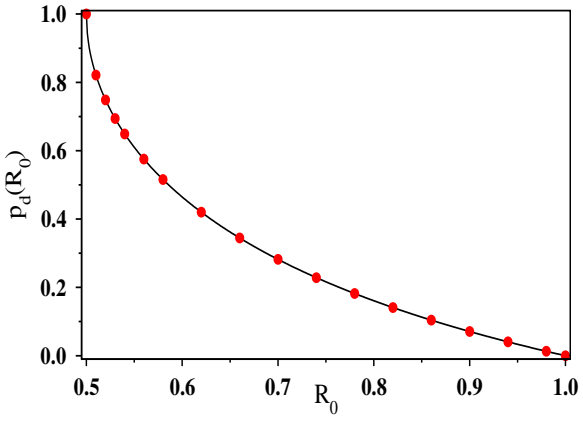

Figure 3.7: The density of dead bonds $p_d(R_0)$ has been plotted against R_0 which never get connected during the entire time evolution. The numerically obtained data for $p_d(R_0)$ using system size $L = 256$ (filled circles) fit excellently well with the functional form given in Eq. (3.11) (solid line).

the quantity $p_d(R_0)$ is calculated as

$$\begin{aligned} p_d(R_0) &= 1 - 2p(\phi)\Delta\phi_c \\ &= 1 - (2/\pi)\cos^{-1}\Big(1/R_0 - 1\Big). \end{aligned} \tag{3.11}$$

In Fig. 3.7, the numerically estimated values of $p_d(R_0)$ for different R_0 and the functional form given in Eq. (3.11) have been plotted. An excellent agreement is observed between the two plots.

Due to the random initial phase angles $\{\phi\}$, different bonds stay connected for different duration of time. Precisely, the fraction of time over which a bond remains connected within a period T is given by

$$f_T(R_0, \Delta\phi) = 1/2 - (1/\pi)\sin^{-1}\Big((1/R_0 - 1)\sec(\Delta\phi/2)\Big). \tag{3.12}$$

For the special case of $R_0 = 1$ and $\Delta\phi = \pi$ we get $f_T = 1$. We can also retrieve the Eq. (3.10) from the fact that for a connected bond we must have $f_T(R_0, \Delta\phi) \geqslant 0$.

3.5.2 Determination of the Second Transition Point

It is clear that information can propagate only through the live bonds and therefore, for a global passage of information across the system, it is necessary that the system must have a spanning cluster of live bonds. This leads us to identify the second transition point R_0^* as the configuration averaged minimum value of R_0 when a spanning cluster of live bonds appears in the system. For every initial configuration of random phase angles $\{\phi\}$, Eq. (3.10) enables us to immediately determine the status of every bond, whether live or dead. This gives a frozen configuration of live and dead bonds. Tuning the value of R_0 from 1/2 density of live bonds monotonically increases from 0 and at a threshold value of $R_0 = R_0^*$, the global connectivity first appears through a spanning path of live bonds. Numerically, the precise value of R_0^* has been estimated using the bisection method in the following way. To start with, we select a pair of values of R_0, namely, R_0^{hi} and R_0^{low}, such that for $R_0 = R_0^{hi}$ there exists a global connectivity through the live bonds, whereas no such connectivity exists for $R_0 = R_0^{low}$. Applying periodic boundary conditions along the horizontal direction, the global connectivity is checked along the vertical direction using the Burning algorithm [56] for $R_0 = (R_0^{hi} + R_0^{low})/2$. If the system is globally connected, then R_0^{hi} is replaced by R_0, otherwise R_0^{low} is replaced by R_0. This way the interval is successively bisected till it becomes smaller than a pre-assigned tolerance value of 10^{-7}. Averaging over a large number of independent configurations $R_0^*(L)$ for the system size L is estimated. The entire procedure is then repeated for different values of L and extrapolated to the asymptotic limit $L \to \infty$ to obtain $R_0^* = R_0^*(\infty)$. We find that the usual extrapolation method using $L^{-1/\nu}$ with $\nu = 4/3$ works very well here as well. Our best estimate for the critical point is $R_0^* = 0.5907(3)$.

To characterize precisely the critical behavior around the second transition point in terms of the live bonds, we have also estimated several critical exponents. The fractal dimension d_f of the largest cluster of live bonds, the exponent γ for the second moment of the cluster size distribution at R_0^*, and the order parameter exponent β around

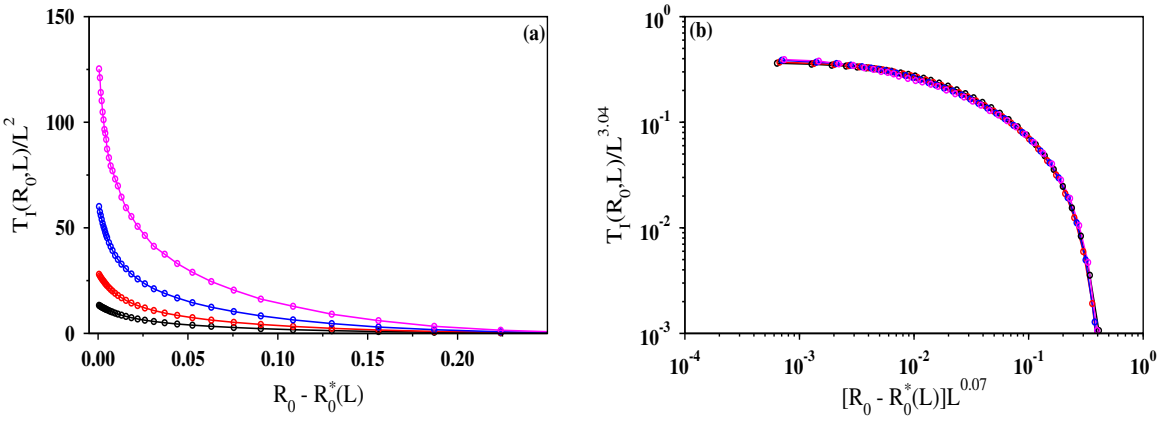

Figure 3.8: (a) Average passage time for information propagation $T_I(R_0, L)/L^2$ has been plotted against the deviation from the critical point $R_0 - R_0^*(L)$ for $L = 32$ (black), 64 (red), 128 (blue) and 256 (magenta) (arranged from bottom to top) using $\omega = 1$ for all the disks. As $R_0 \to R_0^*(L)$, the time $T_I(R_0, L)$ diverges. (b) A scaling by $T_I(R_0, L)/L^{3.04}$ against $[R_0 - R_0^*(L)]L^{0.07}$ exhibits a good data collapse.

R_0^*. The obtained values of the exponents are very much consistent with the ordinary percolation exponents in two dimensions.

An approximate estimate of the critical point R_0^* can also be made by neglecting the local correlations and equating the density of live bonds at the second transition point to the ordinary bond percolation threshold on the square lattice, i.e.,

$$p_l(R_0^*) = 1 - p_d(R_0^*) = 1/2. \tag{3.13}$$

Substituting the functional form of $p_d(R_0)$ as given in Eq. (3.11) to the above equation and solving for R_0^* we obtain $R_0^* = 2/(2 + \sqrt{2}) \approx 0.5858$, which is very close to our numerically obtained value of $R_0^* = 0.5907(3)$.

3.5.3 Information Propagation Time

The time required for the global propagation of information is measured in steps of dt. In Fig. 3.8(a), the average information propagation time $T_I(R_0, L)/L^2$ has been plotted against $R_0 - R_0^*(L)$ for four different system sizes using $\omega = 1$ for all the disks. It is observed that as R_0 approaches R_0^* from above, the propagation time becomes

larger and larger and it diverges as $R_0 \to R_0^*$. For $R_0 < R_0^*$, no such global propagation of information is possible . Further, for a specific value of R_0, the propagation time increases with the size of the system. By suitably scaling the abscissa and ordinate, and plotting the same data we obtain a good data collapse as shown in Fig. 3.8(b). Precisely, the data collapse is obtained when $T_I(R_0, L)/L^{3.04}$ has been plotted against $[R_0 - R_0^*(L)]L^{0.07}$. This is consistent with the variation of the largest passage time which grows as $T_I(R_0^*, L) \sim L^{3.08}$ and thus, the propagation time $T_I dt \sim L^{1.08}$. This exponent is very close to the shortest path fractal dimension of 1.130772(2) [44] for the ordinary percolation in two dimensions.

3.6 Role of the Shift Parameter

We further extend our study by introducing a shift parameter that enhances the disk radii by an amount R_s. Therefore, the radius of a disk now sinusoidally varies between R_s and $R_0 + R_s$ as:

$$R(t) = R_s + (R_0/2)[\sin(\omega t + \phi) + 1]. \tag{3.14}$$

We study the dependence of the first and second transition points on the value of R_s. For a specific value of R_s, it is now more likely that the radii of the disks at the two ends of a bond would satisfy the sum rule. Therefore, the density of connected bonds at any given instant of time t increases as R_s is increased. As a consequence, for a fixed non-zero value of R_s the first transition takes place at a lower value of $R_0 = R_{0c}(R_s)$ compared to its value R_{0c} for $R_s = 0$.

We have studied the variation of the order parameter $\Omega(R_0, R_s, L)$ against R_0 for three different shifts R_s. In Fig. 3.9(a), for each R_s three different system sizes L have been exhibited. Using the same data, we show that the finite-size scaling form

$$\Omega(R_0, R_s, L)L^{\beta/\nu} \sim \mathcal{F}\Big[(R_0/(1 - 2R_s) - R_{0c})L^{1/\nu}\Big] \tag{3.15}$$

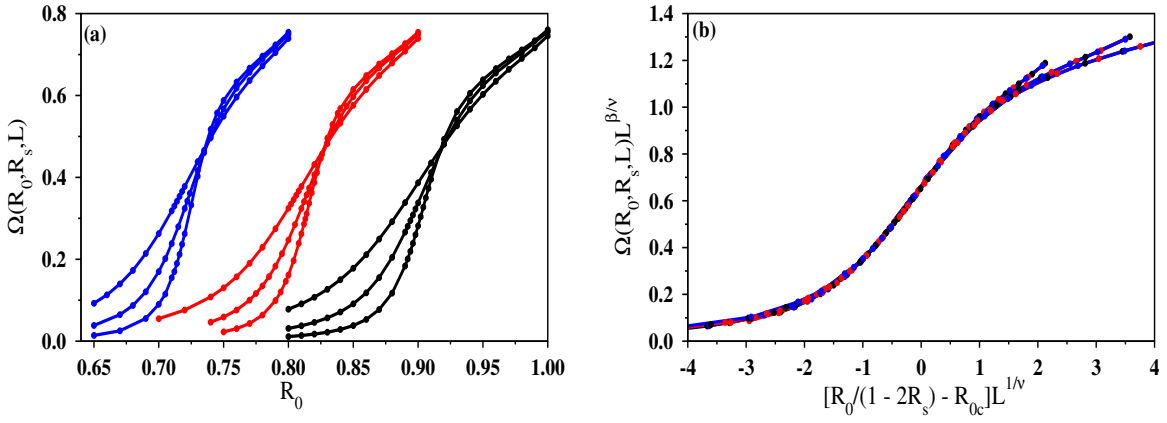

Figure 3.9: For $R_s = 0.001$ (black), 0.05 (red) and 0.1 (blue) (arranged from right to left), and for $L = 64$, 128 and 256 for each R_s. (a) The variation of the order parameter $\Omega(R_0, R_s, L)$ with R_0 has been shown using $\omega = 1$ for all the disks. (b) The same data as in (a) has been scaled suitably. A scaling by $\Omega(R_0, R_s, L)L^{\beta/\nu}$ against $[R_0/(1-2R_s) - R_{0c}]L^{1/\nu}$ with $R_{0c} = 0.908(5)$, $1/\nu = 0.75$ and $\beta/\nu = 0.112(5)$, exhibiting a nice data collapse.

for the order parameter works very well with $R_{0c} = 0.908(5)$ [Fig. 3.9(b)]. The best collapse of data has been obtained using $1/\nu = 0.750(5)$ and $\beta/\nu = 0.112(5)$. Expectedly, the critical exponents are consistent within error bars with the exponents of the ordinary percolation in two dimensions.

It is straightforward to obtain the functional dependence of the first transition point $R_{0c}(R_s)$ on R_s from the scaling of data in Fig. 3.9(b). Clearly, the scaling variable $[R_0/(1-2R_s) - R_{0c}]L^{1/\nu} = 0$ at $R_0 = R_{0c}(R_s)$. This yields

$$R_{0c}(R_s) = (1 - 2R_s)R_{0c}. \tag{3.16}$$

Numerically obtained values of $R_{0c}(R_s)$ match very well with those from Eq. (3.16). Similarly, the second transition point depends on R_s as

$$R_0^*(R_s) = (1 - 2R_s)R_0^*, \tag{3.17}$$

where $R_0^* = R_0^*(0)$. Introduction of the shift parameter R_s effectively reduces the lattice constant by an amount $2R_s$ as the minimal distance between the neighboring disks is

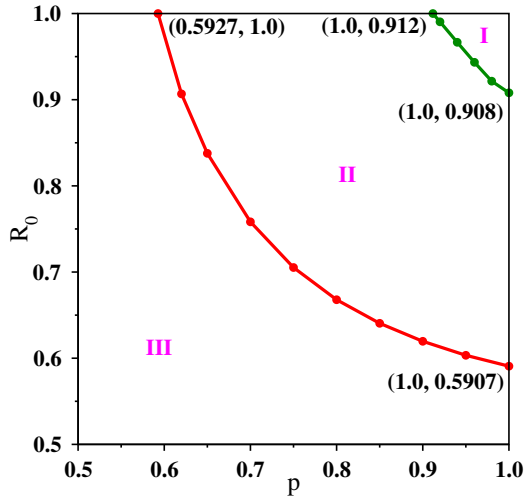

Figure 3.10: Phase diagram has been drawn on $p-R_0$ plane using the angular frequency $\omega = 1$ for all the disks and the shift parameter $R_s = 0$, where R_0 and p denote the maximal radii of the disks and the site occupation probability, respectively. The two distinct critical curves on this plane correspond to the first (green) and second (red) transitions.

$(1 - 2R_s)$. This explains the origin of the factor $(1 - 2R_s)$ in Eq. (3.16) and Eq. (3.17).

3.7 Phase Digram

So far we have considered only a specific situation where every lattice site is occupied by a pulsating disk and therefore, the site occupation probability $p = 1$. Further, the model can be studied for any general value of $p_c \leqslant p \leqslant 1$, where p_c is the site percolation threshold of the corresponding lattice. Initially, a configuration of occupied sites is generated as in the site percolation with site occupation probability p. Then, a random value for the phase angle is assigned with every occupied site and the corresponding disk with radius $R(0)$ at time $t = 0$ is associated with these sites. Subsequently, the system is allowed to evolve with time according to Eq. (3.1). For a given value of p there exists a critical value of $R_{0c}(p)$ where the first transition takes place. Similarly, the second transition point $R_0^*(p)$ also dependent on p. Calculating $R_{0c}(p)$ and $R_0^*(p)$ for various values of p with $R_s = 0$ and $\omega = 1$ for all the disks, we construct a phase diagram on the $p - R_0$ plane. In this plane, we have drawn two critical curves which

represent phase boundaries corresponding to the first and second transitions. The corresponding phase diagram has been shown in Fig. 3.10. Therefore, the whole $p - R_0$ plane gets divided into three separate regions. In region I, there always exists a spanning cluster of connected bonds and thus, information propagates instantly through the system. In region II, a spanning cluster of live bonds exists, but there does not exist a spanning cluster of connected bonds and therefore, finite time is required for the global propagation of information. In region III, no such spanning clusters exist and information can not be transmitted across the system.

3.8 Summary

In the context of studying the global connectivity properties of the wireless sensor networks in the presence of temporal fluctuations of radio transmission ranges, we have formulated a percolation model using a collection of pulsating disks and observed two distinct transition points. Every site of a regular lattice is occupied by a circular disk whose radius vary sinusoidally within $[0, R_0]$. A random phase angle is associated with every pulsating disk and this makes the system heterogeneous. At any given instant of time the set of connected bonds is determined using the sum rule. Precisely, a lattice bond between a pair of neighboring sites is said to be connected only when the disks situated at these sites overlap. The maximal value of the disks radii R_0 is considered as the control variable of the model.

Two different time scales can be associated with the dynamics of information propagation, leading to two distinct transition points. In the time-averaged description, the appearance of global connectivity through the spanning cluster of connected bonds characterizes the first transition point. Our numerical simulations estimate that the transition occurs at $R_0 = R_{0c} = 0.908(5)$, independent of the distribution of the frequencies of the individual disks. A Consideration of the propagation of information within a cluster with infinite speed immediately implies that information transmits

through the spanning cluster instantly for all $R_0 > R_{0c}$. Interestingly, the global transmission of information across the system is also possible for $R_0 < R_{0c}$ when only isolated finite-size clusters of connected bonds are present in the system. The clusters of sites which receive information, store it forever and pass the information when these informed clusters come in contact with the uninformed clusters in the subsequent time steps. The time associated with this global transmission of information is finite and it diverges as R_0 approaches R_0^* from above, $R_0^* = 0.5907(3)$ marks the second transition point. Depending on the value of the phase differences between the disks centered at the ends of the bonds, one can distinguish the whole set of lattice bonds in terms of dead and live bonds. A dead bond can never be connected, whereas a live bond gets connected at least once within a complete time period. Interestingly, the second transition point R_0^* is characterized by the appearance of the global connectivity through a spanning cluster of live bonds in the system. Expectedly, both the transitions exhibit the universal critical behavior of the ordinary percolation transition since the interaction is short ranged. Further, the model has been generalized for any arbitrary value of the site occupation probability p, leading to a phase diagram on the $p - R_0$ plane. This study is useful not only in the context of WSNs but also important from the point of view of the critical phenomena.

For the future investigations, one can study this model by placing the centers of the pulsating disks at random positions on a continuous plane by a Poisson process, like in continuum percolation [7, 30, 130].

Chapter 4

Colored Percolation

4.1 Introduction

In this Chapter [1], we introduce another variant of percolation model which can be viewed as a generalization of the model of AB percolation as described in Sec. 1.4.2 in Chapter 1. In brief, a consideration of assigning A and B atoms at the occupied and unoccupied sites, respectively, in the model of site percolation with any arbitrary site occupation probability p and defining connectivity through the bonds between neighboring dissimilar atoms describes the model of AB percolation [18, 59, 60]. According to this model, the profile of the density of connected bonds is symmetric about the point $p = 1/2$ and decreases monotonically from its maximum value $1/2$ on both sides of this point. Consequently, the system in general exhibits a global connectivity through a sequence of alternating A and B atoms only within a certain interval of p around $p = 1/2$. However, the existence of the global connectivity crucially depends on the geometry of the underlying lattice [60, 61]. For instance, even the maximal density of the connected AB bonds is not sufficient to establish a global connectivity on the square lattice [61, 62], but on the triangular lattice such a connectivity first appears at a density of AB bonds well below its maximum value of $1/2$ [63].

[1] The work reported here is based on the paper "Colored percolation", **Sumanta Kundu**, and S. S. Manna, Phys. Rev. E **95**, 052124 (2017).

Here we investigate a two-dimensional percolation model where the sites of a regular lattice are occupied by atoms with probability p similar to the ordinary site percolation and then, every atom is colored by selecting randomly one of the n distinct colors with a given probability q. The lattice bonds, which have two different colored atoms at their two opposite ends, are marked as connected. The global connectivity is then determined through these connected bonds. We refer this model as "colored percolation". The appearance of the global connectivity at a critical value of $p = p_c$ crucially depends on the values of n and q. Using extensive numerical simulations we have studied the variation of $p_c(q, n)$, whose nature can be predicted using basic concepts of the probability theory. Additionally, we have given a numerical evidence in support of the absence of global connectivity in the AB percolation. In the following, based on our publication [36], we present a detailed study on the percolation properties of the colored percolation model for both the square and triangular lattices.

The organization of the Chapter is as follows. We start by describing the model of colored percolation in Sec. 4.2, where we consider every color to be equally likely. In Sec. 4.3, we generalize the model by introducing a preference towards the selection of a subset of colors. Percolation transition using similarly colored bonds in addition to the dissimilar bonds has been described in Sec. 4.4. Percolation transition mixing the fractions of similarly and dissimilarly colored bonds are reported in Sec. 4.5. The critical properties of the model are presented in Sec. 4.6. Finally, we summarize in Sec. 4.7.

4.2 Model

We start with an initially empty regular lattice of size L, consisting of L^2 number of lattice sites. The sites are then occupied by atoms one by one in the following way. At each step, a vacant site is selected with probability p as in the ordinary site percolation and then, the corresponding site is assigned an atom by selecting its color randomly

among one of the n distinct colors with probability $q = 1/n$. The letters of the Roman alphabet are used to denote the different colors. A bond between a pair of neighboring occupied sites is declared as connected if and only if the atoms at the two ends of the bond are of different colors. Therefore, the other bonds having same colored atoms like AA, BB, etc., are not connected. At any arbitrary stage, the density of atoms in the system is denoted by p and its value is tuned to change the density of connected bonds. The density of connected bonds increases monotonically as p is increased and depending on the value n and the geometry of the lattice, a global connectivity first appears in the system through the set of connected bonds at a critical value of $p = p_c$.

For $n = 2$, every selected site is occupied either by a A atom or by a B atom with probability $q = 1/2$. Like the model of AB percolation, the size of the largest cluster of sites interlinked through the connected bonds never assumes a macroscopic size on the square lattice and therefore, a percolation transition is absent here. On the other hand, our simulation results indicate that on the triangular lattice the percolation transition occurs at $p_c \approx 0.729$.

For $n = 3$, every selected site is occupied by one of the three atoms A, B, and C with probabilities $q = 1/3$. Only the AB, BC, and CA bonds are said to be connected. In this case, there exists a percolation threshold $p_c \approx 0.807$ on the square lattice and $p_c \approx 0.630$ on the triangular lattice. We refer this model as ABC percolation.

Such an extension of the model can be continued with four colored atoms, where A, B, C, and D atoms are distributed with probabilities $q = 1/4$. Here the percolation transition occurs at $p_c \approx 0.734$ on the square lattice and $p_c \approx 0.591$ on the triangular lattice. This model is referred as the $ABCD$ percolation.

This way we systematically increase the number of distinct colored atoms to define further the $ABCDE, ABCDEF, ABCDEFG$, etc., colored percolation models. In brief, we have been able to define an infinite set of percolation models by defining connectivity through the bonds between dissimilar atoms. For very large value of n, hardly any bonds with similar colored atoms at their opposite ends would be found in

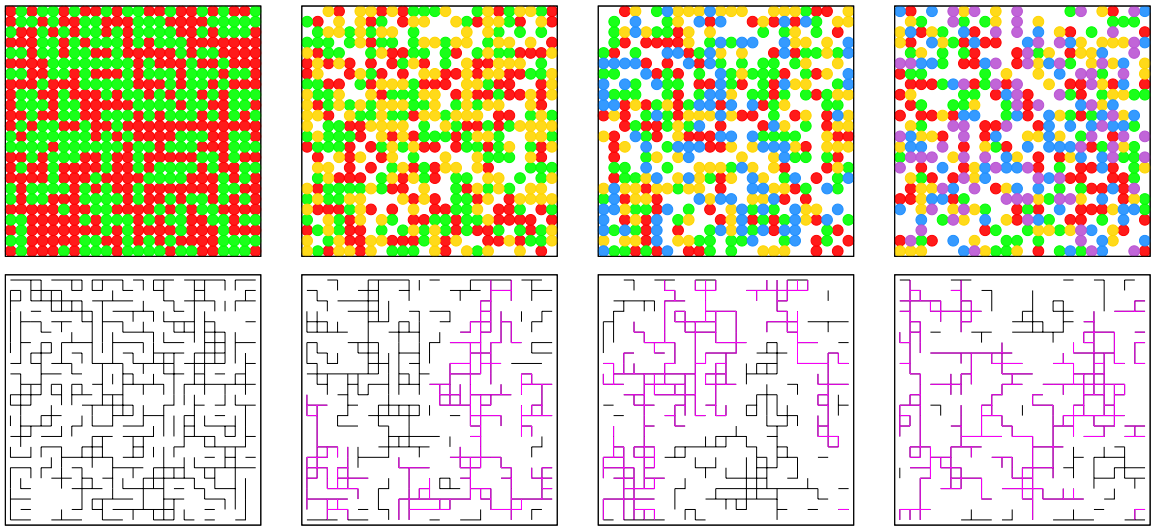

Figure 4.1: Typical configurations of AB, ABC, ABCD, and ABCDE percolation (from left to right) at their critical points have been shown on a 24×24 square lattice with periodic boundary conditions along the horizontal direction. The colors used are: red (A), green (B), yellow (C), blue (D) and orchid (E) and are distributed with uniform probabilities. The corresponding bond configurations with the spanning clusters painted in magenta have been shown in the lower panel. It may be noted that for AB percolation, there is no spanning cluster even when all the sites are occupied.

the system and therefore, this model reduces to the ordinary site percolation in the limit $n \to \infty$. Figure 4.1 shows the images of the typical percolation configurations on the square lattice for four different values of n.

4.2.1 Order Parameter

The size of the largest cluster for a particular value of p and for the system of size L is denoted by $s_{max}(p, L)$ and as before, the scaled average size of the largest cluster is defined as the order parameter $\Omega(p, L) = \langle s_{max}(p, L) \rangle / L^2$. The average is taken over many independent configurations. The variation of $\Omega(p, L)$ against p has been exhibited in Fig. 4.2(a) for six different values of n on the square lattice. As the value of n is increased, more and more connected bonds appear in the system and thereby, the sharp rise in the order parameter curve shifts towards smaller values of p.

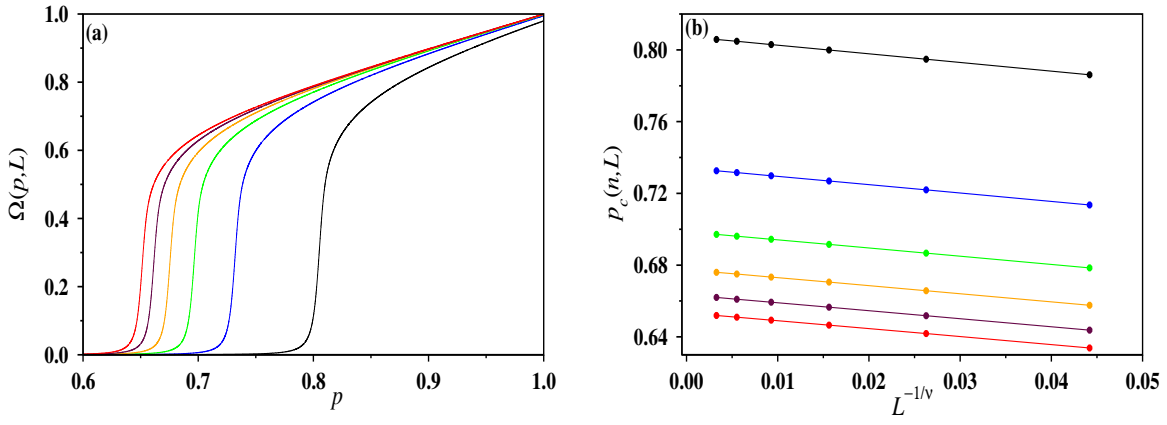

Figure 4.2: For $n = 3$ (black), 4 (blue), 5 (green), 6 (orange), 7 (maroon), and 8 (red): (a) the order parameter $\Omega(p, L)$, has been plotted against the site occupation probability p for the square lattice of size $L = 1024$ (n increases from right to left); (b) plot of the percolation thresholds $p_c(n, L)$ against $L^{-1/\nu}$ using $\nu = 4/3$ (n increases from top to bottom). By extrapolating the straight line in the limit $L \to \infty$, we obtain the asymptotic values of the percolation threshold $p_c(n)$.

4.2.2 Percolation Threshold

The percolation threshold is determined using the method described in Sec. 1.2.1 in Chapter 1. As in the site percolation, here also the size of the largest cluster increases monotonically with increasing the value of p, whereas the variation of the second largest cluster is non-monotonic. In a typical run α, the second largest cluster may merge several times with the largest cluster and thereby causes multiple jumps in the size of the largest cluster. At a specific value of p, when the maximum of the second largest cluster merges with the largest cluster, the maximal jump in the size of the largest cluster takes place. This particular value of p is considered as the percolation threshold p_c^α for the specific run α [36, 43]. For a fixed value of n, a large number of independent runs are considered and the p_c^α values are averaged to obtain $p_c(n, L) = \langle p_c^\alpha \rangle$ for the system size L. In our simulation, periodic boundary conditions are imposed along both the vertical and horizontal directions. We use the Newmann-Ziff algorithm described in reference [42] for the purpose of evaluating the value of $s_{max}(p, L)$ over the entire range of p.

For a given value of n, the $p_c(n, L)$ values are extrapolated as before using

$$p_c(n, L) = p_c(n) - AL^{-1/\nu} \tag{4.1}$$

to obtain the asymptotic value of the percolation threshold $p_c(n)$ in the limit $L \to \infty$, where ν is the correlation length exponent. Using $1/\nu$ as a free parameter we varied its trial values at the interval of 0.001 and found by the least-squares fitting method that the best values for all n differ from 3/4 by at most 0.005. Therefore, in the rest of our calculation we have used $\nu = 4/3$, the exact value of the exponent in two dimensions [6]. The plot of $p_c(n, L)$ against $L^{-1/\nu}$ using a linear scale has been shown in Fig. 4.2(b) for six different values of n. We observe that for each n the data points fit excellently to a straight line. By extrapolating the straight lines in the limit $L \to \infty$ and measuring the y intercepts we estimate the asymptotic values of $p_c(n)$. The values of $p_c(n)$ for first few values of n are listed in Table 4.1 for square and triangular lattices. It is to be noted that, for each value of n, the $p_c(n, L)$ values are calculated numerically using $L = 64, 128, 256, 512, 1024$, and 2048.

Table 4.1: Numerical estimates of the asymptotic values of the percolation threshold $p_c(n)$ for n different colored atoms occur with probability $1/n$ for the square and triangular lattice geometries.

	$p_c(n)$	
n	Square	Triangular
2		0.72890(4)
3	0.80745(5)	0.63005(4)
4	0.73415(4)	0.59092(3)
5	0.69864(7)	0.56991(5)
6	0.67751(5)	0.55679(5)
7	0.66345(5)	0.54782(3)
8	0.65342(8)	0.54130(3)
9	0.64588(5)	0.53634(2)
10	0.64002(4)	0.53245(3)
11	0.63532(5)	0.52931(2)
12	0.63147(4)	0.52672(2)

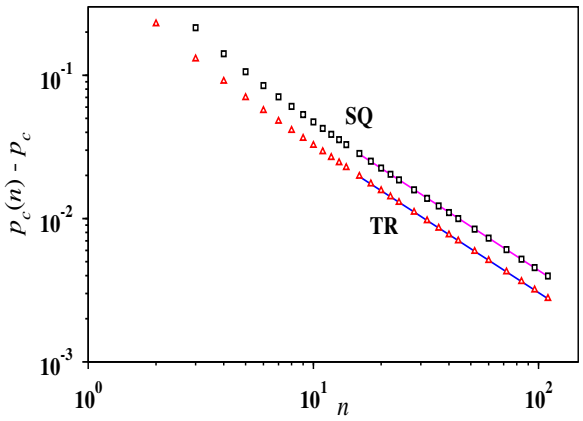

Figure 4.3: Plot of $p_c(n) - p_c$ against n (upto $n = 110$) on a log-log scale, using $p_c = p_c(\text{sq}) \approx 0.592746050$ and $1/2$ for the square and triangular lattices respectively. The slope of the curves in the fitted regime have been found to be 1.020 and 1.017, respectively.

Evidently, the density of connected bonds increases with increasing the number of different colors and as a result, the system is observed to percolate at smaller densities of occupied sites. As all the colors are equally likely, the probability that a bond between two neighboring occupied sites would be a connected one is given by

$$p_b = 1 - 1/n. \tag{4.2}$$

For $n \to \infty$, p_b approaches unity and therefore, for very large value of n the entire scenario is exactly same as the ordinary site percolation. Expectedly, $p_c(n)$ approaches $p_c = p_c(\infty)$, the ordinary site percolation threshold of the corresponding lattice. This $1/n$ dependence of p_b [Eq. (4.2)] should be reflected in the percolation properties of the system also.

To investigate how the asymptotic values of the percolation threshold $p_c(n)$, approach to the value p_c as $n \to \infty$, we first calculate $p_c(n)$ for different values of n up to $n = 110$. Then, we plot the deviation $p_c(n) - p_c$ against n on a double logarithmic scale for the square and triangular lattices. The corresponding plot is shown in Fig. 4.3. Although both the curves have curvatures at their initial regimes, for large values of n they are

quite straight. The slopes of the curves within a window ranges between $n = 16$ and 110 measured as 1.020 and 1.017 for the square and triangular lattices, respectively. We observed that these slopes approach gradually to a value unity as we shift the window to higher values of n. This lead us to conjecture that

$$p_c(n) - p_c \sim n^{-1}, \tag{4.3}$$

for both the lattices, consistent with the expected behavior as mentioned above.

4.3 Preferential Colored Percolation

A straightforward generalization of this model can be achieved by introducing a preference towards the probability of selection of differently colored atoms. In the simplest case, the occurrence of the atoms of a particular color is favored over the others. Let us consider that the atoms of color C to be preferentially selected, whereas all other colored atoms are equally probable. More specifically, we denote the probability of selection of the C atoms by q and for all other atoms it is $(1-q)/(n-1)$. As before, only the bonds between dissimilar atoms are declared as connected.

For a given value of q, if Prob_{ii} denotes the probability that two atoms at the opposite ends of a bond are of same color i, then the probability that a particular bond between a pair of occupied sites would be a connected one is given by,

$$\begin{aligned} p_b(q) &= 1 - \sum_{i=1}^{n} \text{Prob}_{ii} \\ &= 1 - q^2 - (1-q)^2/(n-1). \end{aligned} \tag{4.4}$$

The above expression describes that with increasing the value of q from 0, the $p_b(q)$ first increases, reaches its maximum at $q = q_{min}$, and finally decreases beyond this point. The condition $dp_b(q)/dq = 0$ at $q = q_{min}$ yields the value of $q_{min} = 1/n$. This property of $p_b(q)$ should be reflected in the percolation properties of the system also.

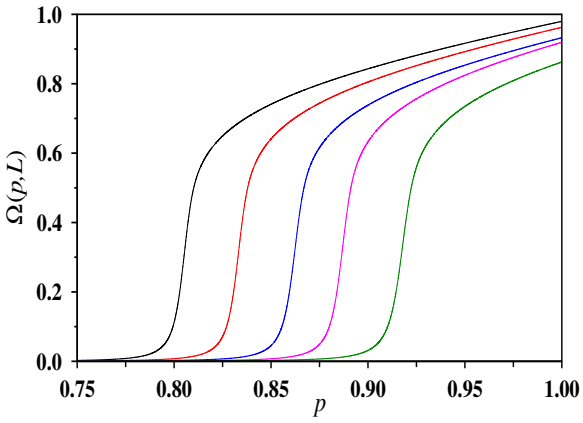

Figure 4.4: Plot of the order parameter $\Omega(p, L)$ against occupation probability p for the preferential ABC percolation on square lattice of size $L = 1024$. The values of q are 1/3 (black), 0.20 (red), 0.53 (blue), 0.12 (magenta), and 0.60 (green) arranged from left to right.

Consequently, the percolation threshold $p_c(q)$ must decrease with q, till it reaches q_{min} and then again increases on increasing q further.

To see this, let us first consider the model for $n = 3$, where the atoms A and B are equally probable and C is selected with probability q. The variations of the order parameter for different values of q have been shown in Fig. 4.4. For $q = 0$, one gets back the $n = 2$ unpreferred colored percolation, and therefore, for the square lattice even a fully occupied lattice does not percolate. Further, on increasing the value of q the BC and CA bonds are created which eventually help the system to establish the global connectivity. Increasing the value of q from zero, it has been observed that there exists a threshold value of $q = q_1$ when the global connectivity first appears, i.e., $p_c(q_1) = 1$. If the value of q is increased further, the percolation threshold $p_c(q)$ continuously decreases till a minimum value of $p_c(q_{min}) \approx 0.807$ at $q = q_{min} \approx 0.333$ is reached. On increasing q even further, $p_c(q)$ increases and reaches the value of unity again at $q = q_2$. Beyond this point the density of connected bonds is no longer sufficient to establish the global connectivity. The variation of $p_c(q)$ for the entire range of q has been shown in Fig. 4.5. For each value of q, first the percolation threshold $p_c(q, L)$ for the system size L is estimated for $L = 256, 512$, and 1024, and then they are extrapolated in the limit

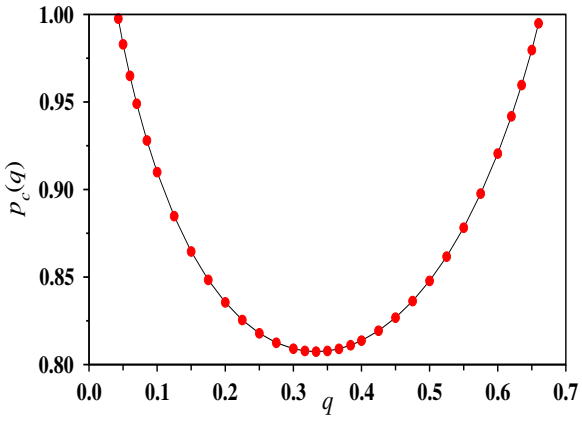

Figure 4.5: For the preferential ABC percolation on the square lattice, percolation threshold $p_c(q)$ is plotted against the parameter q. The minimum of $p_c(q)$ occurs at $q \approx 0.333$ which is in agreement with its estimate of 1/3, using Eq. (4.4).

$L \to \infty$ using Eq. (4.1) to obtain $p_c(q)$.

For the triangular lattice, the curve retains its shape but in this case, even for $q = 0$, there exists a percolation threshold. Since, for $q = 0$ the other two atoms are occupied with probability 1/2, the curve starts with the percolation threshold $p_c(q) \approx 0.729$ for $q = 0$. Similarly, for $q = 0$ and $n = 4$ on the square lattice this model is identical to the ABC percolation and therefore, $p_c(0) \approx 0.807$.

Numerically, the values of q_1 and q_2 are determined using the bisection method described as follows. To estimate q_2, we start with a pair of initial values of q, namely, q^h and q^l such that the system is percolating through a globally connected spanning path for $q = q^h$ but non-percolating for $q = q^l$ at the site occupation probability $p = 1$. We have applied the periodic boundary conditions along the horizontal direction and tested for the global connectivity along its transverse direction using the Burning algorithm [56] for $q = (q^h + q^l)/2$. If the system exhibits global connectivity, then q^h is reduced to q, otherwise q^l is raised to q. This way, the interval $q^h - q^l$ is iteratively bisected until a desired accuracy of 10^{-7} is reached, when $(q^h + q^l)/2$ defines q_2^α for a particular run α. This calculation is repeated over a large number of independent runs and the q_2^α values are averaged to estimate $q_2(n, L)$ for specific values of n and L. Similar procedure has been followed for $q_1(n, L)$. The entire procedure is then repeated

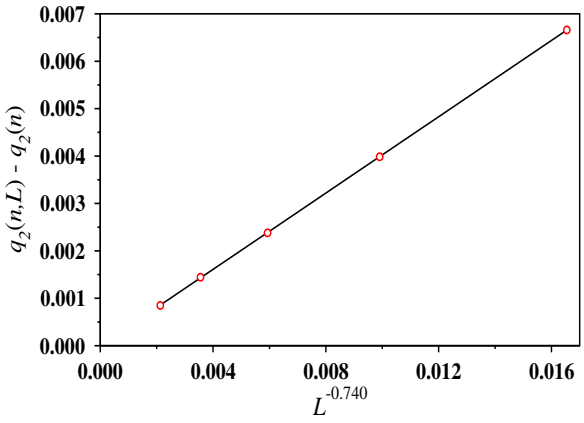

Figure 4.6: For n =3 and for square lattice, plot of $q_2(n, L) - q_2(n)$ against $L^{-0.740}$ with $q_2(n) = 0.6639$ exhibits an excellent straight line which passes very close to the origin. The value of $q_2(n, L)$ is calculated for L = 256, 512, 1024, 2048, and 4096.

for different values of L and extrapolations to $L \to \infty$ using Eq. (4.1) in this case as well, we obtain $q_1(n)$ and $q_2(n)$. For $n = 3$, the best linear fit has been exhibited in Fig. 4.6 by plotting $q_2(3, L) - q_2(3)$ against $L^{-0.740}$, using $q_2(3) = 0.6639(5)$ on the square lattice. Similarly, we have estimated $q_1(3) = 0.0414(5)$.

Therefore, a non-trivial value of $q_1(n)$ exists for $n = 3$ and $n = 2$ on the square and triangular lattices, respectively. It does not exist for all other values of n. On the other hand, $q_2(n)$ exists for all values of $n \geqslant 3$ and $n \geqslant 2$ for the square and triangular lattices, respectively.

The density of connected bonds $p_b(q)$ corresponding to the point $q = q_2(n)$ represents a threshold value in the correlated bond percolation scenario. Beyond this point, the density of connected bonds is no longer sufficient to establish a global connectivity. Neglecting the local correlations and equating $p_b(q_2)$ to p_c^b, the random bond percolation threshold of the respective lattices, we arrive at an expression of $q_2(n)$ using Eq. (4.4),

$$q_2(n) = \left[1 + \left[1 + n[(1 - p_c^b)(n - 1) - 1]\right]^{1/2}\right] \Big/ n. \tag{4.5}$$

Numerically estimated values of $q_2(n)$ for different values of n using bisection method, along with the values obtained from Eq. (4.5) using $p_c^b = 1/2$, are summarized in Table

4.2 for the square lattice. It is observed that the values are close to each other and differ only due to the existence of short range correlations in the system.

4.3.1 Generalized Preferential Colored Percolation

A more general version of the preferential colored percolation model is the situation when m distinct colored atoms are equally probable and the remaining $(n-m)$ colors are also equally probable but occur with different probabilities. Such a generalization can be obtained by assigning an atom of one of the m colors with probability q/m and rest of the $(n-m)$ colors with probability $(1-q)/(n-m)$ at the time of occupying a vacant site. Given that a pair of neighboring sites is occupied, the probability that the bond between these sites would be a connected one has the dependence on q as

$$p_b(q,m) = 1 - q^2/m - (1-q)^2/(n-m). \tag{4.6}$$

Evidently, $p_b(q,m)$ is maximum at $q_{min} = m/n$ and it decreases on both sides of this point. The expression of $p_b(q,m)$ remains unaltered if the value of q is changed from q to $(1-q)$ at the same time m is changed from m to $(n-m)$, i.e., $p_b(q,m) = p_b(1-q, n-m)$. Immediately, it implies that the curve is symmetric about $q = 1/2$ only when $m = n/2$. The percolation threshold $p_c(q,m)$ for specific values of n and m is expected to exhibit such properties appropriately.

Table 4.2: The comparison of $q_2(n)$, evaluated using Eq. (4.5) with its numerical estimates for different values of n for square lattice. For each values of n, numerically $q_2(n,L)$ is calculated for $L = 256$, 512, 1024, 2048, and 4096 and on extrapolation to $L \to \infty$ we obtained $q_2(n)$. Each of the reported value has an error bar of 5 in the last digit.

n	3	4	5	6	7	8
Numerical	0.6639	0.6849	0.6927	0.6969	0.6995	0.7013
Analytical	2/3	0.6830	0.6899	0.6937	0.6961	0.6978

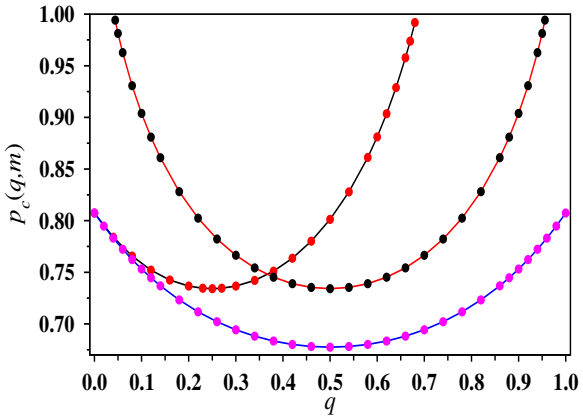

Figure 4.7: The variation of the percolation threshold $p_c(q, m)$ with q for the generalized version of the preferential colored percolation model is shown for $m = 1$, $n = 4$ (black); $m = 2$, $n = 4$ (red); and $m = 3$, $n = 6$ (blue) for the square lattice. The curves are arranged from top to bottom along the line $q = 0.50$.

Again, after extrapolation to the large L limit using Eq. (4.1) with $\nu = 4/3$ we obtain $p_c(q, m)$. In Fig. 4.7, the asymptotic values of the percolation threshold $p_c(q, m)$ have been plotted against q for three pairs of values of m and n for the square lattice. It is observed that all three curves have their own minimum which occur at $q_{min} = 0.25$, 0.50 and 0.50 for $m = 1$, $n = 4$; $m = 2$, $n = 4$; and $m = 3$, $n = 6$, respectively. Clearly, the q_{min} values match excellently with our analytically estimated value of $q_{min} = m/n$. As expected, the curves corresponding to $m = n/2$ are symmetric about the point $q = 1/2$.

4.4 Percolation using Additional Similar Bonds

Let us recall that for $n = 2$ case on the square lattice and for any arbitrary value of the site occupation probability p, the density of AB bonds is maximum for $q = 1/2$. In spite of that no percolation transition is observed on the square lattice since the largest cluster of AB bonds is found to be minuscule even when $p = 1$. In other words, even the maximum number of connected bonds are not sufficient to establish a global connectivity across the system [61].

In this section, we study a new variant of our colored percolation model where in addition to the AB bonds, we allow also a fraction v of similarly colored bonds (like AA and BB) to be connected. Therefore, for $v = 1$, the problem reduces to the ordinary site percolation with the percolation threshold at $p_c(\text{sq}) \approx 0.5927460$ for the square lattice. This suggests that for all values of $p_c(\text{sq}) \leqslant p \leqslant 1$ there should be a critical value of $v = v_c(p)$ for the fraction of bonds between similarly colored atoms, such that percolation transition occurs only for $v \geqslant v_c(p)$.

For $p = 1$, one must include a non-trivial fraction $v_c(1)$ of similarly colored bonds to achieve a percolation transition. On a fully occupied lattice we have used again the bisection method to obtain an accurate estimation of $v_c(1)$. Starting with two initial values of v corresponding to the globally connected and unconnected systems, the gap between them is reduced by successive halving of the interval. As before, the values of $v_c(1, L)$ obtained this way have been extrapolated in the limit $L \to \infty$ to obtain $v_c(1) = 0.0651(5)$. It may be noted that the existence of a non-zero value of $v_c(1)$ is a numerical demonstration of the absence of a percolation transition in the $n = 2$ colored percolation as well as in the AB percolation on the square lattice.

In Fig. 4.8(a), the order parameter $\Omega(v, L) = \langle s_{max}(v, L)\rangle/L^2$ has been plotted against v for three different sizes of the system. For $v = 0$, only the AB bonds are present in the system and the size of the largest cluster is minuscule, which is apparent by the very small value of the order parameter. As the value of v is increased, the order parameter grows monotonically and the sharpest rise occurs at a critical value $v_c(1, L)$ leading to the occurrence of a global connectivity. A finite-size scaling analysis is exhibited in Fig. 4.8(b) indicating a scaling form:

$$\Omega(v, L)L^{\beta/\nu} \sim \mathcal{F}[(v - v_c(1))L^{1/\nu}]. \tag{4.7}$$

Using $v_c = 0.0651$, the best data collapse is observed for $1/\nu = 0.745(5)$ and $\beta/\nu = 0.101(5)$, compared to the exact value of the correlation length exponent $1/\nu = 3/4$ and

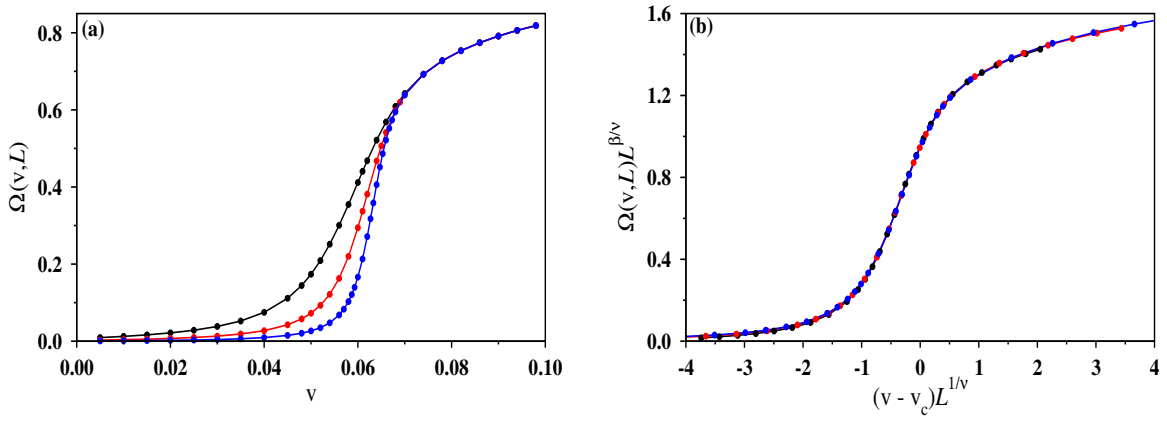

Figure 4.8: (a) For $L = 256$ (black), 512 (red) and 1024 (blue) (arranged from left to right), the order parameter $\Omega(v, L)$ has been plotted with the bond occupation probability v between AA or BB atoms at $p = 1$, for $n = 2$ with $q = 1/2$ colored percolation. (b) By suitably scaling the abscissa and ordinate when the same data as in (a) is replotted, a nice data collapse is observed using $v_c = 0.0651$, $\beta/\nu = 0.101(5)$ and $1/\nu = 0.745(5)$.

$\beta/\nu = 5/48 \approx 0.104$ for the ordinary percolation in two dimensions [6]. In addition, our estimates for the fractal dimension $d_f = 1.896(5)$ of the infinite incipient cluster [15] and the exponent $\gamma = 2.388(5)$ of the second moment of the cluster size distribution at $v = v_c(1, L)$ yield values very much consistent with the exact values of the exponents of $d_f = 91/48$ and $\gamma = 43/18$ for the ordinary percolation which fulfill the scaling and hyperscaling relations in two dimensions: $\gamma/\nu + 2\beta/\nu = 2$ [6].

Repeating this method for many different values of the occupation probability p we have drawn the phase diagram in the $v - p$ plane (Fig. 4.9). This plane is divided into two regions by the critical curve $v_c(p)$ which separates the percolating region (above) from the non-percolating region (below). Three different critical curves are shown for n = 2, 3, and 4. The dependence of the critical fraction $v_c(p)$ on p for a specific value of n is obtained by the quadratic polynomial fit of the data as exhibited in Fig. 4.9:

$$v_c(p) = c_1 + c_2 p + c_3 p^2 \tag{4.8}$$

The values of c_1, c_2, and c_3 are given in the caption of Fig. 4.9.

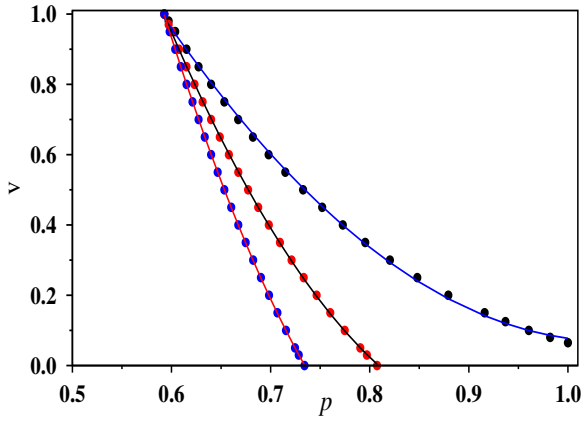

Figure 4.9: Phase diagram of the density v of similarly colored bonds and the site occupation probability p for $n = 2$ (black), 3 (red), and 4 (blue) (arranged from right to left) with $q = 1/n$. The critical curve is fitted very closely by the Eq. 4.8 whose parameters are c_1 = 5.01, 8.28, and 11.47; c_2 = -9.48, -17.92, and -26.25; c_3 = 4.55, 9.50, and 14.47 for n = 2, 3, and 4, respectively.

4.5 Generalized Colored Percolation with Similar and Dissimilar Bonds

In this section we have generalized the model of colored percolation tuning the fractions of the bonds between similar and dissimilar colored atoms using two independent parameters. Specifically, for the site occupation probability $p > p_c$, the bonds between dissimilarly colored atoms are connected with probability u and those between similarly colored atoms are connected with probability v. Therefore, on the $u - v$ plane a critical percolation curve represents the phase boundary between the percolating and the non-percolating phases. In Fig. 4.10(a), we have shown for $n = 2$ and $q = 1/2$ a series of critical percolation curves for different values of the site occupation probability p. Here, the density of connected bonds is given by $p_b(u, v) = (u + v)/2$. The symmetry of this expression under the interchange of u and v is reflected by the mirror symmetry of the curves in Fig. 4.10(a) about the $v = u$ line. This can be generalized further for any value of n as

$$p_b(u, v) = u + (v - u)/n, \tag{4.9}$$

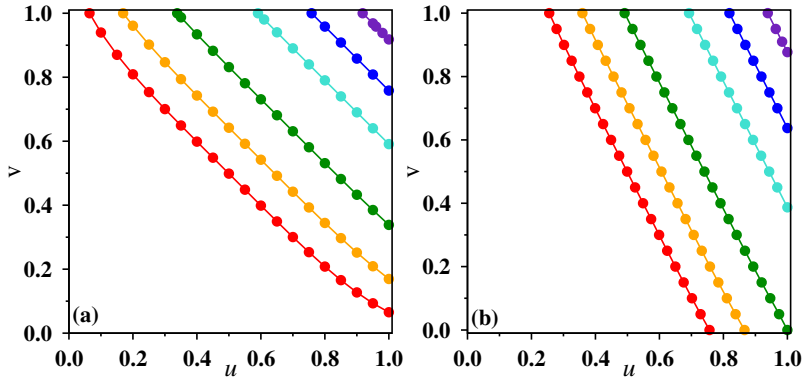

Figure 4.10: Phase diagram of the density of similarly colored bonds v and dissimilarly colored bonds u for fixed values of p for $n = 2$ (a) and $n = 3$ (b), with $q = 1/n$ using $L = 1024$ on the square lattice. The values of p are 1.00 (red), 0.90 (orange), 0.80 (green), 0.70 (cyan), 0.65 (blue), and 0.61 (indigo) (arranged from left to right). For every p, the region above the critical curve depicts the percolating phase.

and therefore, for $n > 2$ the critical curves are not symmetric about the $u = v$ line any more. This has been exhibited in Fig. 4.10(b) for $n = 3$ and $q = 1/3$.

A better visualization of the percolating and non-percolating phases has been exhibited by a three-dimensional critical surface in the $(u - v - p)$ space. Fig. 4.11(a) and (b) exhibit such plots for $n = 2$ and 3, respectively. Any point within the space enclosed by the critical surface represents the percolating phase. The intersections of these critical surfaces with the $u = 1$ plane have been shown in Fig. 4.9 for $n = 2$, 3 and 4.

4.6 Universality Class of Colored Percolation

To confirm that the colored percolation model belongs to the universality class of ordinary percolation, we have estimated a set of critical exponents, e. g., the fractal dimension of the largest cluster, the cluster size distribution exponent and the fractal dimension of the shortest paths right at the percolation threshold of the unpreffered colored percolation.

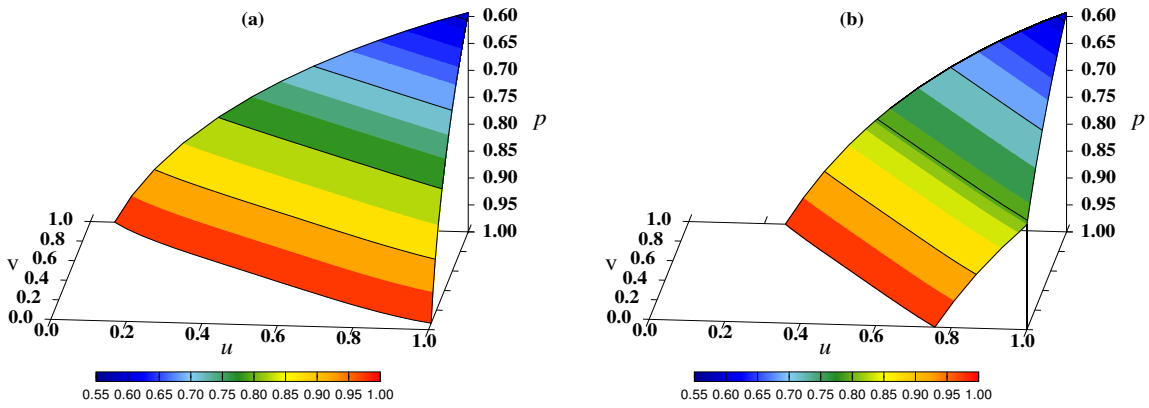

Figure 4.11: 3D phase diagram has been drawn in the $u - v - p$ plane, for $n = 2$ (a) and $n = 3$ (b), with $q = 1/n$ using $L = 1024$ on the square lattice. The colored surface separates the percolating region from the non-percolating region.

Fractal dimension: The scaled average size of the largest cluster at the percolation threshold decreases with the system size L as $\langle s_{max}(p_c, L)\rangle/L^2 \sim L^{d_f-2}$, where d_f is its fractal dimension [15]. Our estimated values of $d_f = 1.897(2)$ for $n = 3$ on square lattice [Fig. 4.12(a)] and 1.895(2) for $n = 2$ on triangular lattice are compared with the fractal dimension $91/48 \approx 1.8958$ of the ordinary percolation in two dimensions.

Cluster Size Distribution: The size s of a percolation cluster is the number of occupied sites in the cluster. Cluster sizes are measured for all clusters right at the percolation threshold, marked by the maximal jump of the largest cluster. In Fig. 4.12(b), the finite-size scaling of the data for the cluster size distribution $D(s)$ has been shown for $n = 3$ on the square lattice. An excellent collapse of the data confirms a power-law variation: $D(s) \sim s^{-\tau}$. Using the best fitted values of the scaling exponents, we estimated $\tau = 2.051(5)$, compared to $187/91 \approx 2.055$ for ordinary percolation in two dimensions [6]. A very similar value of 2.051(5) has been obtained for $n = 2$ on the triangular lattice.

Shortest Path: Right at the percolation threshold, the average length $\langle \ell(n, L)\rangle$ of the shortest path spanning the entire system has been estimated using the Burning algorithm [56]. It is found to scale with the lattice size L as $\langle \ell(n, L)\rangle \sim L^{d_\ell}$, with $d_\ell = 1.133(2)$ for $n = 3$ on the square lattice [Fig. 4.12(c)] and 1.133(3) for $n = 2$

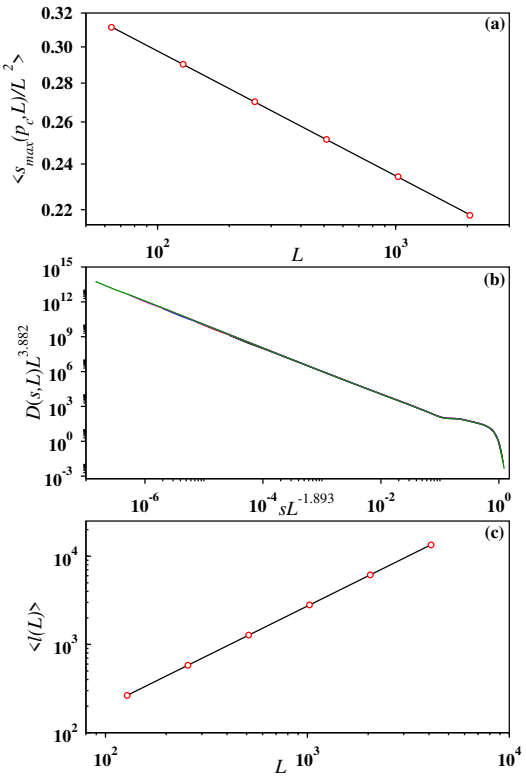

Figure 4.12: Plots for $n = 3$ and $q = 1/3$ at the percolation threshold of the colored percolation on the square lattice. (a) The scaled average size $\langle s_{max}(p_c(L))\rangle/L^2$ of the largest cluster plotted against the system size L gives a value of the fractal dimension $d_f = 1.897(2)$. (b) The finite-size scaling analysis of the cluster size distribution $D(s, L)$ has been exhibited. Plot of $D(s)L^{3.882}$ against $sL^{-1.893}$ shows an excellent data collapse, that yields $\tau = 2.051(5)$. (c) The average shortest path $\langle \ell(L)\rangle$ has been plotted against L for $L = 128$, 256, 512, 1024, 2048, and 4096. The fractal dimension of the shortest path is estimated from the slope as $d_\ell = 1.133(2)$.

on the triangular lattice compared to 1.13077(2) for the ordinary percolation in two dimensions [44].

The same set of critical exponents have been estimated for the preferential colored percolation with $q = 0.60$ and we have obtained very similar matching with the exponents of ordinary percolation.

4.7 Summary

To summarize, we have introduced a model called "colored percolation" and formulated its infinite number of versions in two dimensions. The sites of a regular lattice are occupied by atoms with probability p and then every atom is colored randomly using one of the n distinct colors with uniform probability $q = 1/n$. Here, a lattice bond is defined as connected if and only if the atoms situated at the two opposite ends of the bond are of different colors. Accordingly, the global connectivity is determined through the connected bonds. For $n = 2$, the size of the largest cluster of sites interlinked through the connected bonds remains minuscule on the square lattice even when $p = 1$ and therefore, a percolation transition does not occur here. However, the percolation threshold $p_c(n)$ exists for all values of $n \geqslant 3$ and $n \geqslant 2$ for the square and triangular lattices, respectively. It has been observed that $p_c(n)$ approaches the site percolation threshold value p_c in the limit of $n \to \infty$ as $1/n$ for both lattices.

In the preferential version of the colored percolation model, m out of n colors are selected with probability q/m each and rest of the colors are selected with probability $(1-q)/(n-m)$. It has been observed that $p_c(q, m)$ depends non-trivially on q and has a minimum at $q_{min} = m/n$. The plot of $p_c(q, m)$ against q is asymmetric for general value of m, but it becomes symmetric about $q = 1/2$ only when $m = n/2$.

This model has been generalized by considering the fractions of bonds between similarly and dissimilarly colored atoms as independent parameters. The bonds between dissimilarly colored atoms are connected with probability u, whereas those between similarly colored atoms are connected with probability v. There exists a critical value of the site occupation probability p for each pair of (u, v) values where percolation transition occurs. Estimating the percolation threshold for many different pairs of (u, v), we construct a phase diagram in a three-dimensional $(u - v - p)$ space. A critical surface in this space divides the whole region into two regions, namely, the percolating and the non-percolating regions.

Numerical estimation of different critical exponents lead us to conclude that all versions of the model of colored percolation belong to the ordinary percolation universality class.

Chapter 5

Jamming and Percolation Properties of Random Sequential Adsorption with Relaxation

5.1 Introduction

As discussed in Sec. 1.5 in Chapter 1, the random sequential adsorption (RSA) is a classic model in statistical physics in the context of irreversible adsorption of objects on surfaces. Although the model is simple to describe, it attracted the scientific community a lot as it provides basic concepts of the jamming phenomenon. In addition, at any intermediate stage of the adsorption process, the adsorbed objects in the presence of excluded volume interaction arrange in such a manner that corresponds to a disordered system and therefore, the study of the percolation transition in such a system is quite relevant. Over the last several decades, a large number of studies have been devoted to investigate the role of shapes and sizes of the adsorbed objects on the percolation properties of the system [138–143]. In this Chapter [1], we study how the percolation and jamming properties of a system depend on the mechanism of relaxation.

[1]The work reported here is based on the paper "Jamming and percolation properties of random sequential adsorption with relaxation", **Sumanta Kundu**, Nuno A. M. Araújo, and S. S. Manna, Phys. Rev. E **98**, 062118 (2018).

We introduce a variant of RSA model where the objects in the form of dimers are adsorbed sequentially and irreversibly onto the sites of a regular lattice after going through a well-defined relaxation dynamics. The deposition of a new dimer triggers the relaxation dynamics when it partially overlaps with the previously adsorbed dimers and during the relaxation, a series of dimer displacements may occur to accommodate the new dimer. This leads to a monolayer formation of the adsorbed dimers. We argue that this relaxation dynamics is somewhat different from the stochastic diffusion process considered in the model of accelerated random sequential adsorption (ARSA) [124]. In ARSA, an incoming object starts diffusing when it drops on top of the already adsorbed objects and the diffusion continues until it finds an empty gap where it is then adsorbed irreversibly [124, 144]. Here, based on our publication [113], we present the effect of relaxation dynamics and anisotropy in the orientation of the adsorbed dimers on the jamming and percolation transitions.

The Chapter is organized as follows. We start by describing our model in Sec. 5.2. We present the characteristics of the jamming state and the percolation configuration when the horizontal and vertical orientations of the dimers occur with equal probabilities in Secs. 5.3 and 5.4, respectively. The effect of anisotropy on the jamming and percolation transitions have been discussed in Sec. 5.5. Percolation transition using equal-oriented dimers in the jamming state has been presented in Sec. 5.6. Finally, we summarize in Sec. 5.7.

5.2 Model

An initially empty square lattice of size $L \times L$ with periodic boundary conditions, is the substrate in our model. We consider sequential adsorption of dimers at random positions onto the lattice sites. The two ends of the dimer reside on two neighboring sites of the lattice and thus, adsorption of each dimer occupies a pair of sites. At each adsorption attempt, the orientation (either vertical or horizontal) of the dimer is first

selected randomly with equal probability for both orientations. A pair of neighboring sites are then selected accordingly at random and the dimer is deposited on them.

Depending on the occupation status of the pair of sites, three possible scenarios may arise. First, if the pair of sites are both occupied by previously adsorbed dimers, adsorption fails. Second, if both sites are vacant, the adsorption is successful and the dimer is irreversibly adsorbed on them. Third, if only one of the sites is vacant, a sequence of dimer displacements is triggered, described as follows. When the deposited dimer (A) partially overlaps with a previously adsorbed dimer (B) at one end, the dimer B is displaced by a unit distance along its other end, keeping A fixed. The displaced dimer may again partially overlap with another dimer (C) leading to similar displacement of C. In this way the system of adsorbed dimers thus relaxes and eventually reaches a stable state when no more overlapping of dimers exists. This concerted move completes the "successful" adsorption of dimer A through a relaxation dynamics. Here one assumes the existence of two infinitely separated time scales, as we consider that the relaxation process is always faster than the inter-arrival time of deposited dimers. The trail of dimer displacements originated by depositing A constitute a path which is referred as the "relaxation path". It has been observed that often a relaxation path forms a closed loop. In such a case, the deposition attempt fails and the deposited dimer is discarded. The sequence of dimer adsorption attempts is continued till a jamming state is reached, where no more dimers can be adsorbed.

At any arbitrary stage of the adsorption process, the coverage of the surface is defined as $p = 2n/L^2$, where n is the number of adsorbed dimers. Since there are no desorption events, once a site becomes occupied it remains occupied, though the adsorbed dimers relax their positions during the relaxation process. After relaxation, a stable state configuration is reached where no two dimers overlap with each other. In a stable state configuration of adsorbed dimers, any two neighboring occupied sites are assumed to be connected and said to belong in the same cluster. The number of occupied sites in a cluster is defined as the size of the cluster. An existing cluster

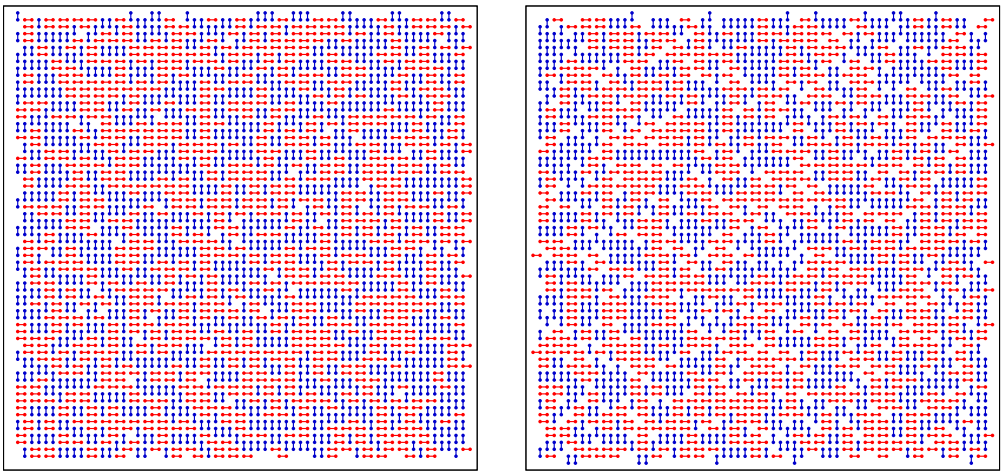

(a) (b)

Figure 5.1: Typical jamming state configuration of the dimers on a 64 × 64 square lattice for the random sequential adsorption model (a) with and (b) without relaxation. The dimers oriented in the horizontal and vertical directions have been painted in red and blue colors, respectively. The single vacant sites are represented by white color.

increases its size by two when at least one of the two end sites occupied by a newly adsorbed dimer becomes nearest neighbor of any of the sites in the cluster. When a new incoming dimer lands along the perimeter of such a cluster (partially overlapping it), that triggers the relaxation dynamics and it stops by displacing a dimer situated at another position on the perimeter of the cluster. Clearly, the relaxation path generated through this process is not at all random in the sense that the dimer displacements take place deterministically, as it is given by the orientation of the dimers adsorbed previously. Therefore, this relaxation is somewhat different from the stochastic diffusion process considered in the ARSA model.

For small values of p, there exists many small isolated clusters. Therefore, the adsorption of dimers is mainly uncorrelated and the occurrence of relaxation process is negligible. On the other hand, for intermediate values of p, successful adsorptions are often associated with relaxation. In this case, the newly occupied pair of sites are positioned at the two ends of the relaxation path and are separated by a distance larger than unity. As discussed above, these two sites are perimeter sites. Given one of the sites, the other can be determined from the overall configuration since the orientations

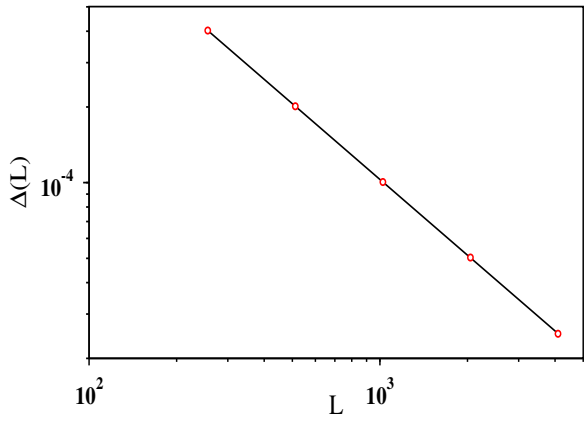

Figure 5.2: The width $\Delta(L)$ of the jamming transition has been plotted against L on a log-log scale for the lattice sizes $L = 256$, 512, 1024, 2048, and 4096. The fitted straight line has a slope 1.002(3).

of the adsorbed dimers belonging to the cluster are already known. Evidently, this introduces spatial correlations between the occupied sites. Such a source of correlation is absent in the model of RSA without relaxation. By further increasing the value of p, the clusters of occupied sites start merging and a percolation transition occurs when a giant cluster emerges that spans between two opposite sides of the lattice. The percolation threshold p_c is defined as the minimum value of p for which such a giant cluster exists in the system. This percolation transition is observed before the jamming transition.

5.3 Jamming Transition

In Fig. 5.1(a), we show a typical jamming state configuration of RSA model with relaxation. A similar jamming configuration obtained for RSA without relaxation has been shown in Fig. 5.1(b) for comparison. By visual inspection, it is clear that the jamming state coverage is higher for our RSA model than that of the RSA without relaxation. This is because, the relaxation dynamics promotes the reorganization and packs the dimers more densely. The averaged fraction of occupied sites at the jamming state defines the jamming coverage p_j. Numerically, we have estimated the

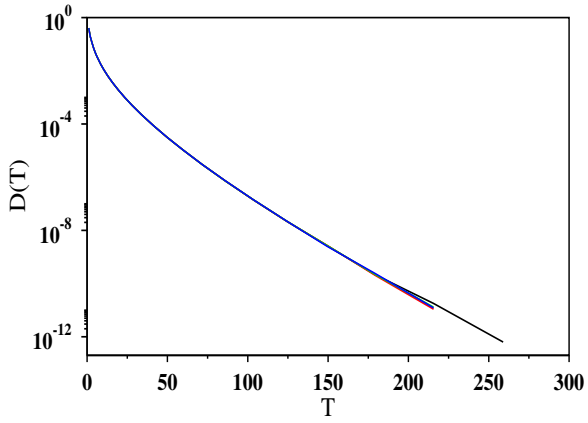

Figure 5.3: Plot of the binned data of the relaxation time distribution $D(T)$ for the entire process of adsorption on a log-lin scale using the lattice sizes $L = 256$ (black), 512 (red), 1024 (green), and 2048 (blue).

jamming state coverage $p_j(L)$ and its standard deviation $\Delta(L) = (\langle p_j^2 \rangle - \langle p_j \rangle^2)^{1/2}$ for different system sizes $L = 256$, 512, 1024, 2048, and 4096. We observe no significant finite-size effects for $p_j(L)$ and its value has been estimated to be 0.99049(3) compared to 0.90682(3) for RSA without relaxation. On the other hand, the value of $\Delta(L)$ indeed decreases systematically with L. To see the variation, we plot $\Delta(L)$ against L on a double logarithmic scale in Fig. 5.2 and find that all the data points fall on a straight line. This suggests a power-law decay: $\Delta(L) \sim L^{-1/\nu_j}$. From slope we have estimated $\nu_j = 1.002(3)$, consistent with a linear decay with $1/L$. A similar analysis also predicts $\nu_j \approx 1$ for the RSA without relaxation.

5.3.1 Relaxation Time

The system reorganizes during the relaxation process originated by depositing a dimer. The duration of time associated with the relaxation process is termed as the "relaxation time" T and it corresponds to the number of successive dimer displacements before a successful adsorption. This relaxation time has been measured for every dimer deposited from the beginning till the jamming state and its distribution $D(T)$ is plotted on a semi-log scale for four different system sizes in Fig. 5.3. Clearly, the tail of the

distribution decays exponentially in time with a characteristic time of ≈ 11.7, in units of dimer displacements. This indicates that the relaxation process reorganizes the system not in all length scales.

5.4 Percolation Transition

As the surface coverage p increases, the size of the largest cluster grows monotonically. Typically, the size of a cluster grows by two factors, e.g., when additional dimers join the cluster at its surface and secondly, when two clusters merge to form a single cluster. At a specific value of $p = p_c$, the system undergoes a percolation transition when a single cluster first connects two opposite sides of the system through a spanning path. Numerically, the precise value of the percolation threshold p_c^α for a specific run α is determined using the bisection method [113] described as follows. We select a pair of initial values of p, namely, p^{h} and p^{l} such that there exists a global connectivity through the spanning cluster for $p = p^{\mathrm{h}}$, but not for $p = p^{\mathrm{l}}$. Starting from an empty lattice the adsorption is continued till the surface coverage $p = (p^{\mathrm{h}} + p^{\mathrm{l}})/2$ is reached. Here, imposing periodic boundary conditions along the horizontal direction the global connectivity between the top and the bottom sides of the lattice is checked using the burning algorithm [56]. If the opposite sides of the lattice are connected by the same cluster, p^{h} is reduced to p, otherwise p^{l} is raised to p. In this way, the interval is successively bisected and the process is terminated when $p^{\mathrm{h}} - p^{\mathrm{l}} < 2/L^2$. At this stage, $(p^{\mathrm{h}} + p^{\mathrm{l}})/2$ defines the value of p_c^α for the run α. The entire procedure is then repeated for a large number of independent runs and the individual percolation thresholds are averaged to obtain the estimated value of the percolation threshold $p_c(L) = \langle p_c^\alpha(L) \rangle$ for the lattice size L. This calculation is then repeated for different values of L and finally, $p_c(L)$ values are extrapolated to obtain the asymptotic value p_c in the limit $L \to \infty$ using,

$$p_c(L) = p_c - AL^{-1/\nu}, \tag{5.1}$$

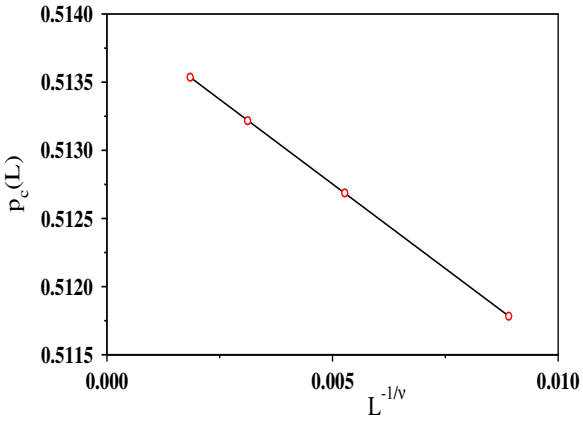

Figure 5.4: Plot of the percolation threshold $p_c(L)$ against $L^{-1/\nu}$ with $1/\nu = 0.756(6)$ for the lattice sizes $L = 512, 1024, 2048$, and 4096. The asymptotic value of the percolation threshold in the limit $L \to \infty$ has been estimated to be 0.5140(1).

where ν is recognized as the correlation length exponent in percolation theory and its value is 4/3 for ordinary percolation in two dimensions [6]. Accordingly, the obtained values of $p_c(L)$ are plotted against $L^{-1/\nu}$ in Fig. 5.4. Tuning the value of $1/\nu$, the data is found to be fit best by a straight line (using the least-squares fit of a straight line with minimal error) for $1/\nu = 0.756(6)$. By extrapolating the fitted line to the limit $L \to \infty$, we estimate $p_c = 0.5140(1)$. A similar procedure yields the value of p_c = 0.5618(1) for the RSA without relaxation and it agrees within error bar with the value of p_c reported in Refs. [145]. Clearly, the relaxation process helps the system to percolate at lower surface coverage.

Qualitatively, one can try to understand the reduction in the value of percolation threshold in the following way. Let us consider a situation where a single vacant site P separates two distinct clusters connected to the top and bottom boundaries of the lattice. In RSA without relaxation, it needs a dimer to be adsorbed precisely on this vacant site to connect the two clusters which results in a percolating state. In comparison, in our model with relaxation, a dimer may be deposited at many other locations, yet due to the relaxation process another dimer may be displaced in such way so that the site P becomes occupied and the two clusters merge together.

To investigate the critical properties of the percolation transition of RSA with

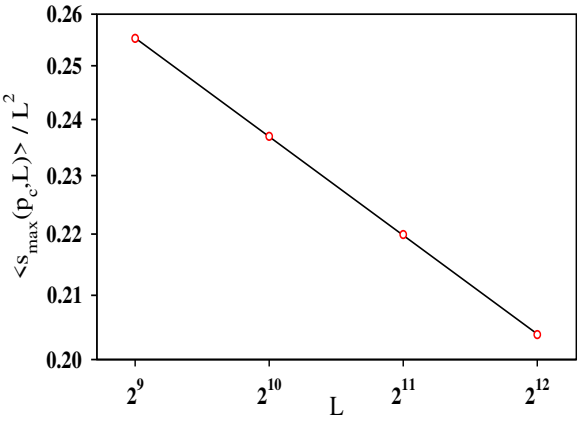

Figure 5.5: Log-log plot of the scaled average size of the largest cluster $\langle s_{max}(p_c, L)\rangle/L^2$ at the percolation threshold p_c for the lattice sizes $L = 512, 1024, 2048$, and 4096 gives the estimate of the fractal dimension $d_f = 1.892(3)$.

relaxation, several critical exponents have been estimated. Using extensive numerical simulations, at $p = p_c$, we have determined the fractal dimension of the largest cluster $d_f = 1.892(3)$ (plot is shown in Fig. 5.5), the exponent $\gamma/\nu = 1.790(2)$ associated with the second moment of the cluster size distribution and the fractal dimension of the shortest path $d_l = 1.1307(5)$. These values are consistent, within error bars, with the values known for the ordinary percolation in two dimensions, namely, $d_f = 91/48$, $\gamma/\nu = 43/24$ [6] and $d_l = 1.13077(2)$ [44].

5.5 Effect of Anisotropy

So far, we have considered that the orientation of the depositing dimers (either vertical or horizontal) is drawn at random with equal probability. We now consider the anisotropic case, where one orientation is preferentially selected compared to the other. More specifically, when the nth dimer is deposited, its orientation is randomly selected with probability p_v or $1 - p_v$ for vertical and horizontal, respectively. In this case, if a deposition attempt fails, another dimer is deposited with the same orientation but at another randomly selected location until the adsorption is successful.

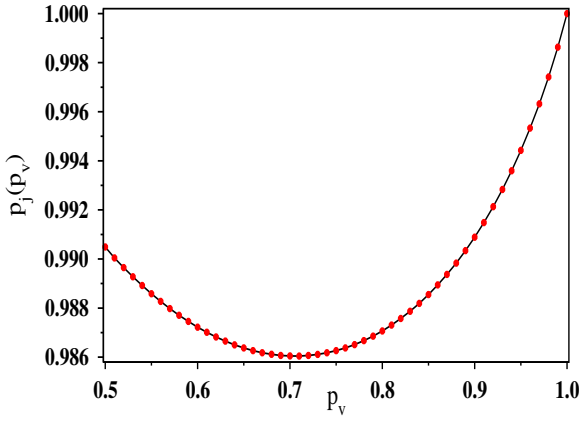

Figure 5.6: For $L = 1024$, the jamming state coverage $p_j(p_v)$ has been plotted against the selection probability p_v of the vertically oriented dimers. The data points are based on the averages over (at least) 10^5 configurations.

5.5.1 Jamming Coverage

For $p_v > 1/2$, we observe that the clusters are elongated along the vertical direction. For this regime, the jamming state corresponds to a configuration where no more vertically oriented dimers can be adsorbed. It turned out that the anisotropy affects significantly the value of the jamming state coverage $p_j(p_v)$. The variation of $p_j(p_v)$ against $1/2 \leqslant p_v \leqslant 1$ has been exhibited in Fig. 5.6, with $p_j = 0.99049$ for $p_v = 1/2$, a minimum value of 0.98605 for $p_v \approx 0.71$, and 1.0 for $p_v = 1$. This variation does not show any appreciable finite-size effects. We also observed that the exponent ν_j that characterizes the fluctuation of the jamming state coverage consistently remains unity (within error bars) for all p_v values. It may be noted that for the RSA without relaxation, $p_j(p_v)$ monotonically decreases from 0.9068 for $p_v = 1/2$ to $1 - e^{-2} \approx 0.8647$ for $p_v = 1$ [146].

5.5.2 Percolation Threshold

The effect of anisotropy on the percolation threshold has also been studied. For a fixed value of the anisotropy parameter p_v, the percolation threshold $p_c(p_v)$ in the limit of $L \to \infty$ has been obtained using the values of $p_c(p_v, L)$ for $L = 256, 512, 1024, 2048,$

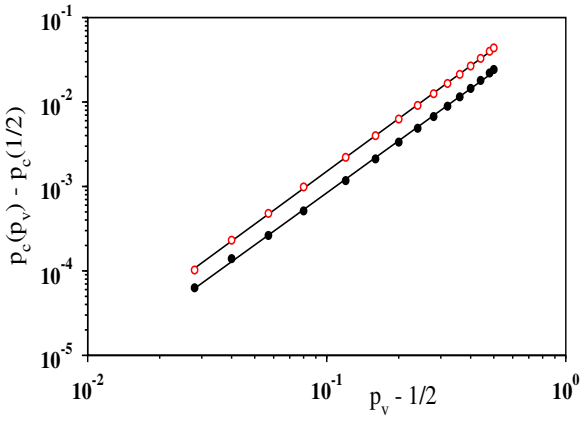

Figure 5.7: Log-log plot of the deviation of the percolation threshold $p_c(p_v) - p_c(1/2)$ against $p_v - 1/2$, p_v being the selection probability of the vertically oriented dimers, with $p_c(1/2) = 0.5140(1)$ and $0.5619(1)$ for the RSA with (open circles) and without (filled circles) relaxation, respectively. Slopes of the fitted straight lines have been measured as 2.05(6) and 2.07(7), respectively.

and 4096, and an extrapolation given by Eq. (5.1). The deviation of the percolation threshold from its value for the isotropic case, i.e., $p_c(p_v) - p_c(1/2)$ has been observed to follow a power-law with $p_v - 1/2$ (Fig. 5.7). On a double logarithmic scale the data points fit quite nicely with a straight line with slope = 2.05(6). Therefore, we conjecture that $p_c(p_v) - p_c(1/2) \sim (p_v - 1/2)^2$. Our simulation results also predict that this behavior holds for the RSA without relaxation (Fig. 5.7). In Table 5.1, the values of $p_c(p_v)$ for a few values of p_v are listed for RSA with and without relaxation.

To identify the universality class of the percolation transition for the anisotropic version of the model, as before we have measured a set of critical exponents, namely ν, γ, d_f and d_l for several values of p_v. It has been observed that the exponents values for RSA with and without relaxation are consistent within error bars with their respective values for the ordinary percolation in two dimensions.

5.6 Percolation of Equal-oriented Dimers

Let us now distinguish the clusters of adsorbed dimers by the orientation of the corresponding dimers in the jamming state. The size s of a cluster is the number

Table 5.1: Our numerical estimates of the percolation threshold $p_c(p_v)$ in the limit $L \to \infty$, for different values of the selection probability p_v of vertically oriented dimers for RSA with and without relaxation. Every reported value has an error bar not more than 2 in the last digit.

	$p_c(p_v)$	
p_v	RSA with relaxation	RSA without relaxation
0.50	0.5140	0.5619
0.58	0.5150	0.5624
0.66	0.5181	0.5640
0.74	0.5232	0.5668
0.82	0.5306	0.5708
0.90	0.5407	0.5764
0.98	0.5539	0.5840
1.00	0.5578	0.5862

of sites occupied by the cluster. In our simulations, we separate out the clusters of occupied sites by the vertically oriented dimers from the horizontal ones and the global connectivity is examined through the neighboring sites occupied by the vertical dimers. It is well known that for RSA without relaxation with $p_v = 1/2$, the largest among all the clusters does not form a spanning path between two opposite boundaries of the lattice [147]. As our model with relaxation dynamics enables more surface coverage, we thus address the question of whether such a spanning cluster appears with relaxation. Identifying different clusters using the Burning algorithm [56] and using many independent configurations, we find that the cluster size distribution $D(s)$ follows an exponential distribution as shown in Fig. 5.8(a). Further, the average size of the largest cluster $\langle s_{max}(p_v, L)\rangle$ is observed to grow logarithmically with the size of the system [Fig. 5.8(b)]. These results clearly indicate that for $p_v = 1/2$, there exist no such spanning cluster and therefore, the system remains in the sub-critical phase of the percolation transition, when clusters are distinguished by the orientation of the dimers in the jamming state. However, $\langle s_{max}(p_v, L)\rangle$ for the RSA with relaxation is higher in comparison to the RSA without relaxation and we see that the ratio between them asymptotically approaches a value ≈ 2.23.

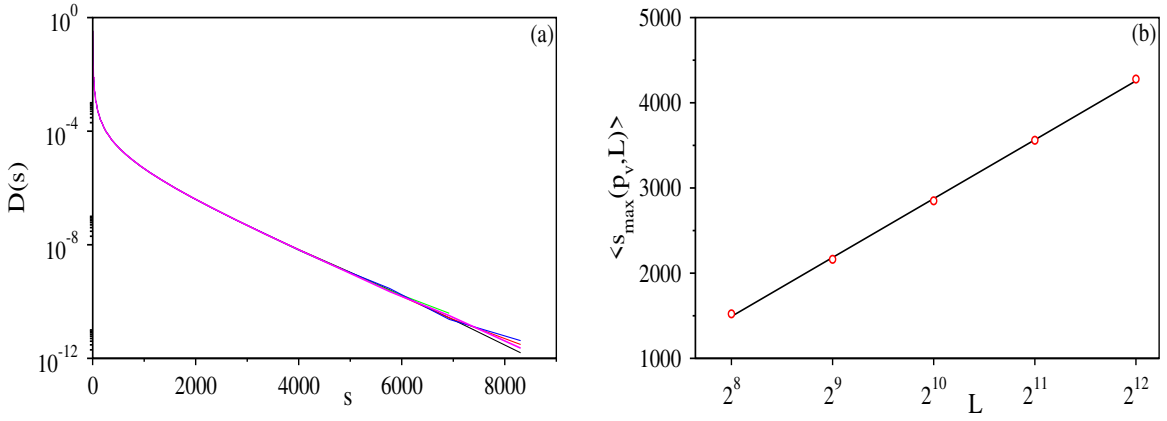

Figure 5.8: Right at the jamming state for the anisotropy parameter $p_v = 1/2$, (a) the binned data for cluster size distribution $D(s)$ of the vertically oriented dimers has been exhibited on a semi-log scale for $L = 256$ (black), 512 (red), 1024 (green), 2048 (blue), and 4096 (magenta); (b) the average size of the largest cluster $\langle s_{max}(p_v, L)\rangle$ for the same values of L has been plotted against L on a lin-log scale. The data points fit considerably well with a straight line indicating the logarithmic growth of the largest cluster.

As the value of p_v is increased from 1/2, the size of the largest cluster $\langle s_{max}(p_v, L)\rangle$ monotonically increases and at a critical value of $p_v = p_{vc}$, its size becomes so large that first time it spans across the system and thus, percolation of equal-oriented dimers occurs. In numerical simulations, imposing periodic boundary conditions along the horizontal direction, global connectivity is checked along the vertical direction.

Tuning the value of p_v and averaging over many uncorrelated jamming state configurations for each p_v, we plot the percolation probability $\Pi(p_v, L)$ in Fig. 5.9(a) for three different values of the surface sizes. The curves become more and more sharp as L is increased. All these curves intersect approximately at the same point $[p_{vc}, \Pi(p_{vc})]$ with $p_{vc} \approx 0.5577$ and $\Pi(p_{vc}) \approx 0.61$, which is slightly lower than the value 0.636454001 [136] obtained using Cardy's formula for cylindrical geometry [137]. Figure 5.9(b), exhibits a scaling plot of $\Pi(p_v, L)$ against $(p_v - p_{vc})L^{1/\nu}$. The best data collapse for all three system sizes corresponds to $p_{vc} = 0.5577(5)$ and $1/\nu = 0.754(5)$, implying a finite-size scaling form

$$\Pi(p_v, L) = \mathcal{F}[(p_v - p_{vc})L^{1/\nu}]. \tag{5.2}$$

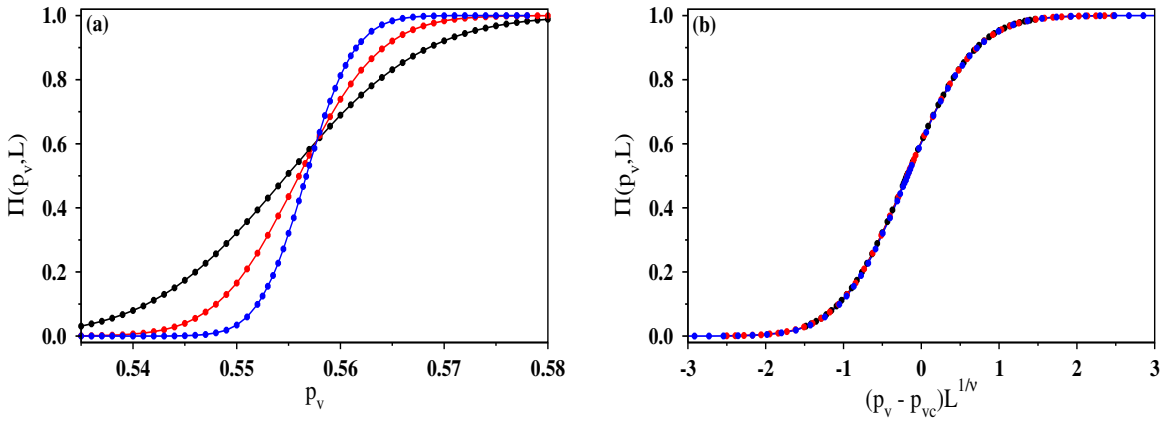

Figure 5.9: (a) For $L = 256$ (black), 512 (red) and 1024 (blue) the percolation probability $\Pi(p_v, L)$ has been plotted against the probability p_v of selection of the vertically oriented dimers. (b) Scaling plot of the same data as in (a). A plot of $\Pi(p_v, L)$ against $(p_v - p_{vc})L^{1/\nu}$ using $p_{vc} = 0.5577(5)$ and $1/\nu = 0.754(5)$ exhibits a nice data collapse.

Similarly, scaling analyses have been performed for the order parameter $\Omega(p_v, L) = \langle s_{max}(p_v, L)\rangle/L^2$ and susceptibility, defined by the fluctuation of the order parameter as $\chi(p_v, L) = \langle \Omega(p_v, L)^2\rangle - \langle \Omega(p_v, L)\rangle^2$ (not shown here). A finite-size scaling form as in Eq. (1.5) works very well for the order parameter. Again, for the susceptibility usual scaling form as the ordinary percolation holds good. We also find that the values of the associated scaling exponents, β and γ follow within error bars the hyperscaling relation $2\beta/\nu + \gamma/\nu = 2$ in two dimensions [6].

The second moment of the cluster size distribution M_2' is defined as

$$M_2' = \sum_k s_k^2/L^2 - \langle s_{max}\rangle/L^2 \tag{5.3}$$

where, s_k is the size of the cluster k. The variation of $M_2'(p_v, L)$ against p_v has been exhibited in Fig. 5.10(a) for the same three system sizes. By suitably scaling the abscissa and ordinate when the same data are re-plotted in Fig. 5.10(b), an excellent data collapse is observed using $p_{vc} = 0.5577(5)$, $1/\nu = 0.754(5)$ and $\gamma/\nu = 1.795(5)$,

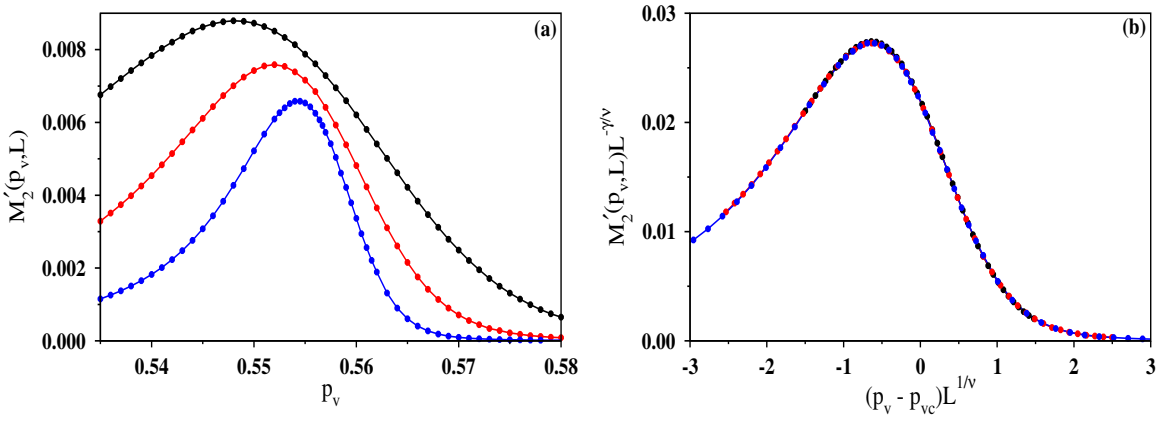

Figure 5.10: (a) For $L = 256$ (black), 512 (red) and 1024 (blue) the scaled second moment $M_2'(p_v, L)/L^2$ has been plotted against the selection probability p_v of the vertically oriented dimers. (b) Finite-size scaling of the same data as in (a). Plot of the re-scaled second moment $M_2'(p_v, L)L^{-\gamma/\nu}$ with the scaling variable $(p_v - p_{vc})L^{1/\nu}$ using $p_{vc} = 0.5577(5)$, $1/\nu = 0.754(5)$ and $\gamma/\nu = 1.795(5)$ exhibits a nice data collapse.

indicating a scaling form

$$M_2'(p_v, L) = L^{\gamma/\nu}\mathcal{G}[(p_v - p_{vc})L^{1/\nu}]. \tag{5.4}$$

The same set of scaling analyses have been performed for RSA without relaxation, and we estimated $p_{vc} = 0.6056(5)$.

5.7 Summary

To summarize, we have introduced and studied a variant of random sequential adsorption (RSA) model in which the objects are adsorbed on a two-dimensional surface after going through a well-defined relaxation dynamics. Specifically, we consider sequential and irreversible adsorption of dimers onto the sites of a square lattice at random positions. When a new incoming dimer partially overlaps with a previously adsorbed dimer, the relaxation dynamics is triggered and during relaxation, a sequence of dimer displacements may take place to accommodate the new dimer. The post-relaxation state is characterized by a monolayer formation of non-overlapping dimers. Every

adsorption followed by the relaxation dynamics includes a pair of new occupied sites separated by a distance larger than unity; given one of the sites the other can be determined from the configuration of dimers adsorbed previously. Therefore, spatial correlations develop in the system. Considering any two neighboring occupied sites as connected, a percolation transition has been observed. when a cluster of occupied sites first spans across the system. Further, the kinetics of adsorption ceases when a jamming state is reached where no more dimers can be adsorbed. The effect of the relaxation dynamics and anisotropy in the orientation of the adsorbed dimers on the percolation and jamming transitions have been investigated here in detail.

We find that the percolation transition for the isotropic case occurs at a critical density of occupied sites $p_c = 0.5140(1)$. The increase of anisotropy, p_v, of the occurrence of vertically oriented dimers results in an increase of the percolation threshold p_c. The value of p_c in the entire range of $1/2 \leqslant p_v \leqslant 1$ has been found to be smaller for our model with relaxation compared to the RSA without relaxation. Estimation of different critical exponents at and around p_c using extensive numerical simulations lead us to conclude that, despite the developed spatial correlations, the model belongs to the same universality class as the ordinary percolation.

The relaxation dynamics helps packing the dimers more densely and thus, the jamming state coverage is higher for RSA with relaxation than without relaxation. Interestingly, a non-monotonic variation of the jamming state coverage with the strength of anisotropy p_v has been observed for RSA with relaxation. Further, in the jamming state, a percolation transition through the cluster of sites occupied by the vertically oriented dimers is observed when the control variable p_v is tuned to the critical value $p_{vc} = 0.5577(5)$. Also here, the directionality does not affect the critical (universal) properties of the percolation transition.

For future investigations, one can study the effect of the size of depositing objects, size dispersion and the dimensionality of the surface on the jamming and percolation transitions in the RSA model with relaxation.

Bibliography

[1] S. Broadbent, and J. Hammersley, *Percolation processes I. Crystals and mazes*, Proceedings of the Cambridge Philosophical Society **53**, 629 (1957).

[2] P. J. Flory, J. Am. Chem. Soc. **63**, 3083 (1941).

[3] P. J. Flory, J. Am. Chem. Soc. **63**, 3091 (1941).

[4] P. J. Flory, J. Am. Chem. Soc. **63**, 3096 (1941).

[5] D. Stauffer, A. Coniglio, and M. Adam, Adv. Polym. Sci. **44**, 103 (1982).

[6] D. Stauffer and A. Aharony, *Introduction to Percolation Theory* (Taylor & Francis, London, 2003).

[7] H. E. Stanley, *Introduction to Phase Transitions and Critical Phenomena* (Oxford University Press, New York, 1971).

[8] D. Sornette, *Critical Phenomena in Natural Sciences: Chaos, Fractals, Self-organization and Disorder: Concepts and Tools* (Springer, New York, 2006).

[9] J. Cardy, *Scaling and Renormalization in Statistical Physics* (Cambridge University press, Cambridge, 1996).

[10] N. Goldenfeld, *Lectures on Phase Transitions and Renormalization Group* (CRC Press, Boca Raton, 2018).

[11] J. T. Ho, and J. D. Litster, Jour. Appl. Phys. **40**, 1270 (1969).

[12] S. Puri, in *Kinetics of Phase Transitions*, edited by S. Puri and V. Wadhawan (CRC Press, Boca Raton, 2009).

[13] B. Mandelbrot, Science **156**, 636 (1967).

[14] B. Mandelbrot, *The Fractal Geometry of Nature* (W.H. Freeman, New York, 1983).

[15] J. Feder, *Fractals* (Springer, New York, 1988).

[16] M. Sahimi, Rev. Mod. Phys. **65**, 1393 (1993).

[17] M. Sahimi, *Applications of Percolation Theory* (Taylor & Francis, London, 1994).

[18] G. Grimmett, *Percolation* (Springer, New York, 1999).

[19] A. A. Saberi, Physics Reports **578**, 1 (2015).

[20] B. Berkowitz, and R. P. Ewing, Surveys in Geophysics, **19**, 23 (1998).

[21] T. Beer, and I. G. Enting , Mathematical and Computer Modelling **13**, 77 (1990).

[22] M. E. J. Newman, Phys. Rev. E **66**, 016128 (2002).

[23] J. D. Murray, *Mathematical Biology* (3rd edn, Springer, Berlin, 2005).

[24] I. Glauche, W. Krause, R. Sollacher, and M. Greiner, Physca A **325**, 577 (2003).

[25] P. Santi, ACM Computing Surveys **37**, 164 (2005).

[26] W. Dargie, and C. Poellabauer, *Fundamentals of Wireless Sensor Networks: Theory and Practice* (Wiley, New York, 2010).

[27] D. J. Watts, Proc. Natl. Acad. Sci. **99**, 5766 (2002).

[28] J. Shao, S. Havlin, and H. E. Stanley, Phys. Rev. Lett. **103**, 018701 (2009).

[29] B. Berkowitz, and I. Balberg, Water Resour. Res. **29**, 775 (1993).

[30] R. Meester, and R. Roy, *Continuum Percolation* (Cambridge University Press, Cambridge, 1996).

[31] N. A. M. Araúujo, P. Grassberger, B. Kahng, K. J. Schrenk, and R. M. Ziff, Eur. Phys. J. Special Topics **223**, 2307 (2014).

[32] D. Lee, Y. S. Cho, and B. Kahng, J. Stat. Mech. **2016**, 124002 (2016).

[33] M. E. Fisher, and J. W. Essam, J. Math. Phys. **2**, 609 (1961).

[34] M. E. Fisher, J. Math. Phys. **2**, 620 (1961).

[35] S. Kundu and S. S. Manna, Phys. Rev. E, **93**, 062133 (2016).

[36] S. Kundu, and S. S. Manna, Phys. Rev. E **95**, 052124 (2017).

[37] P.W. Kasteleyn, and C.M. Fortuin, J. Phys. Soc. Jpn. (Suppl.) **26**, 11 (1969).

[38] R. M. Ziff, C. R. Scullard, J. C. Wierman, and M. R. A. Sedlock, J. Phys. A **45**, 494005 (2012).

[39] J. L. Jacobsen, J. Phys. A: Math. Theor. **48**, 454003 (2015).

[40] A complete list of percolation thresholds is at `en.wikipedia.org/wiki/Percolation_threshold`.

[41] J. Hoshen, and R. Kopelman, Phys. Rev. B **14** 3438 (1976).

[42] M. E. J. Newman, and R. M. Ziff, Phys. Rev. Lett. **85**, 4104 (2000).

[43] A. Margolina, H. J. Herrmann, and D. Stauffer, Phys. Lett. A **93**, 73 (1982).

[44] Z. Zhou, J. Yang, Y. Deng, and R. M. Ziff, Phys. Rev. E **86**, 061101 (2012).

[45] N. V. Dokholyan, S. V. Buldyrev, S. Havlin, P. R. King, Y. Lee, and H. E. Stanley, Physica A **266**, 55 (1999).

[46] R. F. Soares, G. Corso, L. S. Lucena, J. E. Freitas, L. R. da Silva, G. Paul, and H. E. Stanley, Physica A **343**, 739 (2004).

[47] Y. Deng, H. W. J. Blöte, and B. Nienhuis, Phys. Rev. E **69**, 026114 (2004).

[48] K. J. Schrenk, N. Posé, J. J. Kranz, L. V. M. van Kessenich, N. A. M. Araújo, and H. J. Herrmann, Phys. Rev. E **88**, 052102 (2013).

[49] M. Porto, A. Bunde, and S. Havlin, Physica A **266**, 96 (1999).

[50] `https://en.wikipedia.org/wiki/Percolation_critical_exponents`

[51] X. Xu, J. Wang, J.-P. Lv, and Y. Deng, Front. Phys. **9**, 113 (2014).

[52] J. Wang, Z. Zhou, W. Zheng, T. M. Garoni, and Y. Deng, Phys. Rev. E **87**, 052107 (2013).

[53] J. Adler, Y. Meir, A. Aharony, and A. B. Harris, Phys. Rev. B **41**, 9183 (1990).

[54] S. Mertens, and C. Moore, Phys. Rev. E **98**, 022120 (2018).

[55] C. D. Lorenz, and R. M. Ziff, Phys. Rev. E **57**, 230 (1998).

[56] H. J. Herrmann, D. C. Hong, and H. E. Stanley, J. Phys. A **17**, L261 (1984).

[57] A. Coniglio, H. E. Stanley, and W. Klein, Phys. Rev. Lett. **42**, 518 (1979).

[58] Y. Y. Tarasevitch and S. C. Van der Marck, Int. J. Mod. Phys. C **10**, 1193 (1999).

[59] T. Mai, and J. W. Halley, in *Ordering in Two Dimensions* (Elsevier North-Holland, Amsterdam, 1980), p. 369.

[60] J. C. Wierman, Banach Center Publications, Warsaw, **25**, 241 (1989).

[61] M. J. Appel, and J. C. Wierman, J. Phys. A **20**, 2527 (1987).

[62] X. Y. Wu, and S. Y. Popov, J. Stat. Phys. **110**, 443 (2003).

[63] J. C. Wierman, and M. J. Appel, J. Phys. A **20**, 2533 (1987)

[64] F. Sevsek, J. M. Debierre, and L. Turban, J. Phys. A **16**, 801 (1983).

[65] H. Nakanishi, J. Phys. A **20**, 6075 (1987).

[66] M. K. Wilkinson, J. Phys. A **20**, 3011 (1987).

[67] D. Wilkinson and J. F. Willemsen, J. Phys. A **16**, 3365 (1983).

[68] M. Sahimi, Rev. Mod. Phys. **65**, 1393 (1993).

[69] R. Lenormand, and C. Zarcone, Phys. Rev. Lett. **54**, 2226 (1985).

[70] H. Mohammadi, E. N. Oskoee, M. Afsharchi, N. Yazdani, and M. Sahimi, Int. J. Mod. Phys. C **20**, 1871 (2009)

[71] E. T Gawlinski, and H. E. Stanley, J. Phys. A **14**, L291 (1981).

[72] R. Albert, H. Jeong, and A-L. Barabási, Nature **401**, 130 (1999).

[73] R. Pastor-Satorras, A. Vazquez and A. Vespignani, Phys. Rev. Lett. **87**, 258701 (2001).

[74] S. L. Pimm, J. H. Lawton, J. E. Cohen, Nature **350**, 669 (1991).

[75] D. J. Watts and S.H. Strogatz, Nature **393**, 440 (1998).

[76] R. Albert, and A-L. Barabási, Rev. Mod. Phys. **74**, 47 (2002).

[77] P. Erdös and A. Rényi, Publ. Math. Inst. Hung. Acad. Sci. **5**, 17 (1960).

[78] R. Cohen, K. Erez, D. ben-Avraham, and S. Havlin, Phys. Rev. Lett. **86**, 3682 (2001).

[79] R. Cohen, D. ben-Avraham, and S. Havlin, Phys. Rev. E **66**, 036113 (2002).

[80] S. N. Dorogovtsev and A. V. Goltsev, Rev. Mod. Phys. **80**, 1275 (2008).

[81] D. Lee, B. Kahng, Y. S. Cho, K.-I. Goh, D.-S. Lee, J. Kor. Phys. Soc. **73**, 152 (2018).

[82] D. Achlioptas, R. M. D′Souza, and J. Spencer, Science **323**, 1453 (2009).

[83] J. Nagler, A. Levina, and M. Timme, Nature Physics, **7**, 265 (2011).

[84] S. S. Manna, Physica A **391**, 2833 (2012).

[85] P. Grassberger, C. Christensen, G. Bizhani, S.-Woo Son, and M. Paczuski, Phys. Rev. Lett. **106**, 225701 (2011).

[86] R. M. Ziff, Phys. Rev. Lett. **103**, 045701 (2009).

[87] Y. S. Cho, J. S. Kim, J. Park, B. Kahng, and D. Kim, Phys. Rev. Lett. **103**, 135702 (2009)

[88] E. J. Friedman, and A. S. Landsberg, Phys. Rev. Lett. **103**, 255701 (2009).

[89] R. M. D′Souza, and M. Mitzenmacher, Phys. Rev. Lett. **104**, 195702 (2010).

[90] S. S. Manna and A. Chatterjee, Physica A **390**, 177 (2011).

[91] R. M. Ziff, Science **339**, 1159 (2013).

[92] R. A. da Costa, S. N. Dorogovtsev, A. V. Goltsev and J, F. F. Mendes, Phys. Rev. Lett. **105**, 255701 (2010).

[93] O. Riordan and L. Warnke, Science **333**, 322 (2011).

[94] O. Riordan and L. Warnke, Ann. Appl. Prob. **22**, 1450 (2012).

[95] F. Radicchi, S. Fortunato, Phys. Rev. Lett. **103**, 168701 (2009).

[96] F. Radicchi, S. Fortunato, Phys. Rev. E. **81**, 036110 (2010).

[97] R. K. Pan, M. Kivelä, J. Saramaki̇, K. Kaski, J. Kertész, Phys. Rev. E **83**, 046112 (2011).

[98] R. M. Ziff, Phys. Rev. E. **82**, 051105 (2010).

[99] N. A. M. Araújo, and H. J. Herrmann, Phys. Rev. Lett. **105**, 035701 (2010).

[100] K. J. Schrenk, N. A. M. Araújo, and H. J. Herrmann, Phys. Rev. Lett. **105**, 035701 (2010).

[101] Y. S. Cho, S. Hwang, H. J. Herrmann, and B. Kahng, Science **339**, 1185 (2013).

[102] W. Kinzel, Z. Phys. B **58**, 229 (1985).

[103] H. Hinrichsen, Adv. Phys. **49**, 815 (2000).

[104] M. Henkel, H. Hinrichsen, and S. Lübeck, *Non-Equilibrium Phase Transitions, Volume 1: Absorbing Phase Transitions* (Springer, Netherlands, 2008).

[105] J. W. Evans, Rev. Mod. Phys. **65**, 1281 (1993).

[106] V. Privman, Trends in Stat. Phys. **1**, 89 (1994).

[107] E. Kumacheva, R. K. Golding, M. Allard, and E. H. Sargent, Adv. Matter **14**, 221 (2002).

[108] P. C. Lewis, E. Kumacheva, M. Allard, and E. H. Sargent, J. Dispers. Sci. Technol. **26**, 259 (2005).

[109] È. O'Conor, A. O'Riordan, H. Doyle, S. Moynihan, A. Cuddihy, and G. Redmond, Appl. Phys. Lett. **86**, 201114 (2005).

[110] S. Torquato, and F. H. Stillinger, Rev. Mod. Phys. **82**, 2633 (2010).

[111] C. Burda, X. Chen, R. Narayanan, and M. A. El-Sayed, Chem. Rev. **105**, 1025 (2005).

[112] C. L. N. Oliveira, N. A. M. Araújo, J. S. Andrade, and H. J. Herrmann, Phys. Rev. Lett. **113**, 155701 (2014).

[113] S. Kundu, N. A. M. Araújo, and S. S. Manna, Phys. Rev. E **98**, 062118 (2018).

[114] M. C. Bartelt and V. Privman, Int. J. Mod. Phys. B **05**, 2883 (1991).

[115] V. Privman, J. Adhesion **74**, 421 (2000).

[116] A. Cadilhe, N. A. M. Araújo, and V. Privman, J. Phys.: Condens. Matter **19**, 065124 (2007).

[117] P. J. Flory, J. Am. Chem. Soc. **61**, 1518 (1939).

[118] A. Rényi, Publ. Math. Inst. Hung. Acad. Sci. **3**, 109 (1958).

[119] J. Feder, J. Theor. Biol. **87**, 237 (1980).

[120] S. S. Manna and N. M. Svrakic, J. Phys. A **24**, L671 (1991).

[121] B. Bonnier, M. Hontebeyrie, Y. Leroyer, C. Meyers, and E. Pommiers, Phys. Rev. E **49**, 305 (1994).

[122] D. A. King, and M. G. Wells, Proc. R. Soc. London, Ser. A **339**, 245 (1974).

[123] X. C. Guo, J. M. Bradley, A. Hopkinson, and D. A. King, Surf. Sci. **310**, 163 (1994).

[124] G. J. Rodgers, and J. A. N. Filipe, J. Phys. A **30**, 3449 (1997).

[125] M. Cieśla, G. Pajak, R. M. Ziff, Phys. Chem. Chem. Phys. 2015 **17**, 24376 2015.

[126] D. Joshi, D. Bargteil, A. Caciagli, J. Burelbach, Z. Xing, A. S. Nunes, D. E. P. Pinto, N. A. M. Araújo, J. Brujic, and E. Eiser, Sci. Adv. **2**, e1600881 (2016).

[127] D. E. P. Pinto, and N. A. M. Araújo, Phys. Rev. E **98** 012125 (2018).

[128] S. Kundu, A. Datta, and S. S. Manna, Phys. Rev. E **96** 032126 (2017).

[129] B. Lorenz, I. Orgzall, and H. O. Heuer, J. Phys. A **26**, 4711 (1993).

[130] J. Quintanilla, Phys. Rev. E **63**, 061108 (2001).

[131] R. Sollacher, M. Greiner, and I. Glauche, Wireless Networks **12**, 53 (2006).

[132] N. Baccour, A. Kouba, L. Mottola, M. Ziga, H. Youssef, C. Boano, and M. Alves, ACM Trans. Sens. Netw. **8**, 34 (2012).

[133] N. Baccour, A. Kouba, H. Youssef, and M. Alves, Ad Hoc Netw. **27**, 1 (2015).

[134] B. Silva, R. Fisher, A. Kumar, and G. Hancke, IEEE Trans. Ind. Inf. **11**, 1099 (2015).

[135] N. Ahmed, S. Kanhere, and S. Jha, IEEE Commun. Mag. **54**, 52 (2016).

[136] R. M. Ziff, Phys. Rev. E **83**, 020107(R) (2011).

[137] J. Cardy, J. Stat. Phys. **125**, 1 (2006).

[138] V. Cornette, A. J. Ramirez-Pastor, and F. Nieto, Eur. Phys. J. B **36**, 391 (2003).

[139] G. Kondrat, and A. Pekalski Phys. Rev. E **63**, 051108 (2001).

[140] G. D. Garcia, F. O. Sanchez-Varretti, P. M. Centres, and A.J. Ramirez-Pastor, Eur. Phys. J. B **86**, 403 (2013).

[141] Y. Y. Tarasevich, N. I. Lebovka, and V. V. Laptev, Phys. Rev. E **86**, 061116 (2012).

[142] Lj. Budinski-Petković, I. Lončarević, M. Petković, Z. M. Jakšić, and S. B. Vrhovac, Phys. Rev. E **85**, 061117 (2012).

[143] E. J. Perino, D. A. Matoz-Fernandez, P. M. Pasinetti, and A. J. Ramirez-Pastor, J. Stat. Mech. **2017**, 073206 (2017).

[144] S. N. Majumdar, and David S. Dean, Phys. Rev. Lett. **89**, 115701 (2002).

[145] V. A. Cherkasova, Y. Y. Tarasevich, N. I. Lebovka and N. V. Vygornitskii, Eur. Phys. J. B **74**, 205 (2010).

[146] P. L. Krapivsky, S. Redner, and E. Ben-Naim, *A Kinetic view of Statistical Physics*, Cambridge University Press, New York (2010).

[147] N. I. Lebovka, N. N. Karmazina, Y. Y. Tarasevich, and V. V. Laptev, Phys. Rev. E **84**, 061603 (2011).